FINAL
CONTRACT REPORT
VTRC 09-CR11

SHEAR STRENGTH OF A PCBT-53 GIRDER FABRICATED WITH LIGHTWEIGHT SELF-CONSOLIDATING CONCRETE

BENJAMIN Z. DYMOND
Research Associate

CARIN L. ROBERTS-WOLLMANN
Associate Professor

THOMAS E. COUSINS
Professor

Via Department of Civil and Environmental Engineering
Virginia Polytechnic Institute & State University

http://www.virginiadot.org/vtrc/main/online_reports/pdf/09-cr11.pdf

Standard Title Page - Report on Federally Funded Project

1. Report No.: FHWA/VTRC 09-CR11	2. Government Accession No.:	3. Recipient's Catalog No.:
4. Title and Subtitle: Shear Strength of a PCBT-53 Girder Fabricated with Lightweight Self-Consolidating Concrete		5. Report Date: April 2009 6. Performing Organization Code:
7. Author(s): Benjamin Z. Dymond, Carin L. Roberts-Wollmann, and Thomas E. Cousins		8. Performing Organization Report No.: VTRC 09-CR11
9. Performing Organization and Address: Virginia Transportation Research Council, 530 Edgemont Road, Charlottesville, VA 22903		10. Work Unit No. (TRAIS): 11. Contract or Grant No.: 83147
12. Sponsoring Agencies' Name and Address: Virginia Department of Transportation, 1401 E. Broad Street, Richmond, VA 23219; Federal Highway Administration, 400 North 8th Street, Room 750, Richmond, VA 23219-4825		13. Type of Report and Period Covered: Final Contract 14. Sponsoring Agency Code:

15. Supplementary Notes:
This project was financed with Part II State Planning and Research (SPR) funds at an estimated cost of $147,705.

16. Abstract:

Lightweight self-consolidating concrete (LWSCC) is advantageous in the bridge industry because members fabricated with this material have a significantly lower self weight and in its fresh state, LWSCC has a low viscosity that eliminates the need for vibration during fabrication. Unfortunately, lightweight, self-consolidating concrete typically has lower tensile strength and possibly a lower aggregate interlock strength. This combination may result in a lower overall shear strength. In addition, this type of concrete has a lower modulus of elasticity, which leads to higher elastic shortening losses and higher deflections.

In order to evaluate the affect of lightweight, self-consolidating concrete on the shear strength of prestressed concrete bridge girders, the study described herein was performed. A single PCBT-53 bridge girder was fabricated and tested. The girder itself was cast with lightweight, self-consolidating concrete and a composite cast-in-place deck was fabricated using lightweight concrete. In this study, the girder and deck were tested using three different loading conditions. These tests aimed to experimentally quantify the beam's overall web shear strength and flexure-shear strength.

Data pertaining to each test are presented in this report. Results include material properties, deflection plots, strain plots, and temperature change plotted with respect to time. The measured shear strength is compared to several design methods. With respect to web shear strength, the current AASHTO LRFD Sectional Model and the Simplified Method for shear were conservative for the self-consolidating lightweight girder if the measured cracking angle was used in calculations. Both the LRFD Sectional Model and the Simplified Method are recommended for shear design of LWSCC prestressed bridge beams. The tests to evaluate flexure-shear strength were inconclusive because the beam failed in flexure prior to a flexure-shear failure.

17 Key Words:	18. Distribution Statement:
Self-consolidating concrete, lightweight concrete, prestressed concrete bulb tee bridge girders, shear strength	No restrictions. This document is available to the public through NTIS, Springfield, VA 22161.

19. Security Classif. (of this report):	20. Security Classif. (of this page):	21. No. of Pages:	22. Price:
Unclassified	Unclassified	74	

FINAL CONTRACT REPORT

SHEAR STRENGTH OF A PCBT-53 GIRDER FABRICATED WITH LIGHTWEIGHT SELF-CONSOLIDATING CONCRETE

Benjamin Z. Dymond
Research Associate

Carin L. Roberts-Wollmann
Associate Professor

Thomas E. Cousins
Professor

Via Department of Civil and Environmental Engineering
Virginia Polytechnic Institute & State University

Project Manager
Jose P. Gomez, Ph.D., P.E., Virginia Transportation Research Council

Contract Research Sponsored by
the Virginia Transportation Research Council
(A partnership of the Virginia Department of Transportation
and the University of Virginia since 1948)

In Cooperation with the U.S. Department of Transportation
Federal Highway Administration

Charlottesville, Virginia

April 2009
VTRC 09-CR11

DISCLAIMER

The project that is the subject of this report was done under contract for the Virginia Department of Transportation, Virginia Transportation Research Council. The contents of this report reflect the views of the author(s), who is responsible for the facts and the accuracy of the data presented herein. The contents do not necessarily reflect the official views or policies of the Virginia Department of Transportation, the Commonwealth Transportation Board, or the Federal Highway Administration. This report does not constitute a standard, specification, or regulation. Any inclusion of manufacturer names, trade names, or trademarks is for identification purposes only and is not to be considered an endorsement.

Each contract report is peer reviewed and accepted for publication by Research Council staff with expertise in related technical areas. Final editing and proofreading of the report are performed by the contractor.

ABSTRACT

Lightweight self-consolidating concrete (LWSCC) is advantageous in the bridge industry because members fabricated with this material have a significantly lower self weight and in its fresh state, LWSCC has a low viscosity that eliminates the need for vibration during fabrication. Unfortunately, lightweight, self-consolidating concrete typically has lower tensile strength and possibly a lower aggregate interlock strength. This combination may result in a lower overall shear strength. In addition, this type of concrete has a lower modulus of elasticity, which leads to higher elastic shortening losses and higher deflections.

In order to evaluate the affect of lightweight, self-consolidating concrete on the shear strength of prestressed concrete bridge girders, the study described herein was performed. A single PCBT-53 bridge girder was fabricated and tested. The girder itself was cast with lightweight, self-consolidating concrete and a composite cast-in-place deck was fabricated using lightweight concrete. In this study, the girder and deck were tested using three different loading conditions. These tests aimed to experimentally quantify the beam's overall web shear strength and flexure-shear strength.

Data pertaining to each test are presented in this report. Results include material properties, deflection plots, strain plots, and temperature change plotted with respect to time. The measured shear strength is compared to several design methods. With respect to web shear strength, the current AASHTO LRFD Sectional Model and the Simplified Method for shear were conservative for the self-consolidating lightweight girder if the measured cracking angle was used in calculations. Both the LRFD Sectional Model and the Simplified Method are recommended for shear design of LWSCC prestressed bridge beams. The tests to evaluate flexure-shear strength were inconclusive because the beam failed in flexure prior to a flexure-shear failure.

FINAL CONTRACT REPORT

SHEAR STRENGTH OF A PCBT-53 GIRDER FABRICATED WITH LIGHTWEIGHT SELF-CONSOLIDATING CONCRETE

Benjamin Z. Dymond
Research Associate

Carin L. Roberts-Wollmann
Associate Professor

Thomas E. Cousins
Professor

INTRODUCTION

As part of the 2005 Innovative Bridge Research and Construction Program, Virginia received a grant to implement lightweight, self-consolidating concrete (LWSCC) in precast bulb tee (PCBT) bridge girders. Lightweight concrete is advantageous in the bridge industry due to the fact that members fabricated with this material have a significantly lower self weight. This helps facilitate transportation and placement of the beams, and it also reduces the overall dead load of the bridge. This aspect is also very useful to contractors because the erection and handling of large bridge girders is faster and easier with lower capacity cranes. One of the advantages of self-consolidating concrete (SCC), compared to typical concrete, is its low viscosity. This characteristic allows formwork to properly fill during casting without vibration and eliminates many of the typical bug holes present in concrete members. Because vibration is not required during construction, production times are faster and a savings in the overall labor cost can be achieved. The most beneficial aspect of SCC is its ability to flow through congested reinforcement and into tight corners. The bridge industry can take particular advantage of this quality because of the thin webs of bridge girders, and the congested shear reinforcement within these webs.

Unfortunately, lightweight concrete typically has lower tensile strength, and hence lower shear strength, than normal weight concrete of the same compressive strength. In addition, because self-consolidating concretes use a larger percentage of fine aggregates, it is possible that the aggregate interlock contribution to shear strength will also be reduced. The research described in this report was performed to investigate the shear strength of lightweight, self-consolidating concrete, and compare the measured shear strength to existing shear design methods.

PURPOSE AND SCOPE

Purpose

The purpose of this project was to test a full-scale bridge girder fabricated with lightweight, self-consolidating concrete (LWSCC), and compare the measured shear strength to existing shear design methods. Additional data are required due to the fact that LWSCC is a new material and the structural behavior is not widely known. Lightweight concrete and self-consolidating concrete each have a characteristic that can lower the shear strength of prestressed members. When combined, this type of concrete may have a reduced contribution to the overall shear strength of the member. Because of these uncertainties in the calculation of the concrete contribution to the shear strength, one PCBT-53 girder fabricated with LWSCC was tested in the Virginia Tech Structures and Materials laboratory to better understand the behavior of the concrete in shear.

Objectives

This project had two specific objectives. The first was to experimentally determine and record data to quantify the shear strength of one lightweight, self-consolidating concrete bridge girder. One PCBT-53 girder fabricated with LWSCC and a composite cast-in-place lightweight concrete deck was tested to determine loads under which the girder exhibited first cracks, web shear cracks, and flexure-shear cracks. The second goal was to compare the measured shear strength to existing shear design methods to determine if they are adequate for the design of members fabricated with LWSCC.

Scope

The scope of this project is limited to the single PCBT-53 girder. The girder cross-section, reinforcement schedule, and shear design are limited to a single beam. This project does not include a parametric study involving other cross sections, varying design parameters, or alteration of the concrete mix design. The measured shear strength is compared to the shear design method in the AASHTO Standard Specifications for Highway Bridges (2002), the Sectional Design Model from the AASHTO LRFD Bridge Design Specifications (2006), and the Simplified Method presented in NCHRP Report 549 (2007). In addition, a strut-and-tie model approach is investigated to determine strength for one of the two shear tests.

METHODS

Girder Design, Fabrication, and Instrumentation

Introduction

This section provides details on the girder design, girder reinforcement, girder fabrication, and instrumentation. A single 65 ft long PCBT-53 girder was fabricated at Bayshore

Concrete Products Corporation (Bayshore), and then transported to be tested at the Virginia Tech Structures and Materials Laboratory. A timeline for the beam fabrication and testing is as follows:

1. PCBT-53 strands stressed on October 20, 2006, following which instrumentation was installed on the reinforcement skeleton on October 23, 2006.
2. Concrete was poured on October 24, 2006, and steam cured overnight for approximately 16 hours.
3. Strands were cut and the prestress was transferred to the beam on October 25, 2006.
4. The girder was shipped to the Virginia Tech Structures and Materials Laboratory and arrived on December 13, 2006. At this time, the concrete was well over 28-days old.
5. The composite deck formwork was completed on December 21, 2006. The deck concrete was poured on January 9, 2007, and then cured for 14 days.
6. Deck formwork was removed on January 15, 2007, and the deck passed 28-days in age on February 6, 2007.
7. Instrumentation was installed on the beam and composite deck prior to the initial shear test, which took place on February 20, 2007.
8. A subsequent shear test on the same end of the beam with different loading conditions took place on March 1, 2007.
9. The girder was moved and the support conditions altered for a flexure-shear test, and the beam was again instrumented prior to testing.
10. The girder was tested for an anticipated flexure-shear failure on March 27, 2007. The beam was then re-loaded on March 29, 2007, and loaded to ultimate failure.

Girder Design and Fabrication

The PCBT-53 girder reinforcement was designed in two unique stages. First, the anchorage zones were designed for a companion project that was investigating the behavior and design of anchorage zones (beam ends) in prestressed concrete bridge girders, as documented by Crispino (2007). The two ends of the beam are referred to as the north end (12 ksi working stress in the anchorage zone) and the south end (18 ksi working stress in the anchorage zone) throughout the remainder of this report. Secondly, the remaining vertical shear and horizontal shear reinforcement was designed for the shear testing of the PCBT-53. The vertical shear design of the beam, in the critical area for the shear test, was based on the American Association of State Highway Transportation Officials (AASHTO) LRFD Specifications (2006) with an assumed angle of inclination of diagonal compressive stresses of 38 to 39 degrees. The horizontal shear reinforcement was checked after the vertical shear reinforcement design was complete. The majority of the vertical shear reinforcement extended out of the top flange of the beam and into mid-depth of the deck for composite action between the girder and deck. Each vertical shear stirrup that extended out of the beam had an additional horizontal shear stirrup attached as shown in Figure 1. These additional stirrups extended out of the girder at the edges of the top flange and continued into the deck.

The final 65 ft PCBT-53 girder cross section included 32 pretensioned 0.5 in diameter, 270 ksi, 7-wire low relaxation strands. The nominal area for these strands is 0.153 in^2. Six of the strands were harped at the end of the girder. The harping points for these strands were located 30 in from each side of the center line of the girder. There were four additional courtesy strands located in the top flange of the beam. These strands allowed the vertical and horizontal shear reinforcement to be tied off and were each stressed to 4 kips. The 32 main strands were stressed to 75 percent of the 270 ksi ultimate stress (31 kips each). The girder itself was designed using a specified compressive strength of 8000 psi, and the release strength of the

concrete used in the design was 5,500 psi. Since the beam was fabricated with lightweight concrete, the design unit weight was assumed to be 120 pcf. Beam details including cross section views, side elevations, and a final composite cross section are shown in Figure 1 through Figure 4. Vertical shear stirrups throughout the length of the girder consisted of a double leg No. 5 bar, bent at 180° with a standard hook on the bottom. Anchorage zone confinement reinforcement was made up of two pieces spliced together, enclosing all of the straight strands at the ends of the beam. For horizontal shear strength, the 180° bend bars extended out of the beam and additional No. 5 U-stirrups were added in the top flange. The stirrup geometry is presented in Figure 1. Stirrup spacing is shown in Figure 2 and Figure 3 for the north end and the south end of the beam, respectively. Figure 4 shows the top portion of the composite cross section including the horizontal shear reinforcement. Stirrup reinforcing steel material properties are assumed to be those typically used for reinforced concrete design and in accordance with ASTM document A615 (2005). These material properties can be seen in Table 1 for No. 5, Grade 60 rebar, which has a minimum yield strength of 60 ksi.

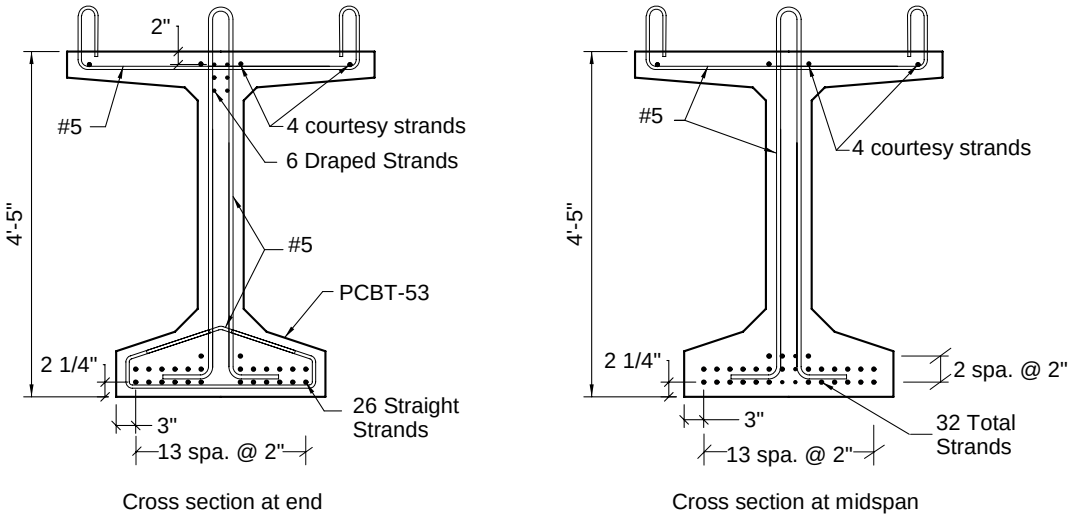

Figure 1. Cross section details of PCBT-53

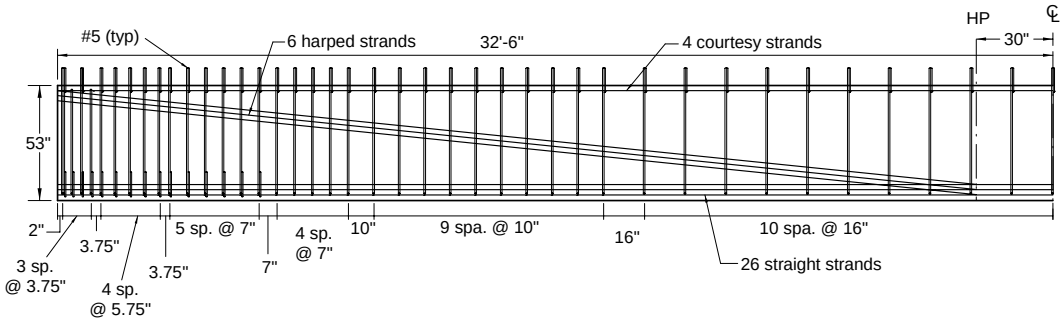

Figure 2. North beam end elevation

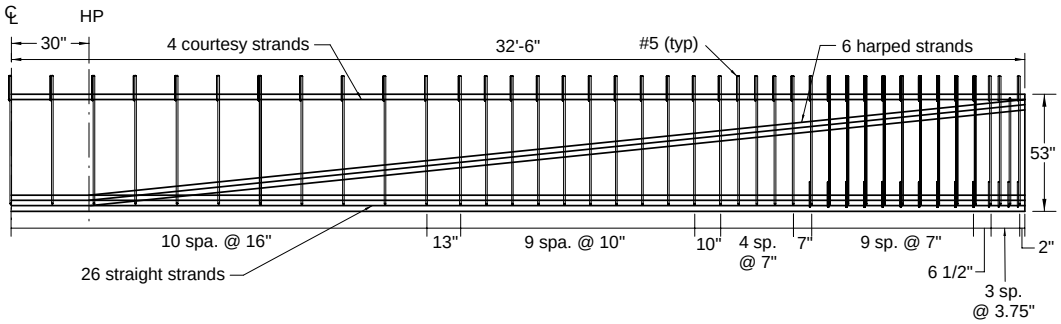

Figure 3. South beam end elevation

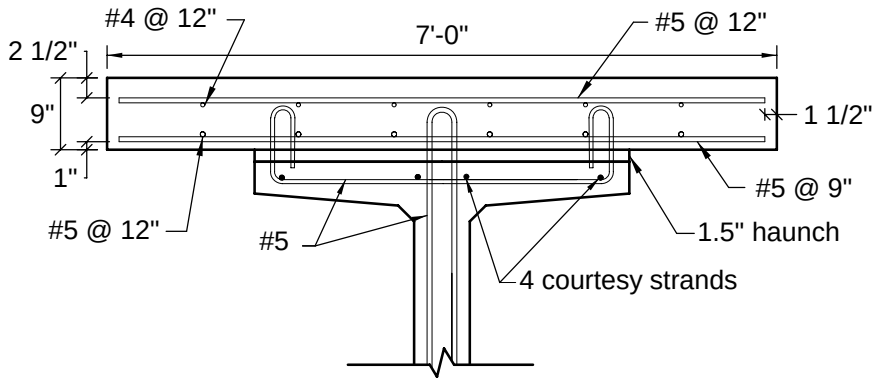

Figure 4. Composite cross section

Table 1. Steel reinforcement design material properties

Diameter of #5 Bar (in)	0.625
Area (in^2)	0.31
Weight (lb/ft)	1.043
Tensile Strength (ksi)	90
Yield Strength (ksi)	60
Modulus of Elasticity (ksi)	29000
Elongation (%)	9

The prestressing strands in this project were those provided by Bayshore, and are a product of the American Spring Wire Corporation (www.americanspringwire.com). Material property testing for strand delivered to Bayshore was conducted by American Spring Wire Corporation and reported to Bayshore via material certification sheets. The results of these tests can be seen in Table 2. The American Society of Testing and Materials (ASTM) document A416 (2005) requires that the minimum yield stress of low relaxation strands should be at least 90 percent of the guaranteed ultimate tensile strength, which is 243 ksi for grade 270 strands. The yield stresses reported by American Spring Wire Corporation are greater than this requirement. ASTM document A416 also requires that the breaking strength should be greater than the guaranteed ultimate tensile strength, and the total elongation should be greater than or equal to 3.5 percent. Values from American Spring Wire Corporation show that all breaking

strengths were greater than the guaranteed ultimate tensile strength and the total elongations of the strands were greater than the 3.5 percent minimum.

Instrumentation was installed at midspan of the rebar cage prior to placing concrete. Two VCE-4200 vibrating wire gages (VWG), manufactured by Geokon (www.geokon.com), were installed on both the bottom straight strands and the top, center courtesy strands. The location of the vibrating wire gages in relation to the entire PCBT-53 cross section can be seen in Figure 5 and Figure 6. Vibrating wire gages, as discussed later, allow for measurement of strain during the pour, cure, and testing. Each vibrating wire gage also contains a thermistor for monitoring temperatures. Small concrete control specimens were also instrumented with vibrating wire gages to monitor the change in strain with no prestress force added to the concrete.

Thermocouples were installed to monitor the temperature of the concrete and formwork during casting, curing, and long-term conditions. The thermocouple locations can be seen in Figure 5 and Figure 6. Data from the VWGs and thermocouples were recorded by a Campbell Scientific CR-23X Micrologger. The data were recorded by the micrologger every 90 minutes except during casting of the beam, casting of the deck, and during testing. The data recording interval was changed to one minute during casting of the beam and testing of the composite system. During casting of the deck, data were recorded every fifteen minutes. These smaller recording windows allowed the researchers to better understand the change in temperature and strain over time in the concrete and strand.

After preparation, the PCBT-53 girder was cast in a single day at Bayshore Concrete Products Corporation. This was a relatively long process because Bayshore had limited experience with casting lightweight, self-consolidating concrete. The mix design of the beam prior to addition of any chemicals at the job site is shown in Table 3. Three ready-mix trucks were rejected by Virginia Department of Transportation personnel who were present to ensure quality and composition of the LWSCC mix. Quality control was ensured when workers took measurements of slump, unit weight, and percent air content. Slump was adjusted during inspection using both regular and high range water reducer. The fresh concrete properties of the LWSCC beam can be seen in Table 4.

Table 2. Prestressing steel material properties

	Diameter (in)	Area (in^2)	Yield Stress (ksi)	Ultimate Stress (ksi)	Elongation (%)	Modulus of Elasticity (ksi)
	0.5035	0.15358	259	285	4.52	29190
	0.5037	0.15358	260	286	5.04	29000
	0.5037	0.15358	256	286	5.04	29060
	0.5035	0.15358	255	282	4.48	28710
	0.5032	0.15281	256	283	4.48	28710
	0.5040	0.15358	255	283	5.00	29050
	0.5030	0.15281	255	281	4.50	29060
	0.5037	0.15358	259	283	4.52	29180
	0.5037	0.15358	257	283	4.52	29110
	0.5032	0.15281	258	284	4.52	29110
	0.5032	0.15281	260	284	4.52	29180
	0.5037	0.15358	262	285	4.54	29060
	0.5035	0.15358	262	285	4.54	29060
	0.5032	0.15281	266	285	4.54	29020
Average	0.5035	0.15331	259	284	4.63	29036
Std Dev	0.0003	0.00038	3.3	1.4	0.2	150

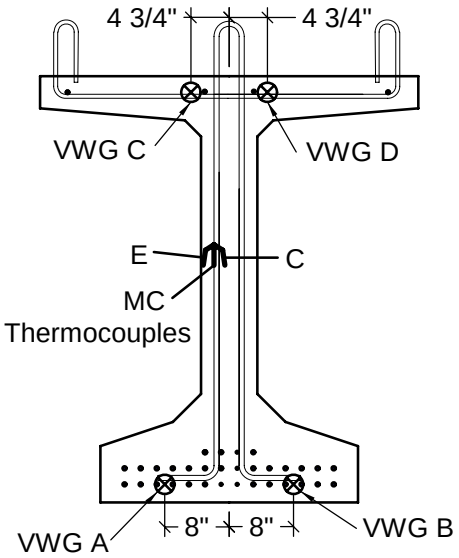

Figure 5. VWG and thermocouple locations

The self-consolidating concrete, as expected, required a minimal amount of external formwork vibration, but workers did provide some internal vibration with pencil vibrators from the top of the formwork. The girder was then subjected to an overnight steam cure after being covered and sealed with blankets. The following morning, an elastic modulus test, a compressive strength test, and a split cylinder test were performed on concrete cylinder samples. Data from these cylinder tests and others can be found in the "Results" section of this report. These cylinders were cured at the same rate and temperature as the beam, and these tests showed that the concrete had already surpassed the target release strength of 5,500 psi. At this time the steam was turned off and the formwork was removed. The concrete test cylinders were also

stripped of their molds and thus were subjected to the same curing conditions as the girder until both the cylinders and girder were transported to the Virginia Tech Structures and Materials Laboratory.

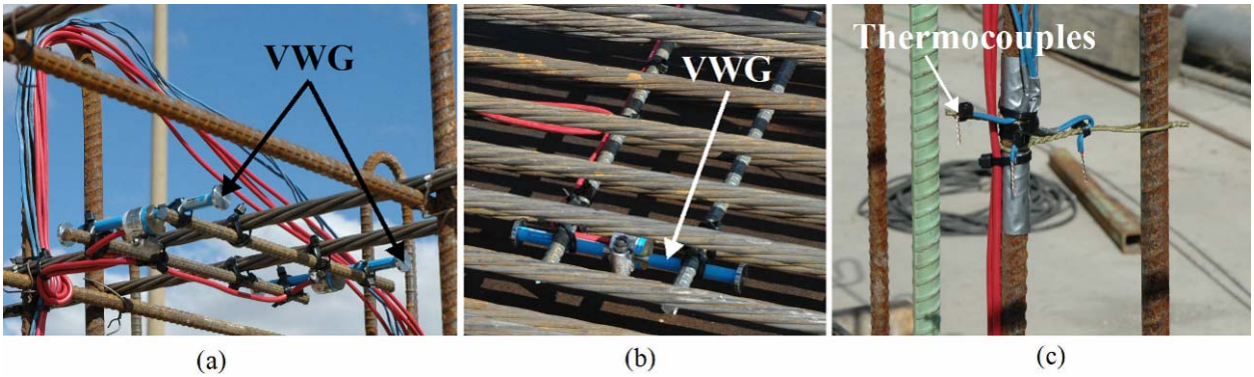

Figure 6. Instrumentation (a) VWG on top strands (b) VWG on bottom strands (c) thermocouples

Table 3. PCBT-53 initial concrete mix design

Component	Initial Mix Design Quantity (per yd^3)
Portland Cement	540 lb
Slag	360 lb
3/4 in Stalite Lightweight Stone	850 lb
Natural Sand	1158 lb
Water	33.5 gal
DCI	3 gal
W/C Ratio	0.31
Target % Air	6

* Note: mixture also has Air Entraining admixture Daravair

Table 4. PCBT-53 fresh concrete properties

Test	Batch 1	Batch 2	Average
Slump Flow (in)	23	20	21.5
Air (%)	4.0	---	4.0
T20 (sec)	7	7	7
Unit weight (lb./$ft.^3$)	120.0	116.8	118.4
Temperature (°F)	56	56	56

Following removal of the formwork, the strands were flame cut with an acetylene torch, starting first with the courtesy strands and the harped strands. Finally, the bottom, straight strands were cut to transfer the prestress force to the beam. The strands were cut simultaneously at both ends of the beam by two workers.

Non-standard lifting devices were used to handle the beam at the Bayshore plant and to unload it from the truck at the laboratory. These lifting devices, as shown in Figure 7, picked the girder up through the top flange using structural steel tubing. This is not the normal way that bridge girders are lifted. Typically, a bundle of prestressing strand is fashioned such that a loop of strand is left exposed for cranes to lift the beams, and the ends of the strand loops extend well into the web of the beam. This LWSCC beam was to be subjected to shear tests at the laboratory in the end region of the beam. Using these atypical lifting devices, no extra strand or stress was put in the test region. The PCBT-53 was lifted initially at Bayshore to test the devices, after which an initial camber measurement was taken. This value and any subsequent measurements that were taken are presented later in this report. The first lift of the beam was successful, and the girder was then transported to the Virginia Tech Structures and Materials Laboratory on December 13, 2006.

Figure 7. Girder lifting device

Upon arrival at Virginia Tech, the beam was lifted off of the delivery truck with tension actuators and the specially fabricated lifting devices. Initial placement of the 65 ft beam resulted in a 63 ft span length measured from center-to-center of each support. Each end of the girder had a 1 ft overhang from the center line of the support beams. The beam was then moved laterally and centered correctly for the initial shear test. Lateral movement of the beam was facilitated by a newly fabricated roller system and low-friction Hilman rollers (www.hilmanrollers.com). The beam delivery and roller system can be seen in Figure 8.

Deck Design, Fabrication, and Instrumentation

Introduction

The final cross section included a composite deck, as seen previously in Figure 4, which was cast at the Virginia Tech Structures and Materials Laboratory with lightweight concrete. The deck had a design compressive strength of 5,000 psi. The deck reinforcement was designed for a fictitious bridge in which the beams were spaced at 9 ft and the deck had a 9 in thickness. For ease of construction and testing at Virginia Tech, the deck was built with only a 7 ft width so that the composite section fit easily between the steel loading frames.

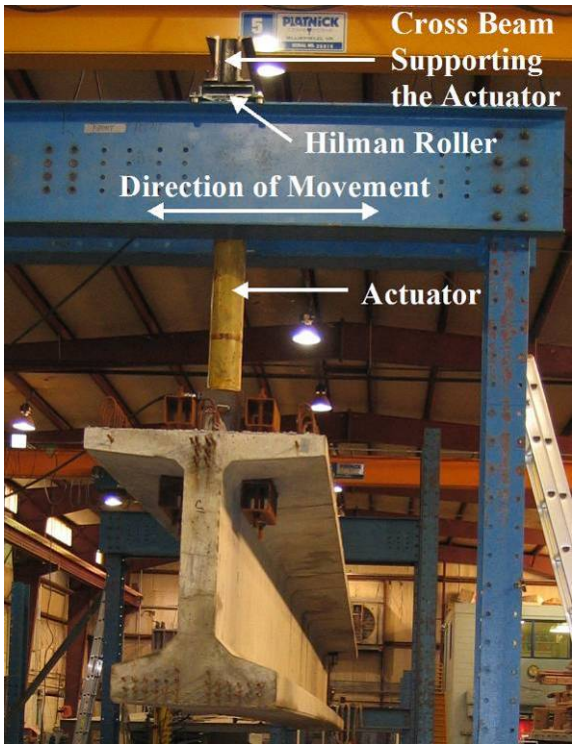

Figure 8. Roller system

Deck Design and Fabrication

Once the beam was set in place for the first test, formwork for the 9 in thick deck was installed as shown in Figure 9. The formwork was designed and installed following the same procedures used by most contractors, with the deck forms supported by the girders. The formwork was installed in 8 ft sections as this is the typical length of plywood sheets and lumber. Holes, 3/8 in in diameter, were drilled at 16 in on center into the edge of the beam top flange and a 3/8 in by 3 ¾ in long Powers Power Stud anchor (labeled F) was driven into each hole. These anchors were then bolted through the vertical 2x6 (labeled H) to support the formwork at the wood-concrete interface. Additional vertical formwork support was provided by 2x4 kickers (labeled K), spaced at 2 ft on center, running from the outer edge of the deck to the bottom bulb of the girder.

Pencil rods with a 1/4 in diameter (labeled B) were installed to run transversely across the 9 in thick deck to provide lateral support from the concrete pressure. Additional longitudinal support was provided for the formwork when two adjoining 8 ft sections were connected. At this connection, the two 2x4 studs (labeled D) on the 9 in tall deck sections were screwed together, and the two 2x6 sections (labeled I) at the ends of the deck formwork were fastened together using two 1/2 in threaded rods. The two ends of the deck were closed to complete the formwork using 3/4 in Plyform plywood and all of the formwork was sealed to protect against water leakage. In addition, PVC tubing was installed to extend the holes for the girder lifting devices so that the composite section could be moved when testing was complete.

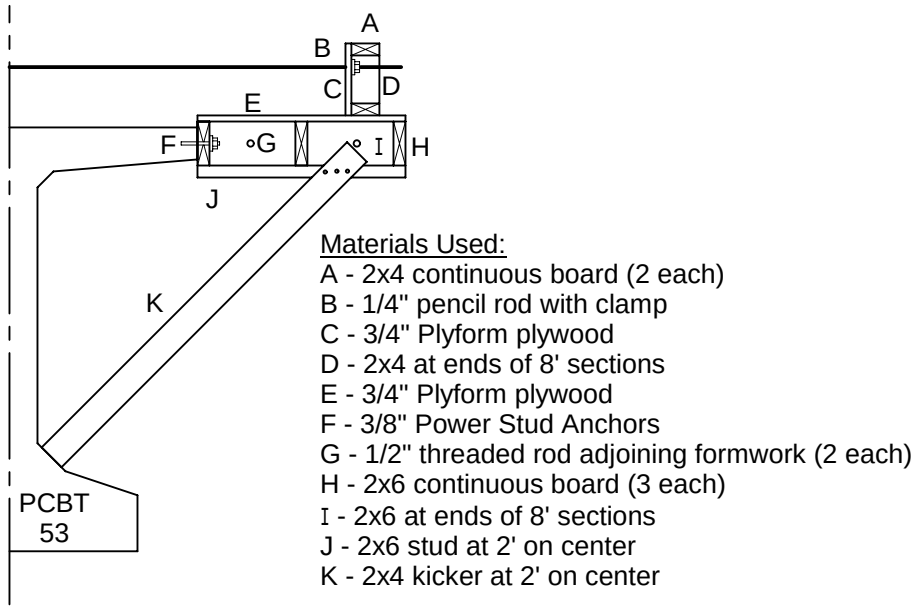

Figure 9. Deck formwork

After sealing the formwork, the reinforcing steel for the deck was placed. The deck reinforcing steel was supported off of low and high chairs and tied together with wire ties. The longitudinal rebar of the deck required splices since the beam was 65 ft long and rebar for this project came in 20 ft sections. These splices were designed as 20 in compression splices and placed as shown in Figure 10. All of the rebar splices are offset to avoid putting a spliced section of reinforcement directly below a loading point for either test one or test two.

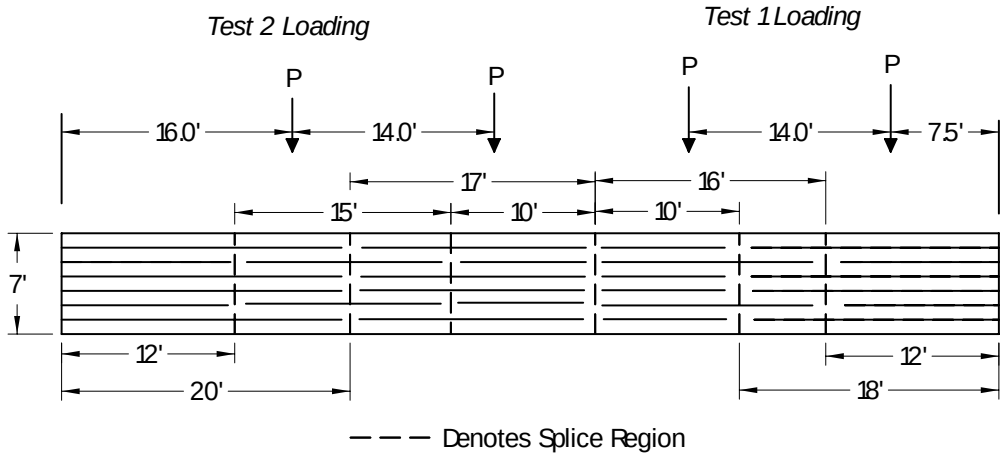

Figure 10. Deck longitudinal reinforcement splices

The mix design for the deck concrete was designed and tested at the Virginia Tech Structures and Materials Lab. Two trial batches of lightweight concrete, as seen in Table 5, were designed and tested before the deck was cast. The first trial batch had too much water, but it did achieve the design compressive strength of 5,000 psi. The second trial mix was redesigned to have less water, cement, and fly ash while having more fine aggregate and lightweight stone. The lightweight stone was a 3/4 in aggregate made by the Carolina Stalite Company of

Salisbury, North Carolina (www.stalite.com). The lightweight aggregate was moisture conditioned according to Stalite's recommendations for handling and batching their expanded slate aggregate. It is important to immerse or sprinkle lightweight aggregate in water for an extended amount of time before using it in concrete batches due to the cellular nature of these aggregates. The absorption rate in lightweight aggregates is higher than most normal weight aggregates. If the stone is not fully moisture conditioned a loss of slump during mixing and delivery of the concrete can occur because water is absorbed during mixing and transportation. Based on cylinder specimen testing, the second mix achieved the desired strength while having the same water to cementitious material ratio as the first mix. Therefore, it was deemed that this mix was to be used for the composite deck.

Prior to pouring the deck, an additional thermocouple was added to the composite section in the deck concrete. This thermocouple was also placed at the center line of the girder and at mid-height of the deck (4.5 in from the top of the deck). This thermocouple was used to track the temperature change of the deck concrete during casting, curing, and testing.

The lightweight concrete for the deck was batched at a nearby ready mix plant and delivered to the lab in three separate batches. The retarder admixture was added to the mix at the plant. The high range water reducing admixture (super plasticizer) was shipped separately and added on site for adjustment of the slump. The local ready mix plant also typically withholds water from every mix to ensure that the desired slump can be achieved at the job site with the addition of water. For the composite deck, water was added to achieve an initial slump of 4 in and then the high range water reducing admixture was added to achieve the desired slump between 7 and 8 in for a good, workable concrete. Fresh concrete properties from the three delivery trucks can be seen in Table 6.

During the casting of the deck, as seen in Figure 11, concrete was transported from the ready mix delivery truck to the girder by an overhead crane and 1 cy concrete bucket. On top of the girder and deck, pencil vibration was used to consolidate the concrete in the formwork. After all the formwork was filled with concrete, the top surface of the deck was bull floated and finished using hand trowels. The top surface of the deck and approximately half of the formwork was covered with water-soaked burlap and plastic sheeting following completion of all concrete finishing. This type of moist cure was applied to the deck for 14 days, even after the formwork was removed at seven days. The State of Virginia department of transportation typically requires a 14 day moist cure for new bridge and deck construction. Concrete cylinder specimens were also cast and subjected to the same curing conditions as the deck itself. The cylinder molds were stripped the same day the deck formwork was removed. The deck was allowed to cure beyond 28 days before the first test was started.

Preparation for testing of the girder started once the 14-day moist cure was completed. All anchors that were driven into the beam were ground off to be flush with the concrete. No cracking from the weight of the deck was visible where anchors were embedded in the concrete. The 32 prestressing strands and the four courtesy strands were ground down so that the frayed ends were no longer evident and approximately 2 in of strand was left protruding from the concrete.

Table 5. Deck concrete mix design

Component	Initial Mix Design Quantity (per yd^3)	Revised Mix Design Quantity (per yd^3)
Portland Cement	588 lb	520 lb
Fly Ash	147 lb	130 lb
Natural Sand	1111 lb	1216 lb
3/4 in Lightweight Stone	950 lb	979 lb
Water	35.5 gal	31.2 gal
Air Entrainment	1 oz	0 oz
Retarder	4 oz	13 oz
Super Plasticizer	0 oz	20 oz
W/C Ratio	0.4	0.4
Target % Air	3-5 %	3-5 %
Target Slump	5-7 in	5-7 in

Table 6. Deck fresh concrete properties

Test	Batch 1	Batch 2	Batch 3	Average
Final Slump (in)	8.5	8.25	8	8.25
Air (%)	3.0	3.25	---	3.125
Unit weight ($lb./ft.^3$)	125.0	123.0	---	124.0

Figure 11. Deck concrete placement

Testing Setup, Procedure, and Instrumentation

Testing Setup and Instrumentation

All tests were performed using a simply supported span and two point loads, which simulated the AASHTO design truck rear axle spacing, as shown in Figure 12. The point loads were 14 ft apart and applied directly to the composite deck using a simulated tire patch. The AASHTO tire patch, which is specified in Article 3.6.1.2.5 in the LRFD Specifications (2006) and in Article 3.30 in the Standard Specifications (2002) as the contact area of a wheel representing either one or two tires, is assumed to be a rectangle with a width of 20 in and a length of 10 in It is also assumed that this tire patch receives a uniformly distributed pressure over the entire area. For these tests, a tire patch was created using steel reinforced neoprene pads that were 24 in long, 10 in wide, and 2 in thick. This pad was not exactly the same dimensions as AASHTO specifies, but was deemed adequate because it was already owned by the laboratory and thus, there was no need to design and purchase a new reinforced neoprene pad. In addition, the researchers believe that the slight deviation from the specified AASHTO tire patch dimensions did not influence the test results.

Each test setup consisted of a simply supported beam and two load frames representing the AASHTO truck rear axle spacing. To achieve the simply supported, pin-and-roller support conditions, a single, solid, 4 in thick steel cylinder that was the full width of the bottom bulb (32 in) was used to support each end of the beam. Because this steel cylinder would only touch the beam across a single line, a steel plate was used between the roller and the beam to distribute the load. This steel plate was 14 in long and 32 in wide, hence the entire bottom bulb of the girder was supported through this plate to the steel cylinders. Figure 13 depicts both the roller and pin support conditions with the additional steel plate in place to distribute the load. The girder and rollers sat on steel W-shapes with stiffeners welded under the top flange where the beam rested on the support. The steel beams were W14x90 shapes.

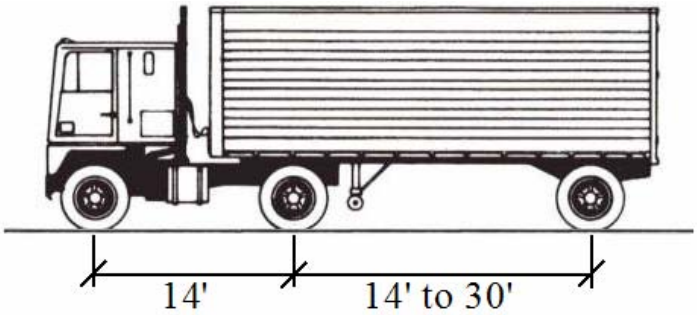

Figure 12. AASHTO design truck

A hydraulic actuator was mounted to a steel load frame to apply load at each point. These load frames were bolted to the reaction floor to ensure a closed loading system. These actuators applied a single point load through a series of plates increasing in size and ultimately sitting on the neoprene tire patch. The actuators were connected to an electric pump in parallel, and the hydraulic fluid pressure was monitored during testing.

Figure 13. Beam end support conditions

The applied load from each actuator was monitored during two of the tests using individual load cells. The remaining tests only used the higher capacity load cell to measure the applied load and an assumption was made that the loads were equal during the test and subsequent analysis. For this reason, a comparison was done using load vs. displacement plots to determine if the percent difference in load reported between the two load cells was significant. Figure 14 and Figure 15 show a comparison of the two load cell values as reported at different displacements. A typical percent difference was in the range of 1.5 to 1.8 percent. The maximum percent difference, as evident in the initial flexure-shear test, was approximately 3.4 percent. Based on these small percent differences, the researchers felt that the assumption to set the applied loads equal in both actuators for data analysis was not unconservative. In addition, the researchers believe that the slight difference should not influence the test results.

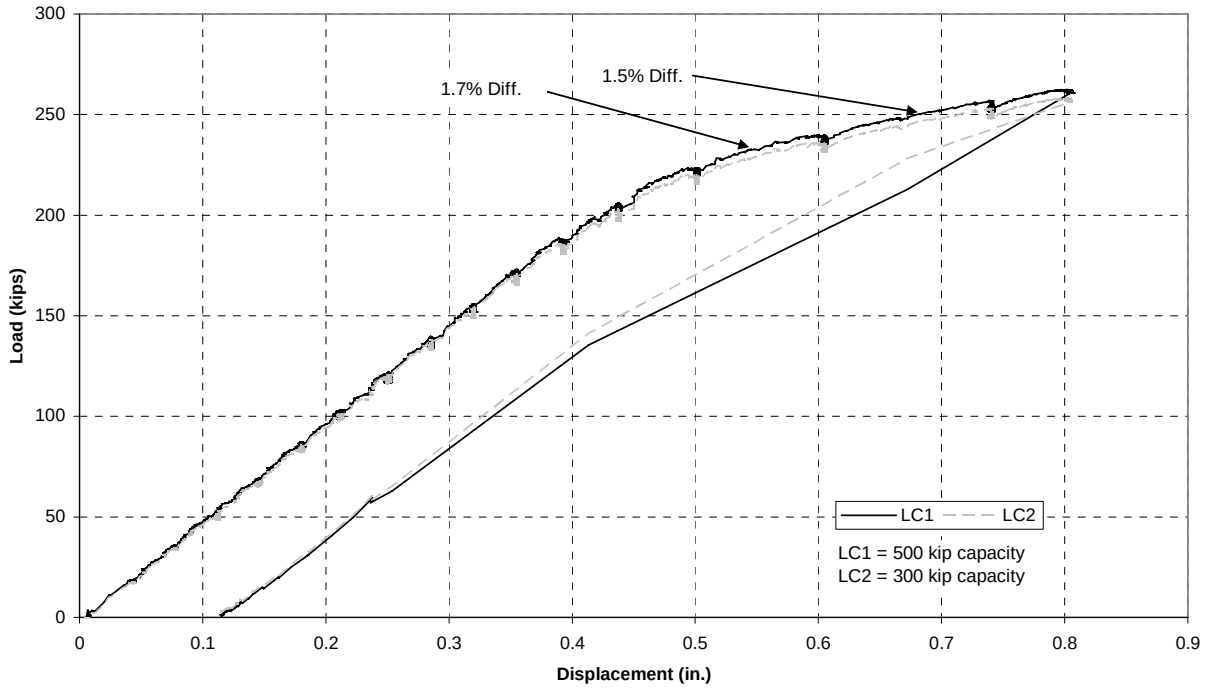

Figure 14. Shear test #1 load cell comparison

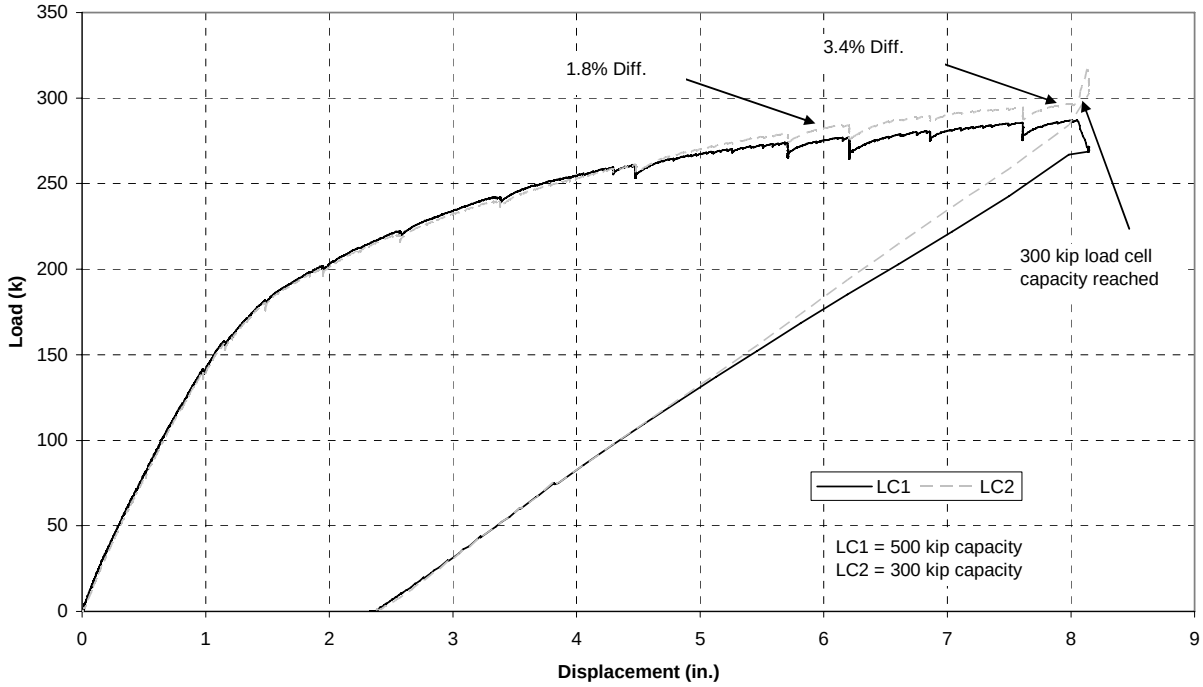

Figure 15. Flexure-shear test #1 load cell comparison

Several different kinds of instrumentation were used to monitor load, deflection, strain, and strand slip during each test. As previously discussed, four vibrating wire gages were installed within the beam to monitor prestress loss, temperature change, and curvature. This was achieved by recording the change in strain over time. A load cell was used under each individual actuator to monitor load, with one load cell having a 500 kip capacity while the other had a 300 kip capacity. The load cells were calibrated before the testing began and were shown to exhibit a linear relationship between load and voltage to their specified capacity. Deflection was measured at various points under the girder during testing using displacement transducers (referred to as wire pots for the remainder of the report) manufactured by Celesco Transducer Products, Inc. (www.celesco.com). These wire pots were located directly below each loading point and below midspan of the girder. The wire pots measured deflection to an accuracy of 0.01 in and had a stroke of approximately 10 in

Strain was measured in two different ways at two different parts of the composite system. During the first test of the beam, concrete surface strains were measured to determine when and where the first crack initiated in the bottom bulb using a detachable mechanical strain gage (DEMEC) and surface mounted gage points manufactured by Mayes Instruments Limited, from England (www.mayes.co.uk). The DEMEC strain gage has a gage length of 200 mm (roughly 7 7/8 in) and measures changes in strain between the surface mounted points to an accuracy of ± 5 με. The DEMEC strain gage apparatus consists of a main beam with two conical locating points, one fixed and the other able to pivot on a knife edge. Figure 16 shows a top view and a side view of the DEMEC gage apparatus; the main beam, fixed locating point, and pivoting locating point are visible in the figure. The locating points are positioned in the surface gage points that are stainless steel discs attached to the girder with a five minute epoxy. Movement of the pivoting point is measured by the dial gage located on the main beam, and reported by the digital readout. The stainless steel discs were affixed to each side of the girder at the lowest level of

prestressing strands, directly below the point of maximum applied moment created by the loading setup, so that five strain measurements could be taken. Figure 17 shows the steel discs affixed to the side of the girder. The first flexural crack was monitored and observed through the use of these strain readings and a plot of load vs. strain. When the plot became nonlinear, the beam was visually inspected for cracking to determine if a flexural crack was present.

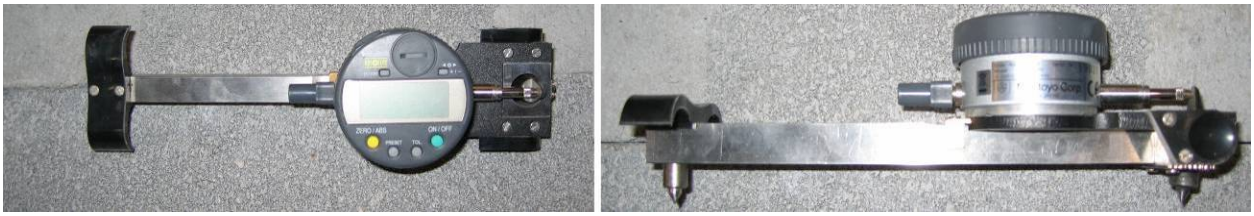

Figure 16. DEMEC gage

Secondly, strain was measured at the extreme compression fiber of the composite system with surface mounted, resistance-based strain gages produced by Vishay (www.vishay.com). Each strain gage had a gage length of 4 in so that the gage gave an average strain across the mortar paste and the 3/4 in coarse aggregate in the deck concrete. These strain gages were placed 6 in from the outer edge of the deck and 6 in from the bearing pad. Figure 18 shows the locations of the compressive fiber strain gages in plan view.

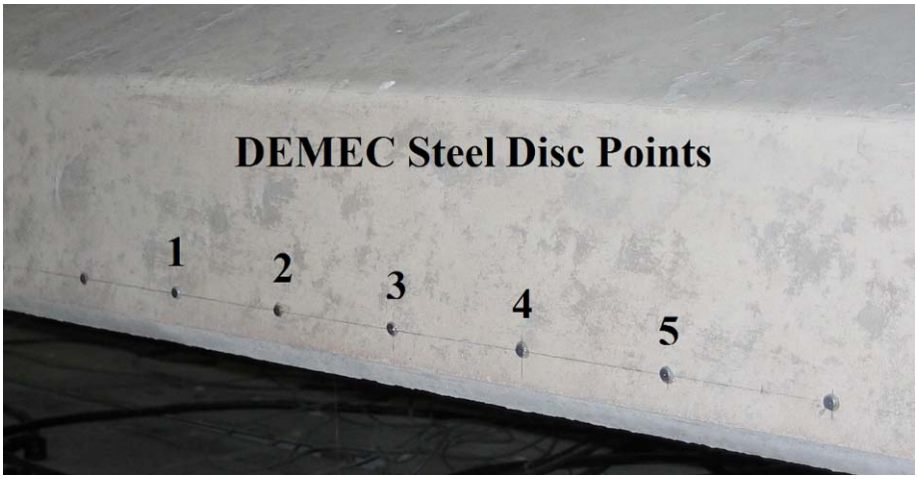

Figure 17. DEMEC steel disc affixed to the girder

Finally, strand slip was measured on four of the prestressed strands along the bottom row. This enabled the researchers to determine if a development length failure took place. Strand slip was monitored using linear variable differential transformers (LVDT), produced by Trans-Tek Inc., of Ellington, Connecticut (www.transtekinc.com). The LVDTs have a total plunger range of approximately 0.15 in and were calibrated to measure movement as small as one thousandth of an inch. Each LVDT was fastened to the appropriate strand using a small bracket fabricated at Virginia Tech. The spring loaded spindle touched the face of the end of the girder itself and detected movement of the strand relative to the end of the beam. If the strand slipped inward, the LVDT spindle would retract inward yielding a displacement measurement. Figure 19 (b) and (c) show how and where (triangles represent strands with LVDTs) each of the four LVDTs were

mounted to monitor strand slip. The other 22 strands (not including the harped strands) were marked 1 in from the face of the concrete with a piece of duct tape as shown in Figure 19 (a) to physically record slip with a ruler.

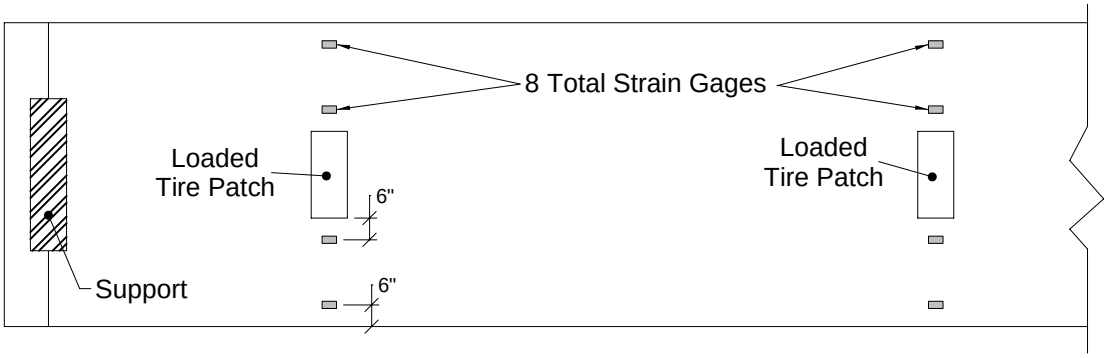

Figure 18. Strain gage plan view

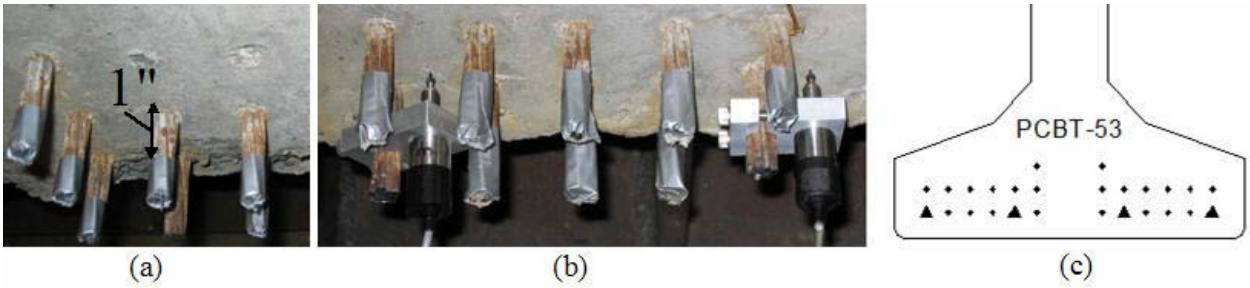

Figure 19. Strand slip (a) duct-taped strands (b) LVDTs on strands (c) location of LVDTs

Data from each test were collected with a Vishay Measurements System 5000 scanner and Strain Smart 5000 data acquisition software installed on the laboratory computer. Data were collected at a sample rate of one second for each test setup. Prior to testing, all instrumentation installed on the girder was directly calibrated within this system. The accompanying data files from Strain Smart 5000 were reduced into Microsoft Excel files for further analysis following the completion of each test.

Web Shear Strength Testing

The focus of the first test on the beam and the initial test setup was to collect data pertaining to the predicted web shear strength of the girder. The 65 ft girder was simply supported with a span of 63 ft and a 1 ft overhang past the center line of each support. The two load frames were placed at a distance of 7.5 ft and 21.5 ft from the south end of the beam. The support conditions were set up to allow for the pinned end to be the tested end of the beam and the roller end to be the non-tested end of the beam. The test setup, load placement, and instrumentation locations are shown in Figure 20.

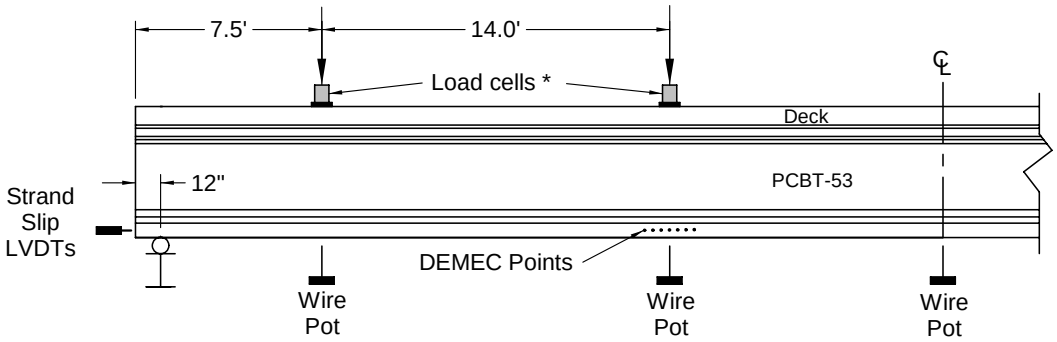

* Strain gages transversely linear with load cells

Figure 20. Shear test #1 setup and instrumentation

During this initial test, the load was increased in 20 kip increments until the DEMEC plot of load vs. strain became nonlinear and visible flexural cracks were detected. From this point on the DEMEC plot was not used and cracks were marked after each load increment of 20 kips was achieved. As this test proceeded, the capacity of the 300 kip load cell was reached, and the test was halted for a few minutes while this load cell was taken out of the overall setup. The test was then continued uninterrupted back up to the 300 kip per actuator limit and beyond, with the 500 kip capacity load cell still in place.

During the testing process a few different setbacks occurred. First, as the test was approaching the limiting maximum load, as controlled by the steel loading frame bolted connections, the researchers were unsure about the accuracy of their load when comparing the load cell values to the pressure gage in line with the actuators. The load cells had been calibrated with the Satec universal test machine in the Virginia Tech Structures and Materials Laboratory, which was later found to be out of calibration. This was a minor setback as the load cells were re-calibrated on a different universal testing machine in the laboratory and the loads from the previous loading were linearly scaled to be accurate.

Testing was again started after the load cells had been re-calibrated. During this re-calibrated test, the 300 kip capacity load cell was not used due to the fact that it would have to be taken out of the setup when loads exceeded 300 kips, which was expected. Load was applied continuously until 290 kips was reached on each actuator, after which load was applied in 10 kip increments and new cracks were marked.

The second setback occurred after the load cells had been re-calibrated. The maximum available load as limited by the steel loading frame was again reached during the testing of the beam. Unfortunately, this loading configuration with actuators located at 7.5 ft and 21.5 ft from the end of the beam did not produce a high enough shear force at the end of the beam to initiate the desired failure. To resolve this problem a second shear test was planned on the same end of the beam.

The focus of the second shear test on the beam was the same as the first, to collect data pertaining to the predicted web shear failure. The 65 ft girder was still simply supported with a span of 63 ft and a 1 ft overhang past the center line of each support. The two load frames were then moved and placed at a distance of 7.5 ft and 10.5 ft from the south end of the beam. The

test setup, load placement, and instrumentation used are shown in Figure 21. This test was started and proceeded without use of the 300 kip capacity load cell due to the fact that it would have to be taken out of the setup when loads exceeded 300 kips, which was expected. The test was uninterrupted beyond 300 kips per actuator with the 500 kip capacity load cell in place. Load was applied continuously until 170 kips was reached on each actuator, after which load was applied in 20 kip increments and new cracks were marked. After the load per actuator reached 250 kips, the load was increased to 290 kips and then in 20 kip increments until 330 kips per actuator was achieved. Beyond 330 kips, the load was increased at 10 kip increments until an ultimate load of 353 kips was reached.

The researchers believe that this test setup came close to reaching the ultimate shear failure desired because there was clear evidence of concrete spalling in the web of the PCBT-53. Again, the ultimate strength of the steel load frame bolted connections was the limiting case. The researchers believe that if approximately 5 to 10 kips more could have been applied, the web of the girder would have become more completely crushed. McGowan (2007) states that during tests of two normal weight, self-consolidating PCBT-45 bridge girders it was observed that full compression failure occurs soon after evidence of concrete spalling in the web is detected.

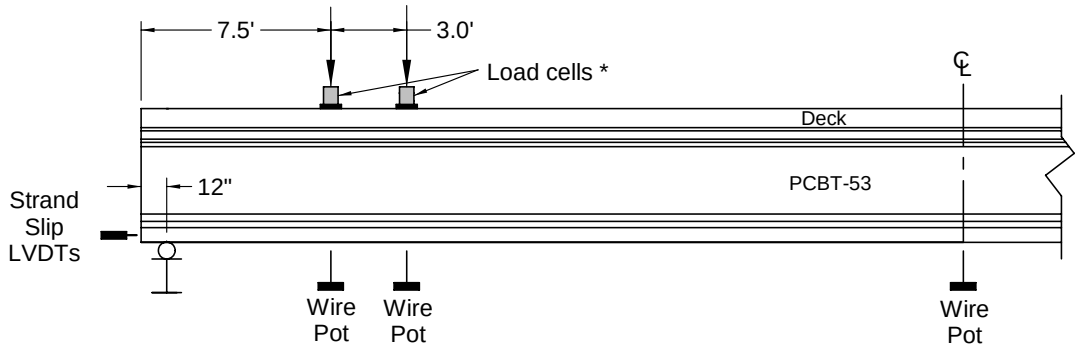

* Strain gages were not moved from shear test #1
(they are transversely at 7.5' and 21.5' from the end)

Figure 21. Shear test #2 setup and instrumentation

Flexure-Shear Strength Testing

The focus of the third and final test on the beam was to collect data pertaining to the predicted flexure-shear failure. The 65 ft girder was moved longitudinally after conclusion of the shear test on the south end of the beam, by Abbott Rigging, Inc. of Rocky Mount, VA. This resulted in a simply supported span of 59 ft. This was achieved with a 5 ft overhang past the center line of the support at the south end of the beam and a 1 ft overhang past the center line of the support at the north end of the beam. During the move by Abbott, the support conditions were changed to allow for the pinned end to be the tested end of the beam and the roller end to be the non-tested end of the beam. The two load frames were placed at a distance of 16 ft and 30 ft from the north end of the beam as shown in Figure 22. As this test proceeded, the capacity of the 300 kip load cell was exceeded, and the test was halted for a few minutes while this load cell was removed. This load cell was initially left in during the test to evaluate the accuracy of the two load cells in relation to each other; it allowed for a comparison of how the two loads differed

as the hydraulic pressure was increased. The test was then continued uninterrupted up to the 300 kip per actuator limit and beyond with the 500 kip capacity load cell still in place.

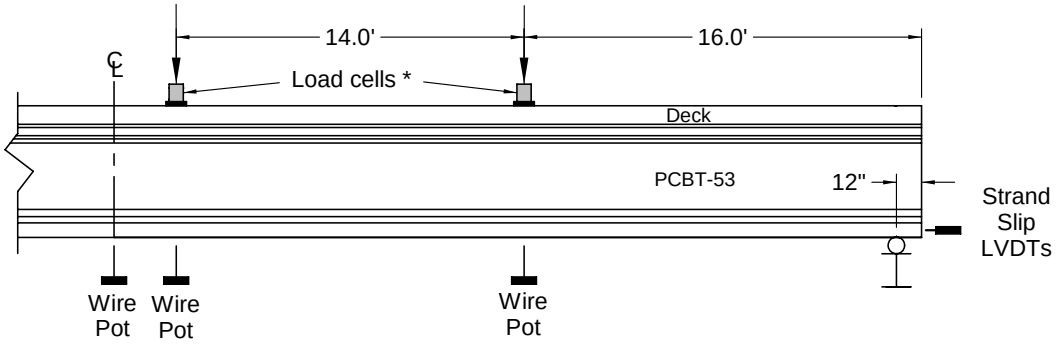

* Strain gages transversely linear with load cells

Figure 22. Flexure-shear test setup and instrumentation

A problem was encountered with this test setup, due to the large deflections occurring due to the flexural dominated loading. The roller supported end of the beam approached the support edge at large loads as shown in Figure 23. To avoid this problem during subsequent tests, steel angles were welded to the steel support beams to prevent the pin from completely rolling off. The girder was then lifted off of the support with hydraulic actuators to re-adjust the pinned support and allow it to roll farther.

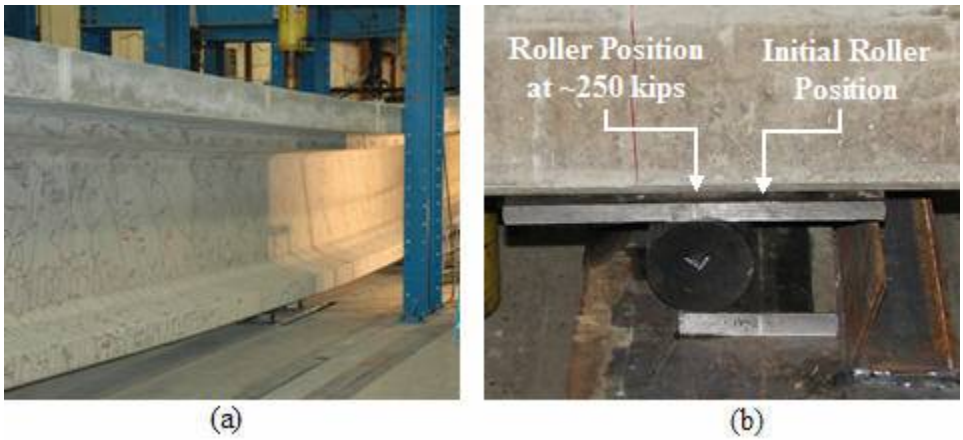

Figure 23. Support condition problems (a) large deflections (b) disconcerting roller position

Once the support conditions were adjusted, the flexure-shear testing was resumed. The PCBT-53 was loaded without using the 300 kip capacity load cell. This allowed the test to run smoothly because loads were expected to exceed 300 kips per actuator near ultimate failure of the beam. Ultimate failure of the girder was achieved during the flexure-shear test as discussed in the "Results" section of this report.

The PCBT-53 was then cut in half to aid in handling and removal of the beam. The concrete was separated using a pneumatic jack hammer and the strands were cut at the centerline of the beam using an acetylene torch. Each half of the beam was then rotated by Abbott Rigging,

Inc. as shown in Figure 24. This configuration allowed for the composite deck to sit directly on the truck bed eliminating any possibility of the section overturning during transportation.

RESULTS

Concrete Material Properties

PCBT-53 Concrete Properties

The PCBT-53 girder was cast in a single day using two batches of LWSCC. The girder was then subjected to an overnight steam cure and the formwork was stripped the following day. Throughout the life of the beam, tests were performed on cylinders stored both at Virginia Tech and at the Virginia Transportation Research Council (VTRC). Typically, two or three cylinders were broken for each type of test at VTRC and usually only one cylinder was broken for each test at Virginia Tech; the average of the results is reported.

Figure 24. Removal of one half of the PCBT-53

Compressive strength tests were done in accordance with ASTM Document C39 (2005), and the results and strength gain plots for the PCBT-53 can be seen in Table 7 and Figure 25. The splitting tensile tests were completed following ASTM Document C496 (2005), and the results and corresponding plot can be seen in Table 8 and Figure 26. Finally, the modulus of elasticity tests were completed following ASTM Document C469 (2005), and the results for the PCBT-53 can be seen in Table 9, and Figure 27 is the corresponding plot.

Table 7. PCBT-53 compressive strength data

Time (days since pour)	VTRC Data (psi)		VT data (psi)		Average f'_c (psi)
	Batch 1 (n)	Batch 2 (n)	Batch 1 (n)	Batch 2 (n)	
1	8,920 (1)	7,750 (2)	-------	-------	8,340
7	8,380 (3)	7,900 (3)	-------	-------	8,140
14	9,280 (3)	8,790 (3)	-------	-------	9,040
28	9,230 (3)	8,690 (3)	-------	-------	8,960
56	9,660 (3)	9,260 (3)	-------	-------	9,460
77 (Deck Poured)	9,630 (2)	-------	10,500 (1)	9,950 (1)	10,000
119 (Shear Test #1)	-------	-------	10,300 (2)	10,800 (1)	10,550
128 (Shear Test #2)	-------	-------	-------	-------	-------
154 (Flexure-shear Test #1)	-------	-------	10,900 (1)	10,500 (1)	10,700
156 (Flexure-shear Test #2)	-------	-------	-------	-------	-------

(n) = the number of cylinders used to determine each value

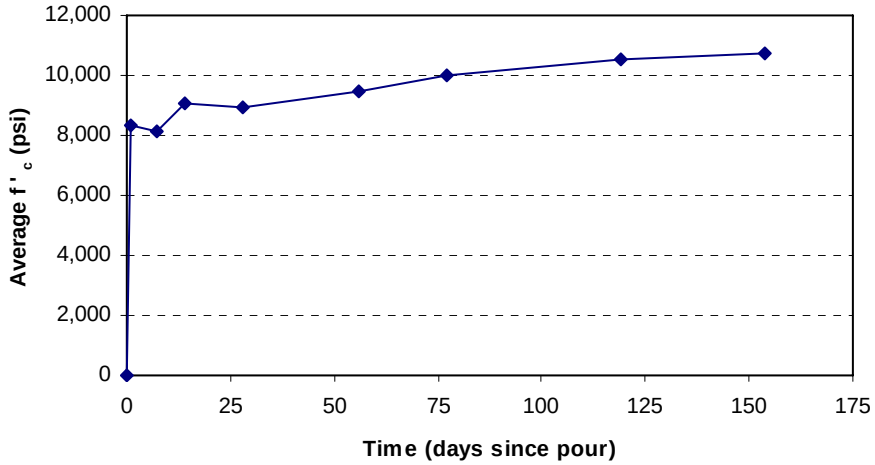

Figure 25. PCBT-53 compressive strength plot

Table 8. PCBT-53 splitting tensile data

Time (days since pour)	VTRC Data (psi)		VT data (psi)		Average f_r (psi)
	Batch 1 (n)	Batch 2 (n)	Batch 1 (n)	Batch 2 (n)	
1	626 (2)	558 (1)	-------	-------	592
7	640 (2)	600 (2)	-------	-------	620
14	670 (2)	665 (2)	-------	-------	668
28	665 (2)	640 (2)	-------	-------	653
56	700 (2)	640 (2)	-------	-------	670
77 (Deck Poured)	-------	-------	875 (1)	696 (1)	786
119 (Shear Test #1)	-------	-------	836 (1)	756 (2)	796
128 (Shear Test #2)	-------	-------	-------	-------	-------
154 (Flexure-shear Test #1)	-------	-------	875 (1)	855 (1)	865
156 (Flexure-shear Test #2)	-------	-------	-------	-------	-------

(n) = the number of cylinders used to determine each value

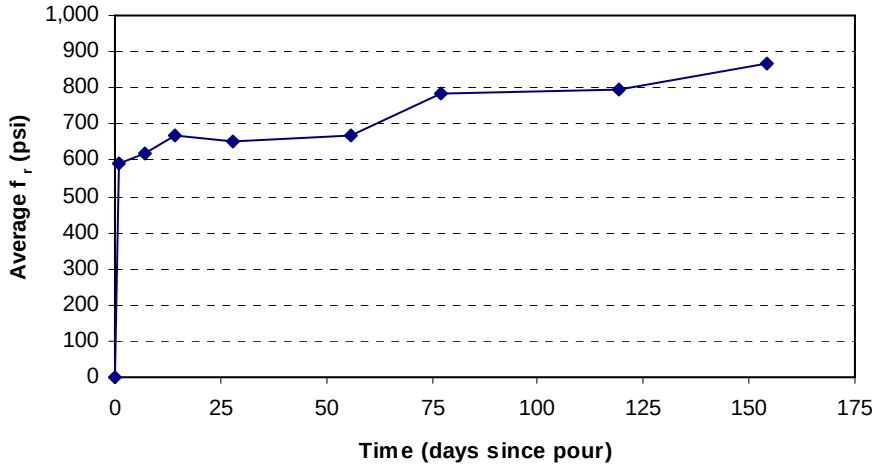

Figure 26. PCBT-53 splitting tensile plot

Table 9. PCBT-53 modulus of elasticity data

Time (days since pour)	VTRC Data (ksi)		VT data (ksi)		Average E_c (ksi)
	Batch 1 (n)	Batch 2 (n)	Batch 1 (n)	Batch 2 (n)	
1	3,640 (1)	3,550 (1)	-------	-------	3,600
7	3,580 (5)	3,510 (5)	-------	-------	3,550
14	3,360 (5)	3,260 (5)	-------	-------	3,310
28	3,450 (5)	-------	-------	-------	3,450
56	3,320 (5)	-------	-------	-------	3,320
77 (Deck Poured)	3,540 (2)	-------	3,130 (1)	3,000 (1)	3,220
90	3,250 (4)	-------	-------	-------	3,250
119 (Shear Test #1)	-------	-------	3,300 (1)	3,250 (1)	3,280
128 (Shear Test #2)	-------	-------	-------	-------	-------
154 (Flexure-shear Test #1)	-------	-------	3,250 (1)	3,140 (1)	3,200
156 (Flexure-shear Test #2)	-------	-------	-------	-------	-------

(n) = the number of cylinders used to determine each value

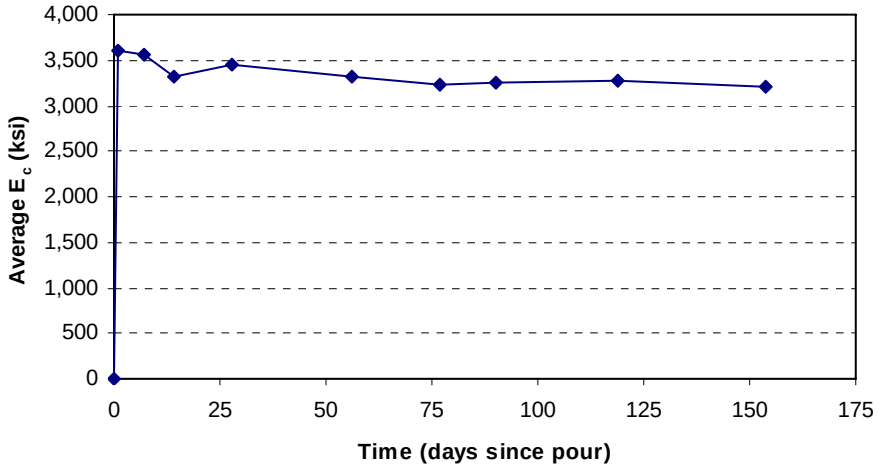

Figure 27. PCBT-53 modulus of elasticity plot

Note that the modulus of elasticity dropped over the life of the beam. This was evident at Virginia Tech during testing of the cylinders in the laboratory. There is also evidence that the modulus of elasticity readings dropped during experiments at VTRC. Figure 27, shows the decline in the elastic modulus, and the first five points on the graph are those corresponding to VTRC tests. The final four points on the plot correspond to Virginia Tech data.

Vibrating wire gages (VWG), each with an internal thermistor, and thermocouples were also installed in the PCBT-53 and the additional shrinkage blocks prior to casting of the concrete to track the change in temperature over time. Time zero in both cases corresponds to the beginning of the concrete pour. From Figure 28 it can be seen that the VWGs reported only one location that exceeded the 71° Celsius maximum temperature limit set by AASHTO LRFD

Construction Specifications (2004) in Article 8.11.3.5. The maximum temperature reported by VWG number three in the top of the beam was approximately 72° Celsius, which is very close to the specified temperature. The VWGs located in the shrinkage specimens were not connected to the Campbell Micrologger until after the steam curing process began due to human error. This leaves a blank in the data recorded by the VWGs in those specimens.

The thermocouple data show that all measured locations in the girder exceeded the maximum allowed temperature as shown in Figure 29. This is interesting to note because of the large difference between these readings and those recorded by the VWGs. The difference in the maximum temperatures shown in Figure 28 and Figure 29 is significant but unexplained. The shrinkage specimens exhibited an interesting change in thermocouple temperature while steam curing. They indicate a sharp increase in temperature correlating with the girder temperatures, but then the blocks lost approximately 20° Celsius over a four to six hour time period. This may be from someone removing the blocks from underneath the steam blankets, or some other type of curing conditions felt by the blocks. The temperature began a sharp decline when the steam was turned off approximately 19 hours after the pour started. At this time the formwork was also removed from the girder and the concrete was exposed to the ambient temperature. A jump in temperature can be seen in both plots two days after casting the concrete. This temperature rise could be due the fact that the station or ambient temperature also saw a sharp increase at that time.

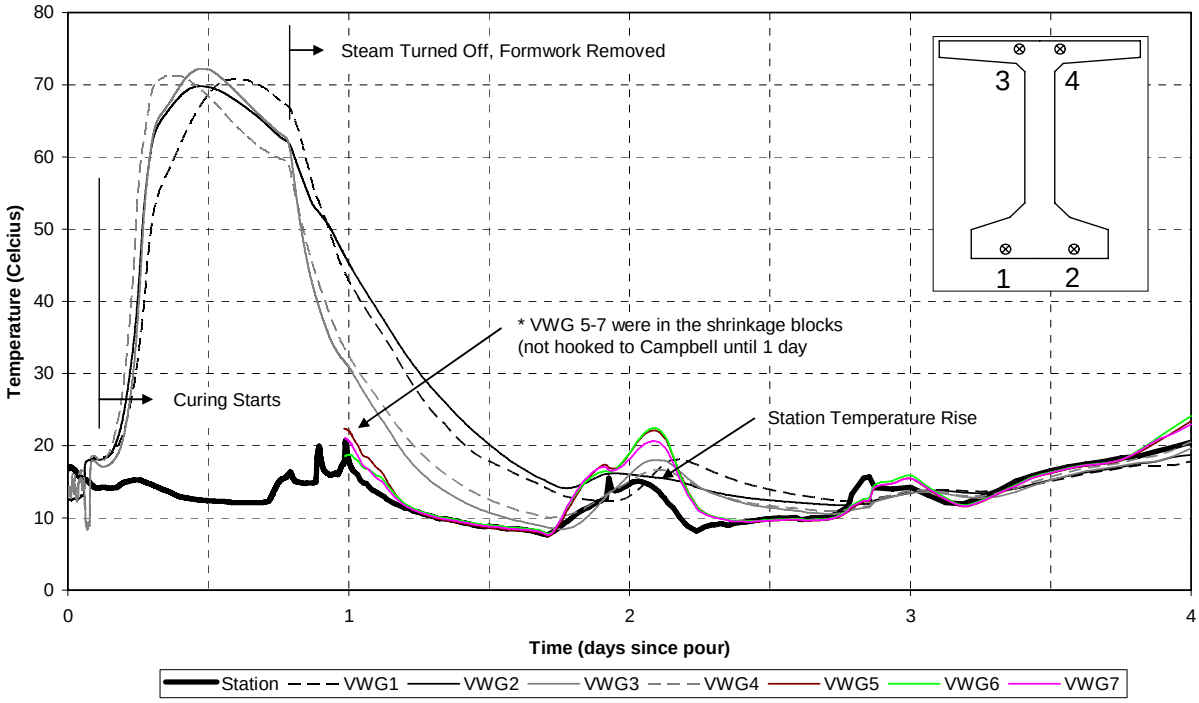

Figure 28. VWG temperature change over time

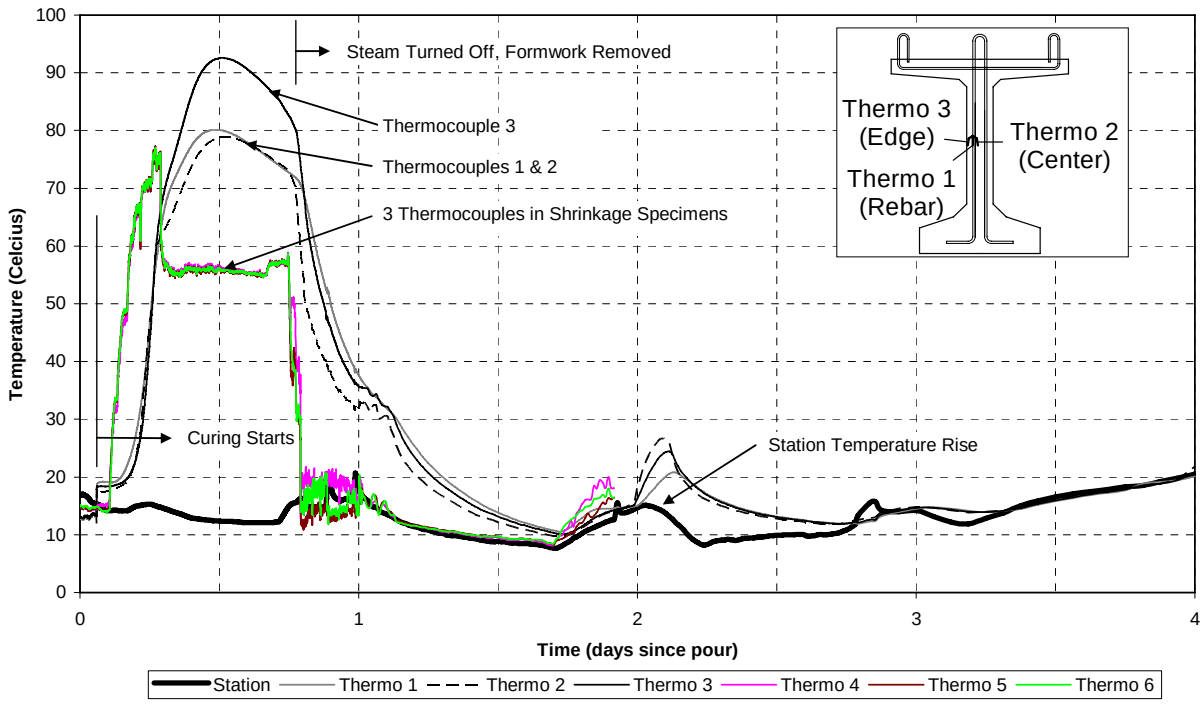

Figure 29. PCBT-53 thermocouple temperature change over time

The vibrating wire gages were also used both in the PCBT-53 and the additional shrinkage specimens to track the change in strain over time. Time zero again corresponds to the beginning of the concrete pour. The strain recorded by the VWGs was adjusted using a recommended temperature correction factor. This factor, using the coefficients of thermal expansion for steel and concrete, is used because the concrete and the tensioned wire within the gage do not expand the same amount. The coefficients of thermal expansion were assumed to be 12.2 and 9.0 με/°C for steel and lightweight concrete, respectively. The coefficient of thermal expansion value for steel was provided by Geokon who manufactured the VWGs, and the coefficient of thermal expansion for lightweight concrete is reported in the AASHTO LRFD Specifications Article 5.4.2.2 (2006). Strain recorded by the vibrating wire gages is shown in Figure 30. Any changes in strain observed should not be due to thermal expansion or contraction since the temperature correction is made for all of the gages. Therefore, the strains observed should most likely be due to shrinkage effects or expansion of the girder concrete from hydration. The VWGs located in the shrinkage specimens were not connected to the Campbell Micrologger until after the steam curing process began due to human error. This leaves a blank, as shown in the plots, in the strain data recorded by the VWGs in those specimens.

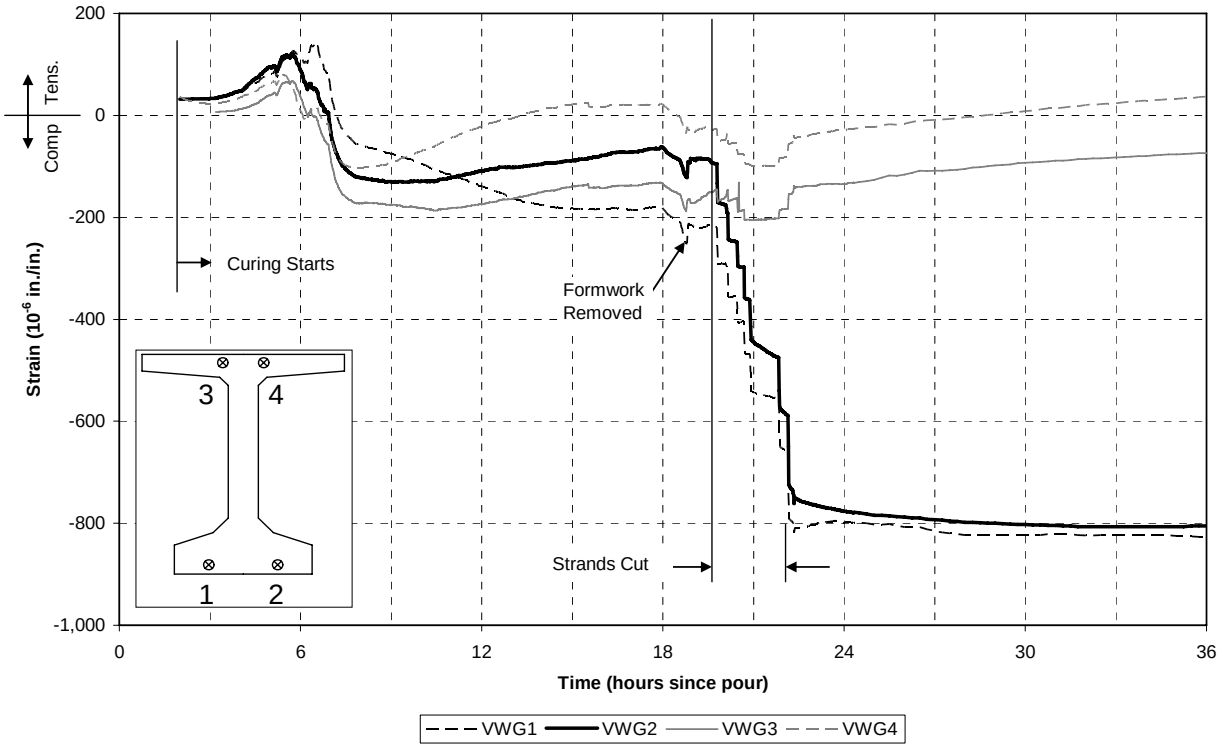

Figure 30. VWG strain over 36 hours since casting

Early age strains and stresses are very difficult to explain due to the rapid change in the concrete's properties such as the modulus of elasticity and the coefficient of thermal expansion. Keeping this in mind, some observations may be made from the strain vs. time data. There is a clear increase in strain around six hours after casting of the PCBT-53, which is subsequently followed by a drop in strain, from tensile to compressive strains. The increase in strain may be attributed to hydration and the expansion of the concrete, while the drop to compressive strain is most likely due to the fact that the formwork is restricting the expansion of the concrete. Another explanation for the drop to compressive strain may be that the contraction is due to autogenous and drying shrinkage. The strain increased (added tensile strain) in three of the four VWGs between nine and 18 hours after curing started. This additional tensile strain can be attributed to restricted contraction in the concrete provided by the pretensioned strands in the beam itself. It is interesting to note that VWG 1, in the bottom of the beam, did not seem to follow this trend.

The formwork was taken off of the beam about 19 hours after curing started. At this time, a small drop in strain in all four of the VWGs occurred. When the strands were flame torched and the prestress force was released onto the beam, the bottom strands (VWG 1 and 2) were subjected to a compressive strain, or drop in strain, and the top strands (VWG 3 and 4) were subjected to a tensile strain, or rise in strain. This is because the prestress is forcing the girder to camber upwards at mid-span.

Deck Concrete Properties

The composite deck was cast on top of the PCBT-53 girder January 9, 2007, in a single day at the Virginia Tech Structures and Materials Laboratory. The deck was subjected to a 14 day moist cure, and the formwork was removed seven days after concrete placement. Throughout the life of the deck, tests were performed on cylinders stored at Virginia Tech. Typically, three cylinders were broken for each type of test (one from each batch), and the average of the results is reported.

Compressive strength tests were done in accordance with ASTM Document C39 (2005), and the results can be seen in Table 10 and in Figure 31. The deck's splitting tensile strength data were collected following ASTM Document C496 (2005), and the results and corresponding plot can be seen in Table 11 and Figure 32, respectively. Finally, the modulus of elasticity tests were completed following ASTM Document C469 (2005), and the results for the deck can be found in both Table 12 and Figure 33.

Table 10. Deck compressive strength data

Time (days since pour)	VT data (psi)			Average f'_c (psi)
	Batch 1 (n)	Batch 2 (n)	Batch 3 (n)	
4	4,580 (1)	4,220 (1)	4,620 (1)	4,470
7	5,050 (1)	4,930 (1)	4,300 (1)	4,760
14	5,770 (1)	6,000 (1)	6,290 (1)	6,020
28	7,640 (1)	7,240 (1)	6,370 (1)	7,080
42 (Shear Test #1)	8,000 (1)	7,800 (1)	7,080 (1)	7,630
51 (Shear Test #2)	-------	-------	-------	-------
77 (Flexure-shear Test #1)	8,200 (1)	8,400 (1)	-------	8,300
156 (Flexure-shear Test #2)	-------	-------	-------	-------

(n) = the number of cylinders used to determine each value

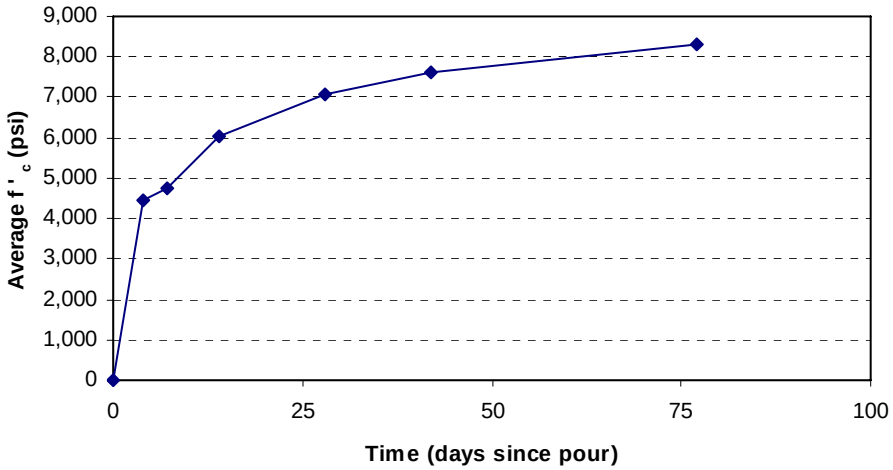

Figure 31. Deck compressive strength plot

Table 11. Deck splitting tensile data

Time (days since pour)	VT data (psi)			Average f_r (psi)
	Batch 1 (n)	Batch 2 (n)	Batch 3 (n)	
4	-------	-------	-------	-------
7	607 (1)	517 (1)	477 (1)	534
14	547 (1)	647 (1)	567 (1)	587
28	647 (1)	716 (1)	657 (1)	673
42 (Shear Test #1)	716 (1)	696 (1)	637 (1)	683
51 (Shear Test #2)	-------	-------	-------	-------
77 (Flexure-shear Test #1)	706 (1)	696 (1)	-------	701
156 (Flexure-shear Test #2)	-------	-------	-------	-------

(n) = the number of cylinders used to determine each value

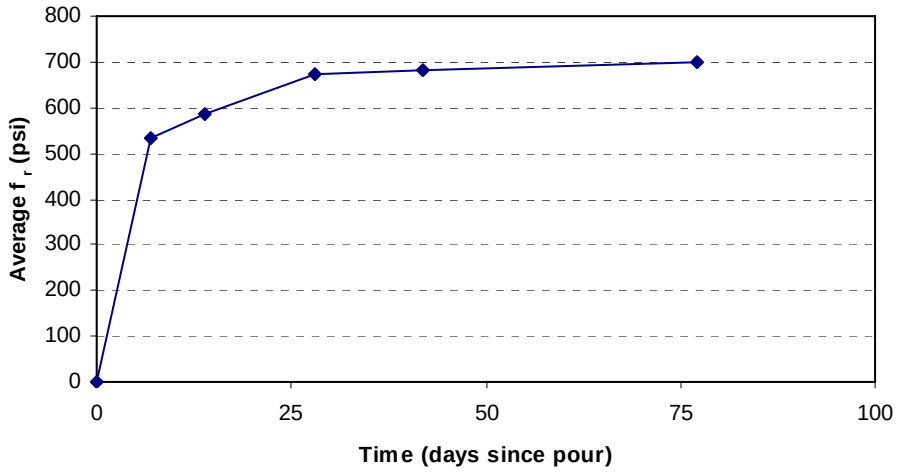

Figure 32. Deck splitting tensile plot

Table 12. Deck modulus of elasticity data

Time (days since pour)	VT data (ksi)			Average E_c (ksi)
	Batch 1 (n)	Batch 2 (n)	Batch 3 (n)	
4	-------	-------	-------	-------
7	2,850 (1)	2,960 (1)	2,570 (1)	2,793
14	3,070 (1)	3,000 (1)	-------	3,035
28	2,940 (1)	2,920 (1)	2,680 (1)	2,847
42 (Shear Test #1)	2,960 (1)	2,950 (1)	2,681 (1)	2,864
51 (Shear Test #2	-------	-------	-------	-------
77 (Flexure-shear Test #1)	3,190 (1)	3,060 (1)	-------	3,125
79 (Flexure-shear Test #2)	-------	-------	-------	-------

(n) = the number of cylinders used to determine each value

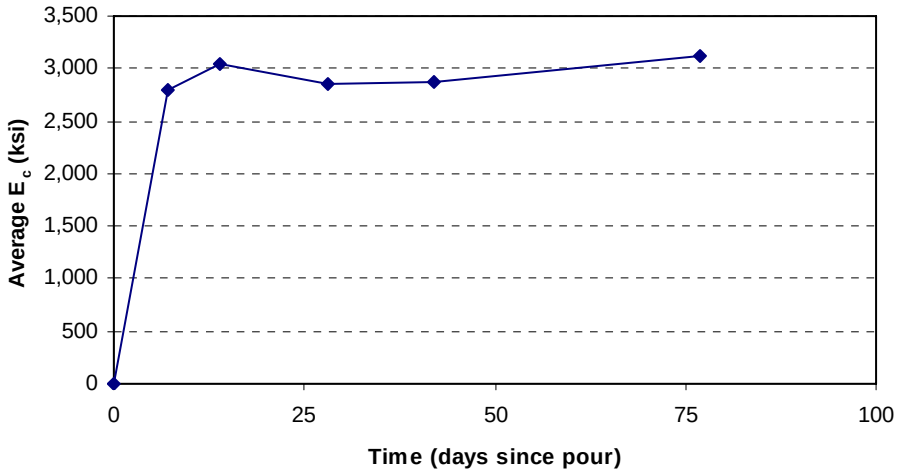

Figure 33. Deck modulus of elasticity plot

Deck instrumentation consisted of a single thermocouple to measure the temperature change during the curing process of the deck concrete. Time zero corresponds to the beginning of the deck concrete pour. This thermocouple was placed at mid-span of the composite system and at mid-height of the deck (4.5 in below the surface of the concrete). The temperature change over time can be seen in Figure 34. The maximum temperature achieved during the curing process was approximately 43° Celsius and the temperature returned to the laboratory ambient temperature approximately eight days after casting of the deck.

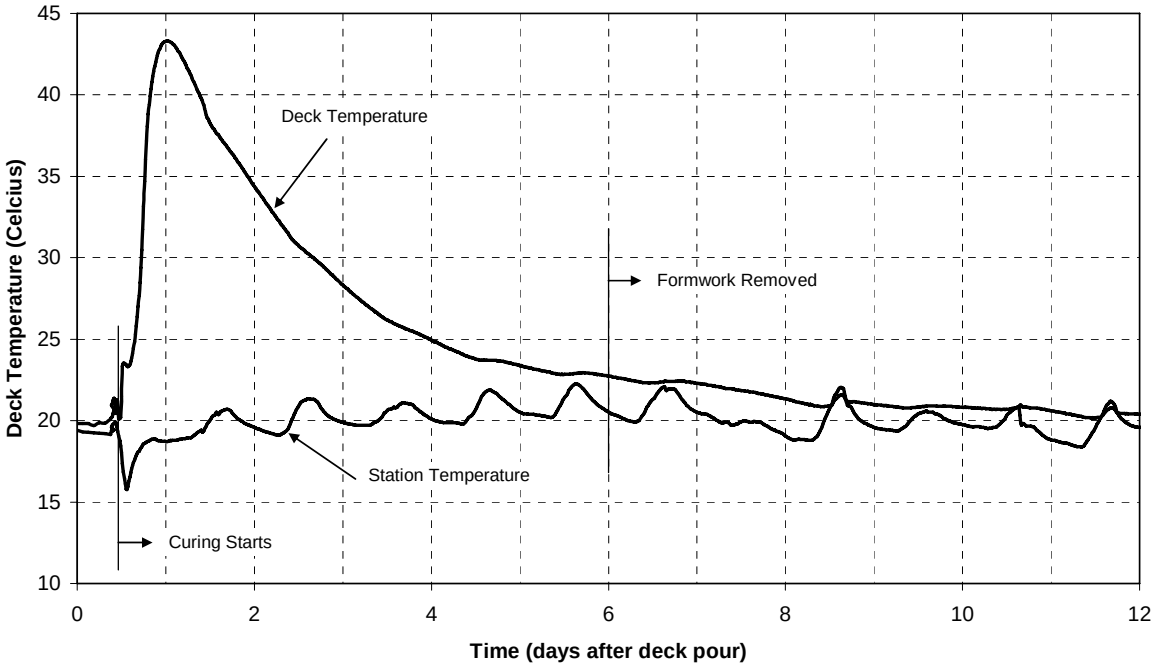

Figure 34. Deck thermocouple temperature change over time

The change in strain, as recorded by the girder vibrating wire gages, experienced by the PCBT-53 as the composite deck was cast and cured can be seen in Figure 35. It is evident that the weight of the deck concrete caused compression in the top of the girder and induced tension in the bottom of the girder. The plot also shows that the top of the beam experienced a small amount of tension while the bottom of the beam had a small amount of compression. This can be attributed to the top flange of the beam expanding from the hydration temperature effect. The deck heated up the top flange of the beam causing it to expand (increase in strain) followed by a short cooling period (decrease in strain) during which the net difference before and after this phenomena is noted. This net difference could be due to some strain or stress locked in the beam. After the formwork was removed on January 15, 2007, the concrete was again allowed to contract.

Camber Monitoring

The PCBT-53 girder was cast on October 24, 2006, in a single day at Bayshore Concrete. After the girder was subjected to an overnight steam cure and the formwork was stripped, the girder was lifted using the unique lifting devices for two reasons. The first was to analyze the anchorage zones of the beam after lifting, which is outside the scope of this project and was part of the research done by Crispino (2007). The second reason was to ensure that the lifting devices would work properly. The first camber measurement of 0.67 in was taken following this initial lift after the beam was set back into the casting bed. No more camber measurements were taken between this time and when the beam was setup for the initial shear test. The second and final measurements of the camber reflected a value of 1.25 in and this was taken twice with the first time occurring nine days after the deck was cast and the next occurring 16 days after the deck was cast. Both of these times the camber measurements were the same. The final camber measurements were taken using a rotating laser level and a folding carpenters rule.

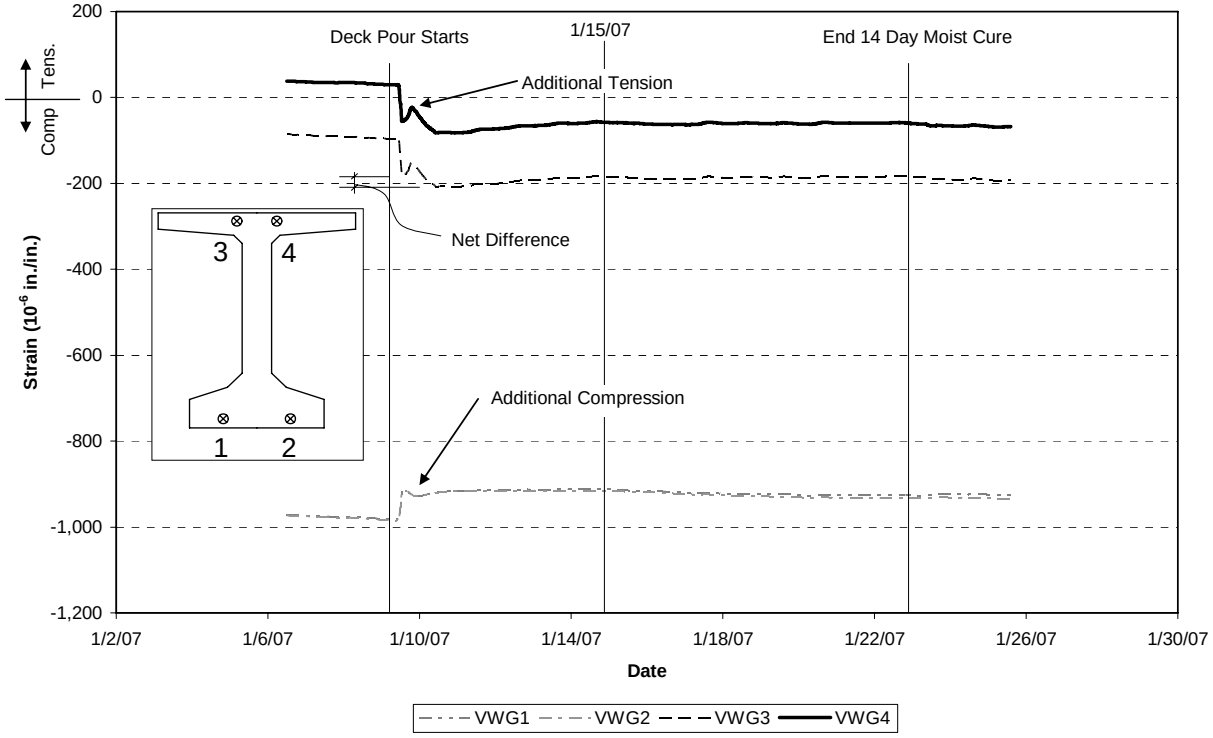

Figure 35. PCBT-53 VWG strain over time as composite deck is cast

Shear Testing Results

Shear Test #1

The testing instrumentation setup for both the initial shear test and the following shear test after the load cells were re-calibrated is shown in Figure 36. Note the location of the wire pots, load cells, and strain gages because the accompanying plots are labeled in the same fashion.

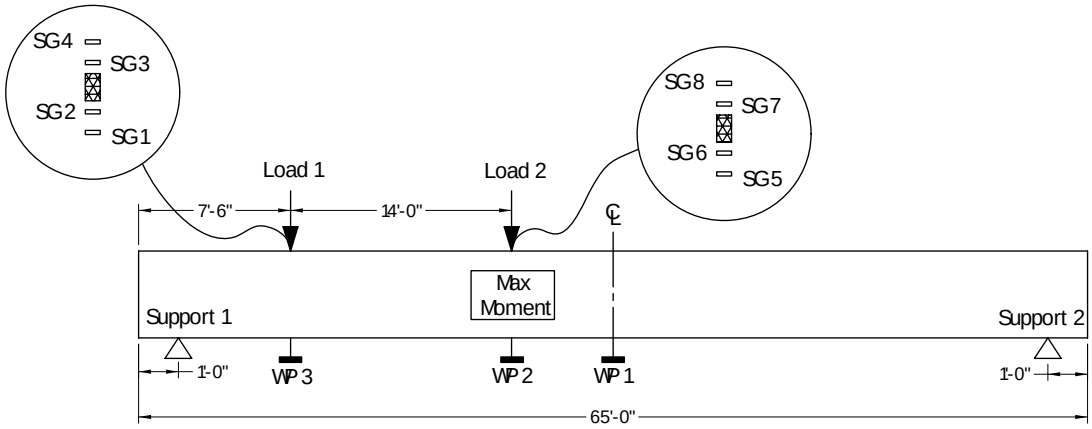

Figure 36. Shear test #1 instrumentation labels

During this initial test, the load was increased in 20 kip increments. The first cracks were noticed at approximately 80 to 85 kips per actuator (support reaction of 170 to 178 kips) and these consisted of some crazing cracks at the top of the bulb under Load 2. These cracks did not cross the DEMEC region and thus were not visible on the plot. The first true flexural crack crossed the bottom of the bulb at approximately 150 to 160 kips per actuator (support reaction of 280 to 296 kips), and this is when the plot of load vs. strain became nonlinear. This region was being tracked with the DEMEC points and the plot of load vs. strain can be seen in the Appendix.

The first web shear crack, shown in Figure 37 with the corresponding crack angle, in the PCBT-53 occurred around 180 kips per actuator, which is equivalent to a support reaction of 327 kips. These first shear cracks formed at an angle of approximately 39 degrees running from the support towards the first loading point. Just beyond this load (at a support reaction of 350 kips), the beginning of non-linear behavior can be seen. Figure 38 shows the non-linear behavior as the load was increased until the 300 kip capacity load cell was removed from the system. Unloading of the girder was a fast process because of the hydraulic pressure built up inside the actuators. During this unloading process, illustrated in Figure 38, the researchers had limited control of how fast the load was removed; hence, the plateau at a support reaction of 140 kips in Figure 38. This event is typical for all of the different tests and times of loading with differences in the load remaining after the hydraulic fluid recovered. It is important to note that all of the plots of support reaction vs. deflection throughout the study contain a calculated support reaction based on the two applied actuator loads and the self weight of the composite member.

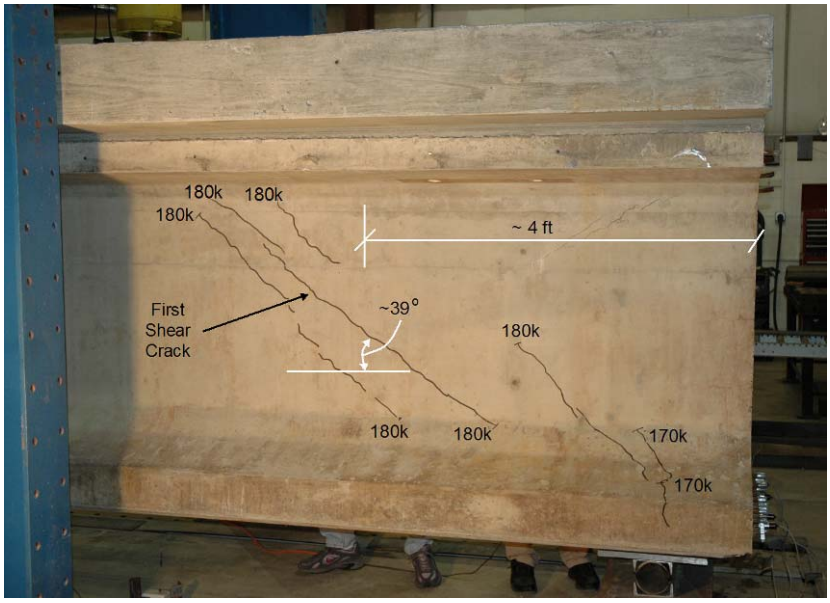

Figure 37. Initial web shear cracks (noted loads are per each actuator)

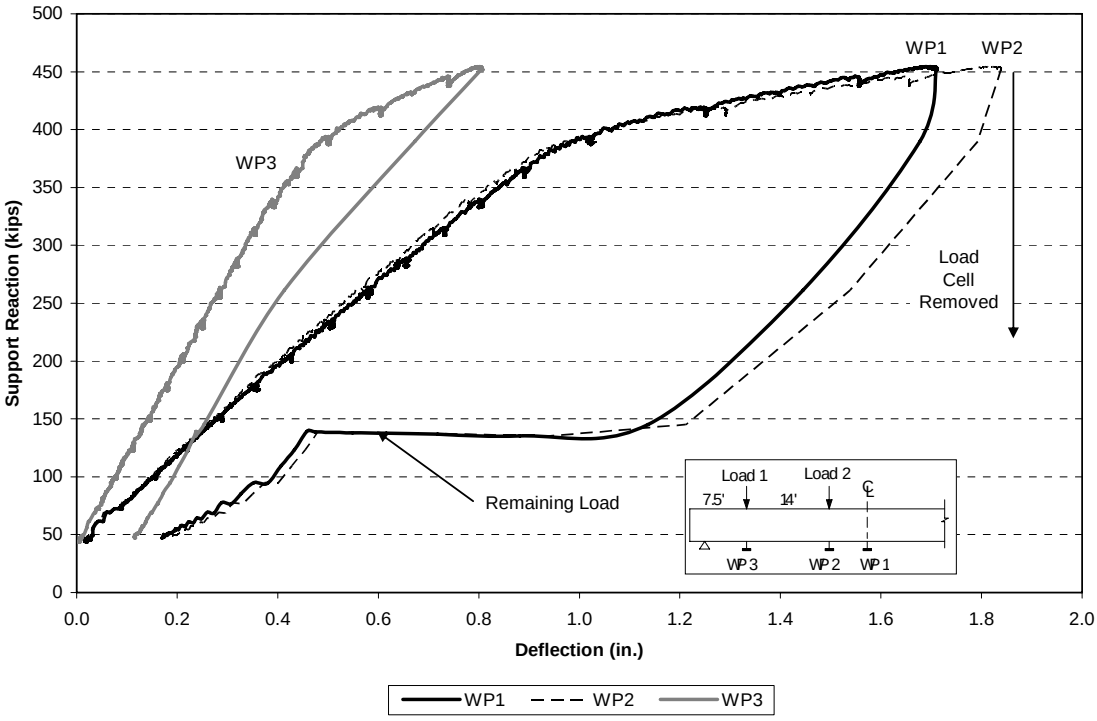

Figure 38. Shear test #1 initial loading displacements

Figure 39 shows the support reaction vs. displacement during the second test that occurred after the 300 kip load cell was removed. The plot again shows non-linear behavior when the support reaction reaches approximately 300 kips. This load is lower than the first time the beam was loaded, since the concrete was previously cracked. The first flexure-shear crack did not propagate toward Load 2 until a support reaction of 437 kips. At this point, additional flexure-shear cracks opened until the test was stopped at a load of approximately 290 kips per actuator (support reaction of approximately 500 kips) for the re-calibration of the load cells with a new universal testing machine as previously mentioned.

The maximum deflection achieved was approximately 2.8 in (see Figure 39), measured at the point of maximum moment under the load applied at 21.5 ft from the end of the beam. During this test, no strand slip was noticed from visual inspection or from the recorded data.

The maximum compressive strain during this test was approximately 1,300 με. This strain was recorded on the top of the deck under the point load located 21.5 ft from the end of the beam. Figure 40 shows the measured strains at the load point 21.5 ft from the end of the beam. The maximum strain was recorded at an applied moment of approximately 5,800 k-ft. Figure 41 shows the strains measured during this test by the gages under the load located at 7.5 ft from the end of the beam. Figure 40 and Figure 41 show clear evidence of a shear lag effect, and this was present for each test performed on the girder. Due to the shear lag effect, elements in close proximity to the load are subjected to large stresses while other elements near the edges of the member are less affected by the applied load. In this case, the strain gages that were closer to the web of the PCBT-53 recorded a higher strain than those located at the outer edge of the composite deck. It is important to note that all of the plots of moment vs. strain throughout the

study contain a calculated moment (at point of maximum applied moment) and support reaction based on the two applied actuator loads and the self weight of the composite member.

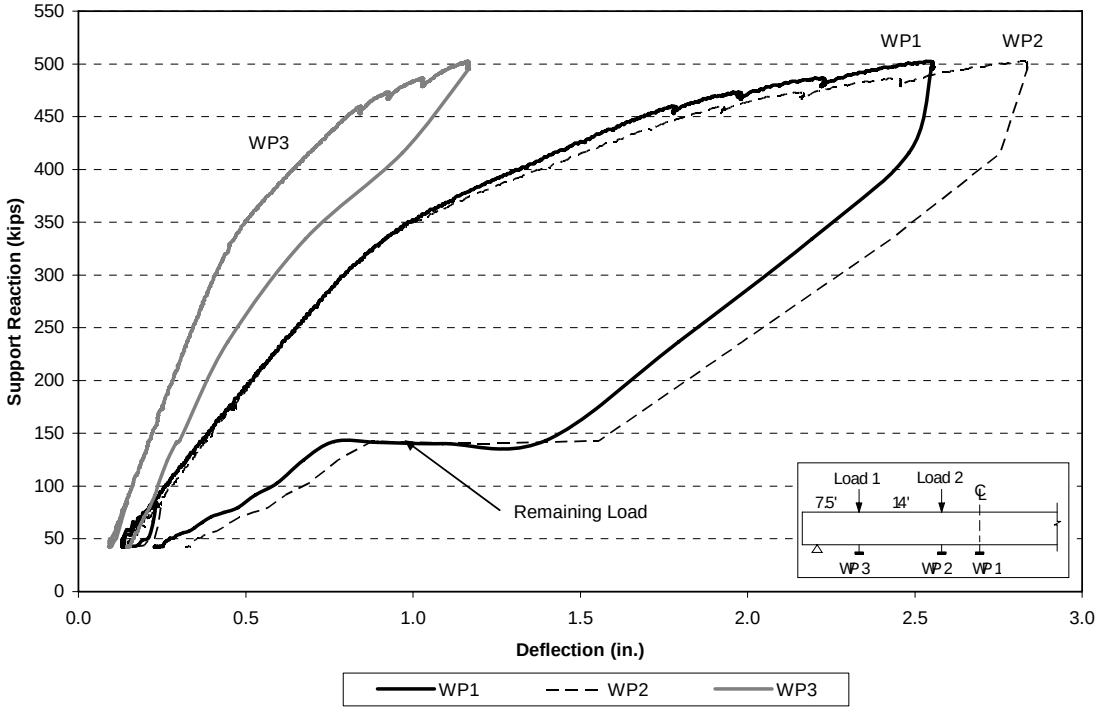

Figure 39 Shear test #1 displacements after removing 300k load cell

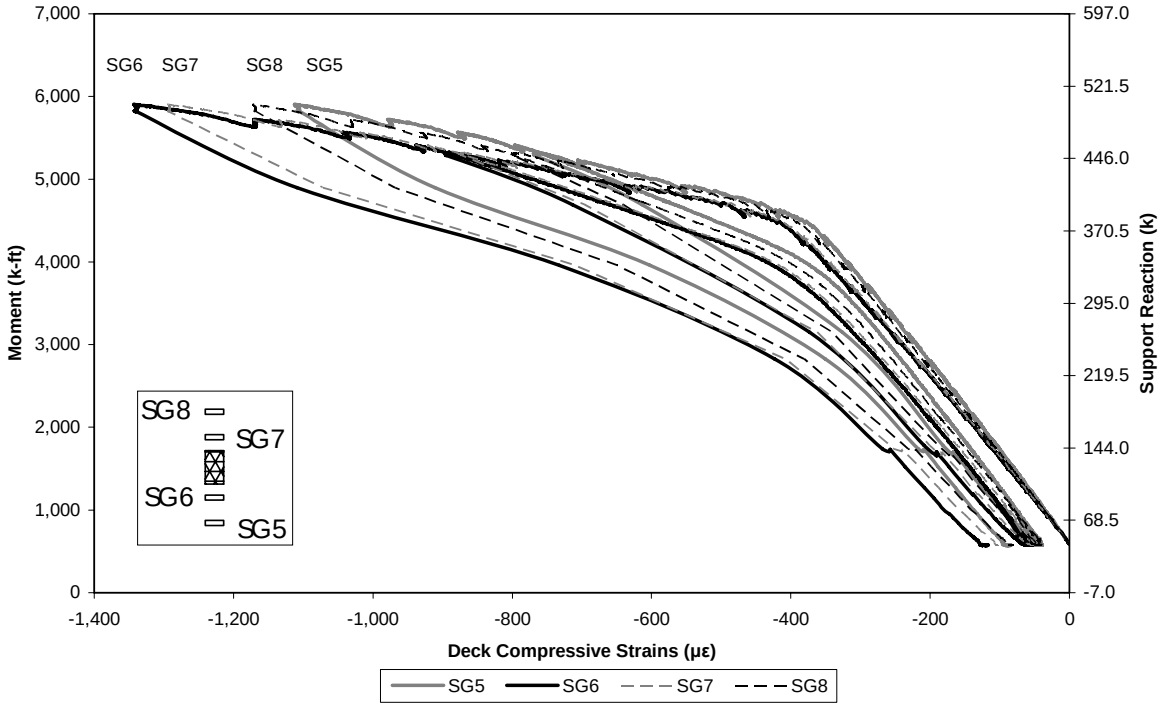

Figure 40. Shear test #1 deck strains under the load at 21.5 ft from end of girder

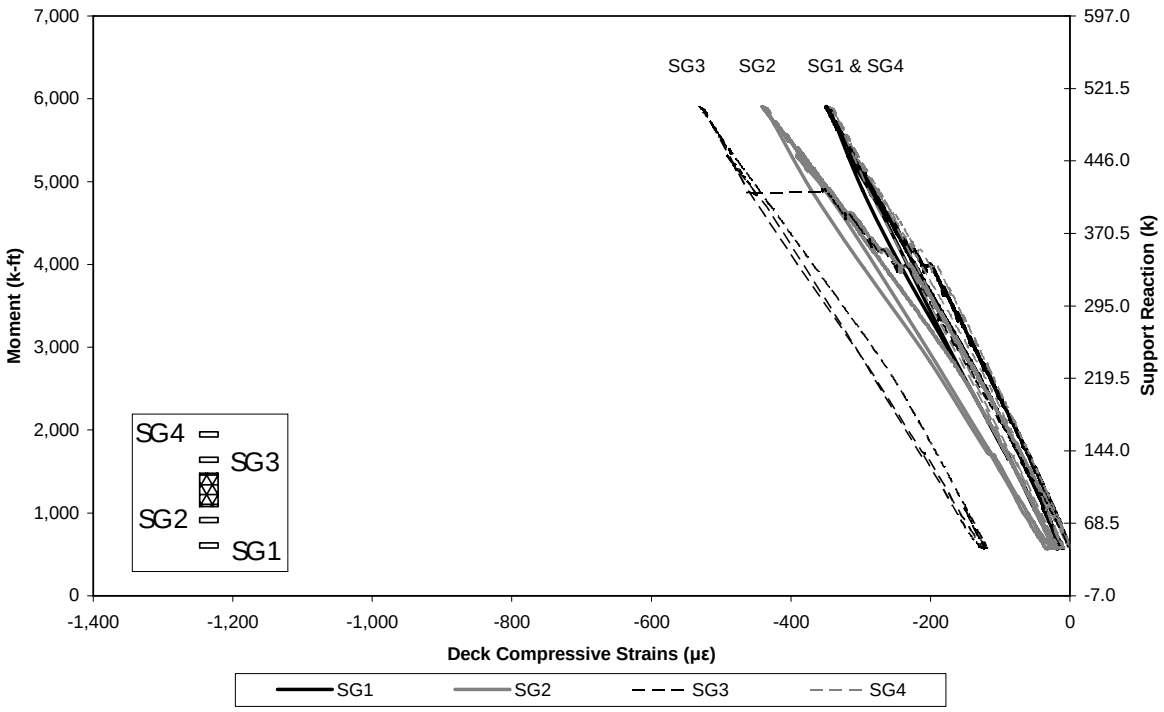

Figure 41. Shear test #1 deck strains under the load at 7.5 ft from end of girder

Re-calibrated Shear Test

During this re-calibrated test, load was applied continuously until 290 kips was reached on each actuator (achieving a support reaction of 500 kips), after which load was applied in 10 kip increments and new cracks were marked. Crack widths were measured during re-loading of the beam. At approximately 290 kips per actuator, or a support reaction of 500 kips, the shear cracks under the loading point closest to the support were measured to be approximately 0.010 in wide, and a flexure-shear crack under the second point of loading was measured to be 0.025 in wide. The first flexural cracks propagated roughly 1.5 in into the deck at approximately 310 kips per actuator (530 kips support reaction). At this point, horizontal cracks were also forming parallel to the strand near the point of maximum moment.

A plot of support reaction vs. deflection for this re-calibrated shear test is shown in Figure 42. Plastic hinging in the PCBT-53 was evident from the deflection of the beam during testing and from the plot of support reaction vs. deflection plot (Figure 42) when the load is not increasing but the deflection is still increasing. This plastic moment and hinging were beginning to initiate around 330 kips per actuator (560 kip support reaction). A maximum deflection of approximately 4.5 in was achieved during this test. Again, no strand slip was noticed from visual inspection or from the recorded data.

The maximum compressive strain during this test was approximately 2,700 με. This strain was recorded under the point load located at 21.5 ft from the end of the beam. Figure 43 shows a maximum recorded moment of approximately 6,500 k-ft. Figure 44 shows the deck strain under the actuator located at 7.5 ft from the end of the beam. Again, in both plots there is evidence of the shear lag effect.

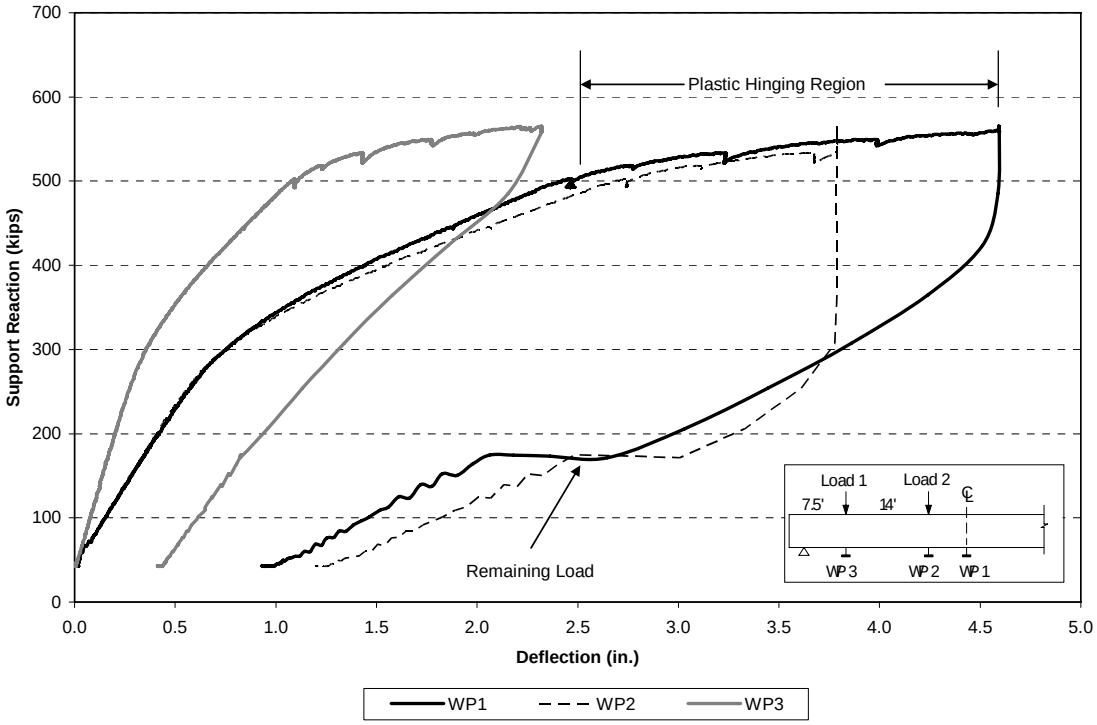

Figure 42. Re-calibrated shear test displacements

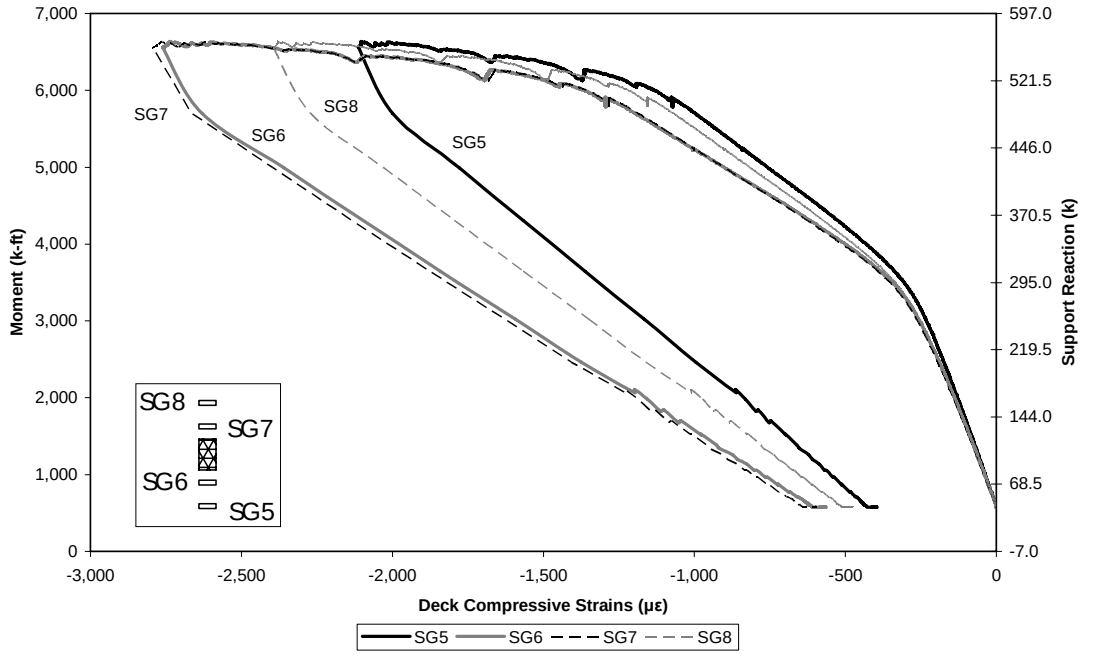

Figure 43. Re-calibrated shear test deck strains under the load 21.5 ft from girder end

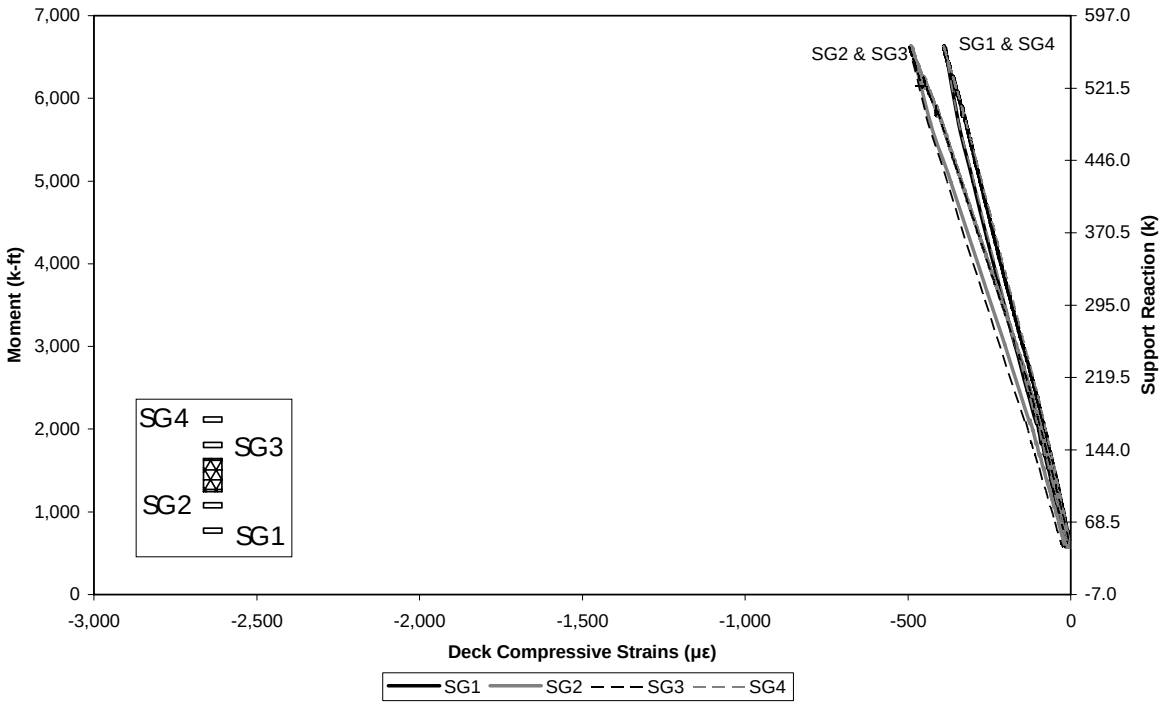

Figure 44. Re-calibrated shear test deck strains under the load 7.5 ft from girder end

Shear Test #2

The focus of the second shear test on the beam was the same as the first, to collect data pertaining to the predicted web shear failure, but the loading configuration was altered to induce higher support reactions. The testing instrumentation setup for the second shear test is shown below in Figure 45. Note the location of the wire pots, load cells, and strain gages because the plots shown are labeled the same way.

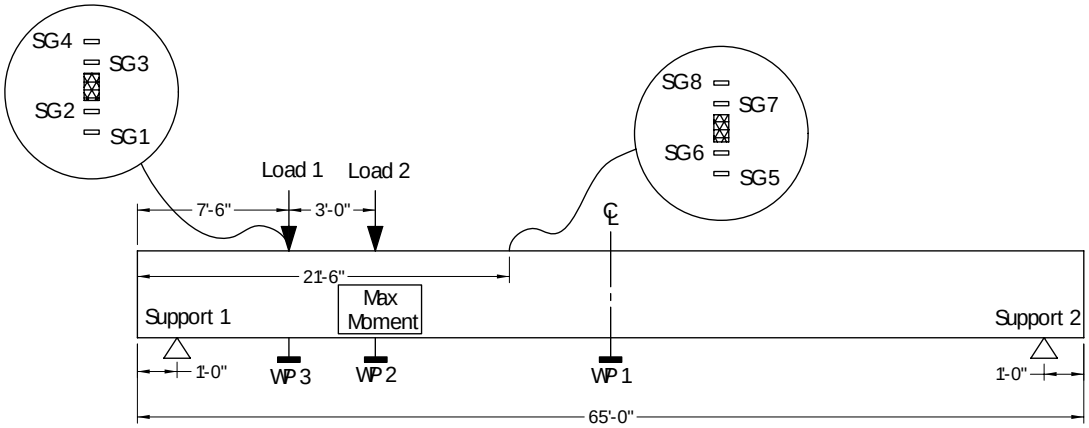

Figure 45. Shear test #2 instrumentation labels

This test was started with a continuously applied load until 170 kips was reached on each actuator (support reaction of approximately 342 kips), after which load was applied in 20 kip increments and new cracks were marked. After the load per actuator reached 250 kips, or a support reaction of 481 kips, the load was increased directly to 290 kips (support reaction of 551

kips) and then in 20 kip increments until 330 kips per actuator was achieved, or a support reaction of 621 kips. Beyond 330 kips, the load was increased at 10 kip increments until an ultimate load of 353 kips per actuator (support reaction of approximately 661 kips) was reached.

Additional web shear cracks began to form when a load of approximately 170 kips per actuator (support reaction of 340 kips) was applied. The cracks were near the point of maximum moment, or the applied load at 10.5 ft from the end of the beam. New horizontal cracks parallel with the strand formed when the load per actuator reached 250 kips (support reaction of 480 kips). New flexural cracks and web cracks formed and extended as more load was applied. Eventually, the ultimate strength of the steel loading frame bolted connections was reached, and the testing was stopped.

The maximum load reached during this test was 353 kips per actuator or a support reaction of 661 kips, and at this point some flaking of concrete in the web of the girder was noticed. This flaking in the web was located between load 1 and support 1. This type of cracking indicates an imminent web crushing failure and the researchers believe this form of total failure would have occurred if an additional 5 to 10 kips could have been applied to the girder. Figure 46 illustrates the initial signs of web shear failure in the beam where the concrete was starting to crush.

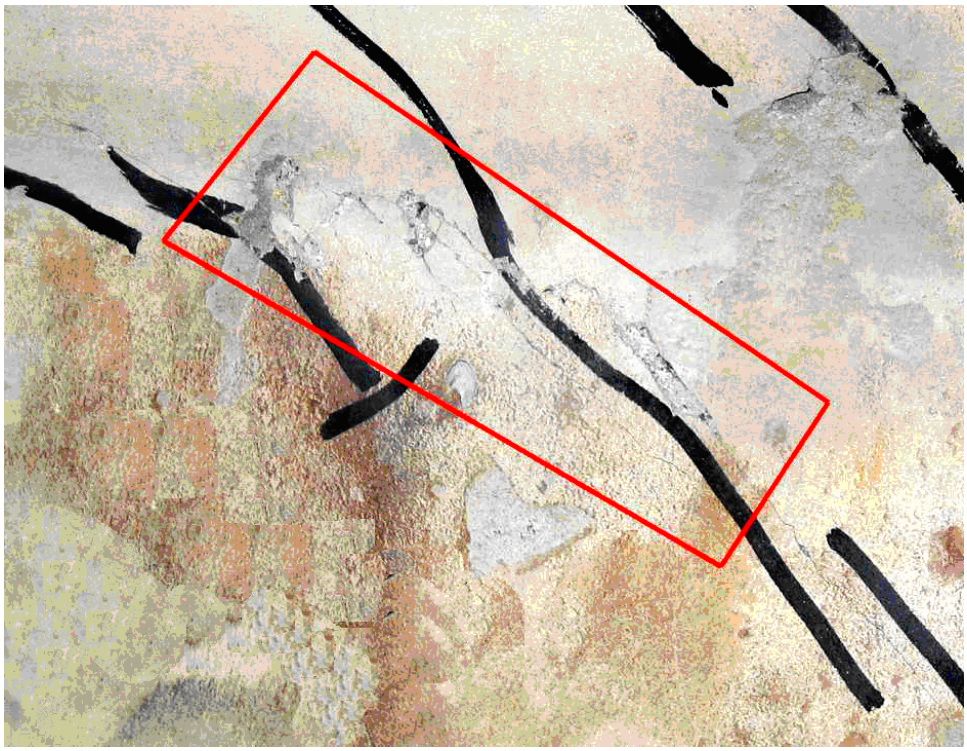

Figure 46. Indication of web shear failure

The maximum deflection achieved was approximately 2.6 in, which was measured at midspan of the 63 ft simply supported span. This deflection was achieved when the maximum load of 353 kips per actuator (support reaction of 661 kip) was applied. Figure 47 presents the support reaction vs. displacement curve. It is interesting to note from this figure there was

virtually no linear "reaction vs. displacement" behavior of the girder in this test, due to the extensive damage from the previous test. The plot of reaction vs. deflection seems to be curved, with a very short linear behavior region. No strand slip was noticed from visual inspection or from the data recorded.

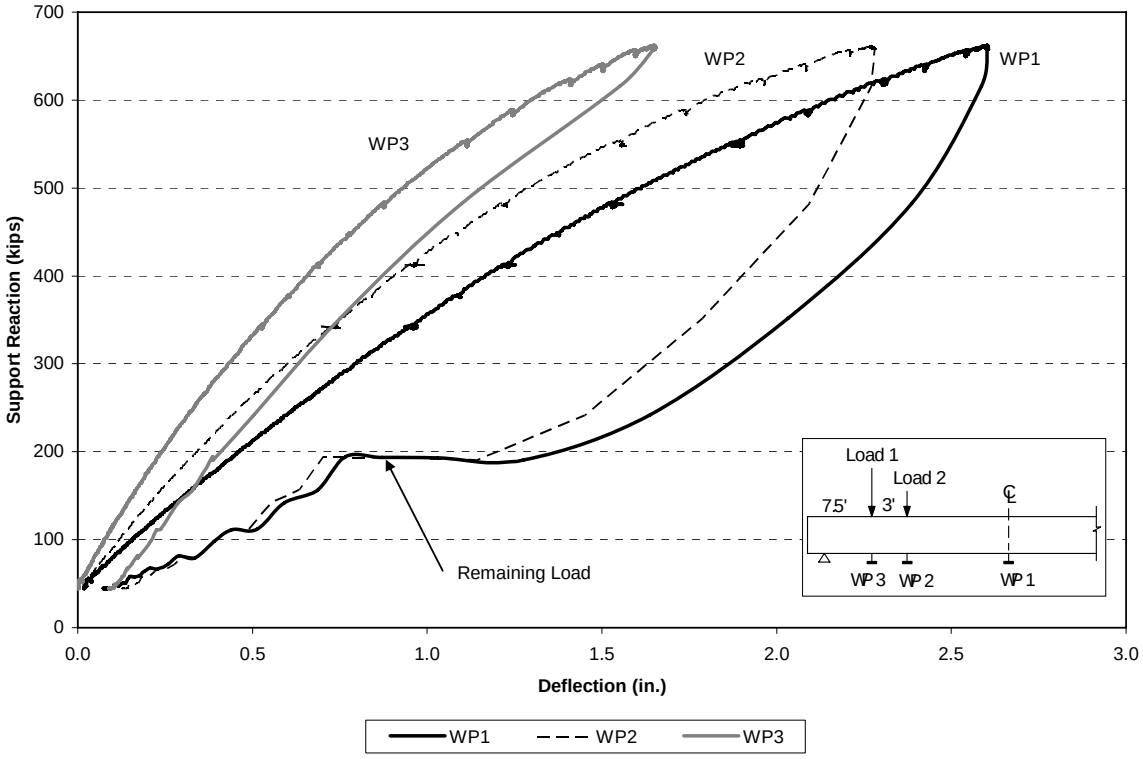

Figure 47. Shear test #2 displacements

The maximum compressive strain achieved during shear test #2 was approximately 700 με. This strain was recorded under the point load located at 7.5 ft from the end of the beam. Figure 48, a plot of moment vs. strain at 7.5 ft from the end of the beam, shows that the maximum recorded moment was approximately 5100 k-ft. This plot also shows evidence of the typical shear lag effect. Figure 49 shows the deck compressive strains at 21.5 ft from the end of the girder. Due to movement of the second load point to 10.5 ft from the end of the girder, no strain measurements were made at the location of maximum applied moment.

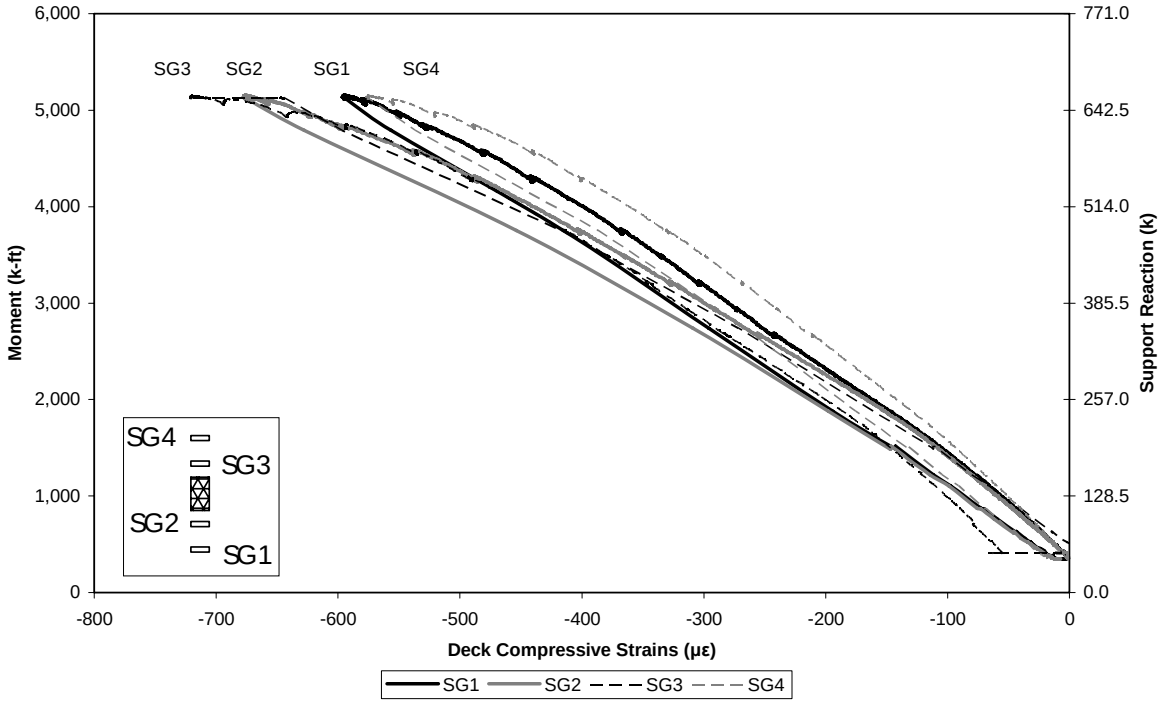

Figure 48. Shear test #2 deck strains at 7.5 ft from girder end

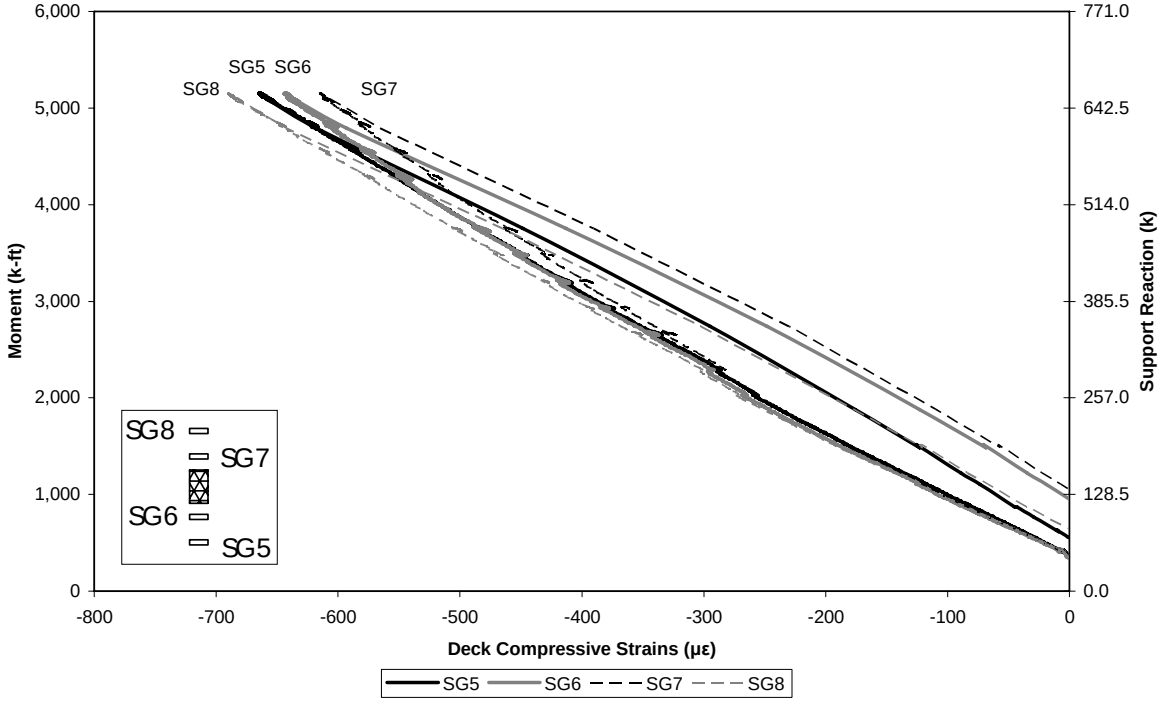

Figure 49. Shear test #2 deck strains at 21.5 ft from girder end

Flexure-Shear Testing Results

During the flexure-shear test, the girder was loaded at three different stages. The first stage (flexure-shear test #1) had both of the load cells in place and load was applied until the 300 kip load cell reached capacity. The load cell was then removed and the second loading stage of the beam took place. This stage is not specifically discussed in this report because the support conditions were not deemed safe. Finally, the girder was re-loaded (flexure-shear test #2) after the support conditions had been fixed and load was applied until the girder reached a state of ultimate failure and could no longer be tested.

The testing instrumentation setup for both of the flexure-shear tests is shown in Figure 50. Note the location of the wire pots, load cells, and strain gages because the plots shown are labeled the same way. The wire pot located on the steel support (support 2) is not shown.

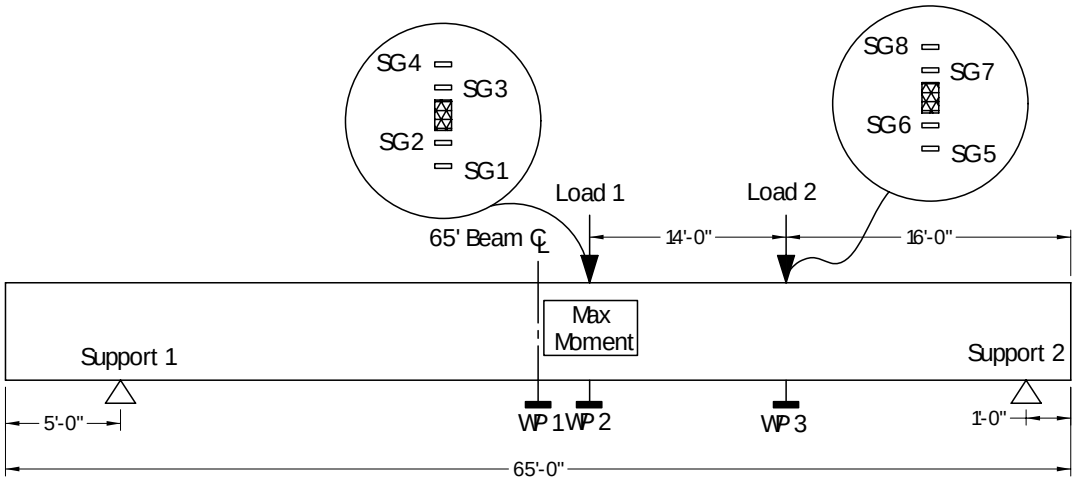

Figure 50. Flexure-shear test instrumentation labels

Flexure-Shear Test #1

The initial flexure-shear test took place with a constant loading until 140 kips per actuator was reached (support reaction of 217 kips). The first new flexural crack was then detected under the load located 30 ft from the end of the beam. The first new web shear crack appeared under the loading point at 16 ft from the end of the beam when the load in each actuator reached 155 kips or a support reaction of 236 kips. In addition, a new flexural crack appeared under Load 2 at the same applied load. The first flexure-shear crack formed when a flexural crack turned toward the loading point located at 30 ft from the end of the beam, and this occurred at a load of 180 kips per actuator (support reaction of 268 kips).

A horizontal bottom flange splitting of the concrete, as shown in Figure 51, occurred between the center line of the beam and Support 1 when the load per actuator reached 220 kips (support reaction of approximately 318 kips). At this point, the region of the beam being tested also had a horizontal crack form in the bottom bulb of the girder between Load 1 and Load 2. The loading was increased and new flexure-shear cracks formed, along with more horizontal cracks, until the actuator located 30 ft from the end of the beam ran out of stroke at a load of approximately 290 kips per actuator (support reaction of 406 kips). At this point, there were

wide flexure-shear cracks and horizontal bottom flange splitting cracks between the loading point located at 30 ft from the end of the beam and Support 1.

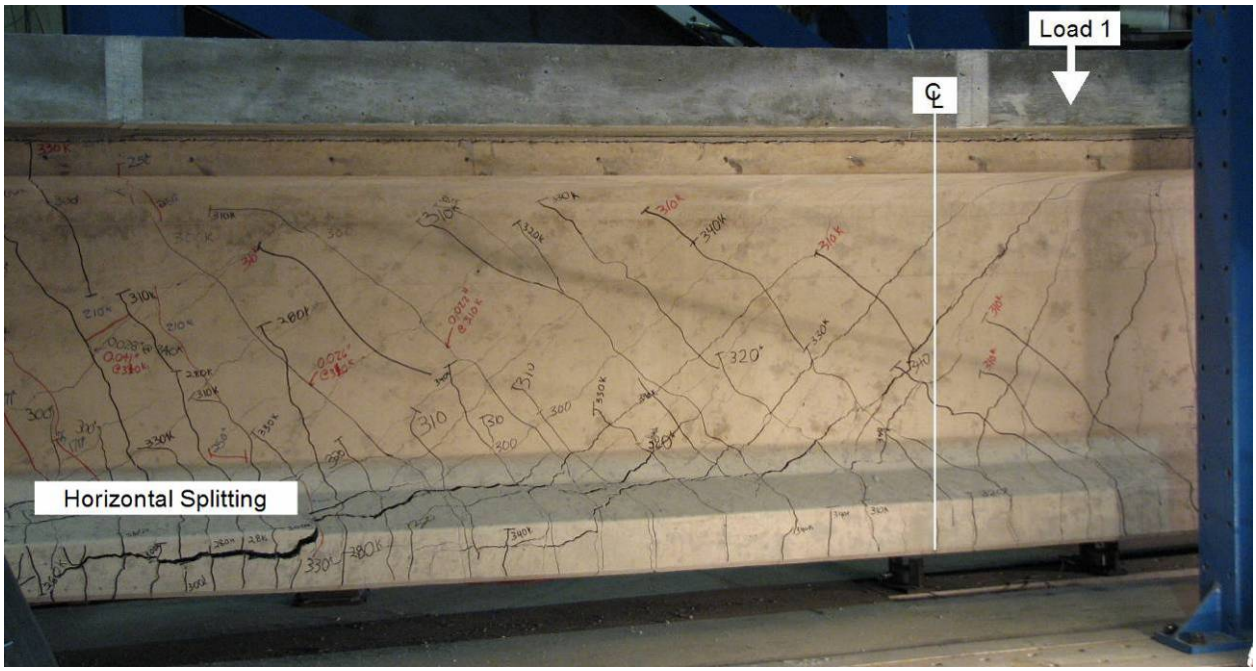

Figure 51. Horizontal bottom flange splitting failure

The maximum deflection achieved was approximately 10.5 in, which was measured at the center line of the 65 ft beam. This deflection was achieved when the maximum load of 290 kips per actuator (support reaction of 406 kips) was applied, and this pushed the wire pots to the extent of their stroke. The plot of support reaction vs. displacement, as seen in Figure 52, shows the measured displacements. Figure 52 also shows that the support reaction vs. displacement plot begins to look non-linear at a support reaction of approximately 200 kips. No strand slip was noticed from visual inspection or from the data collected.

The maximum compressive strain achieved during this test was approximately 3,400 με. This strain was recorded under the point load located at 30 ft from the end of the beam. A plot of maximum moment vs. strain at Load 1, as seen in Figure 53, shows that this strain was present under an applied moment of approximately 7,000 k-ft. It can be noted that this value exceeds the typically assumed design failure strain of concrete in compression of 0.003 in/in. Finally, Figure 54 shows the moment vs. strain data for the remaining four strain gages in this setup located 16 ft from the end of the beam under Load 2. As with previous tests, the shear lag effect is visible in both plots.

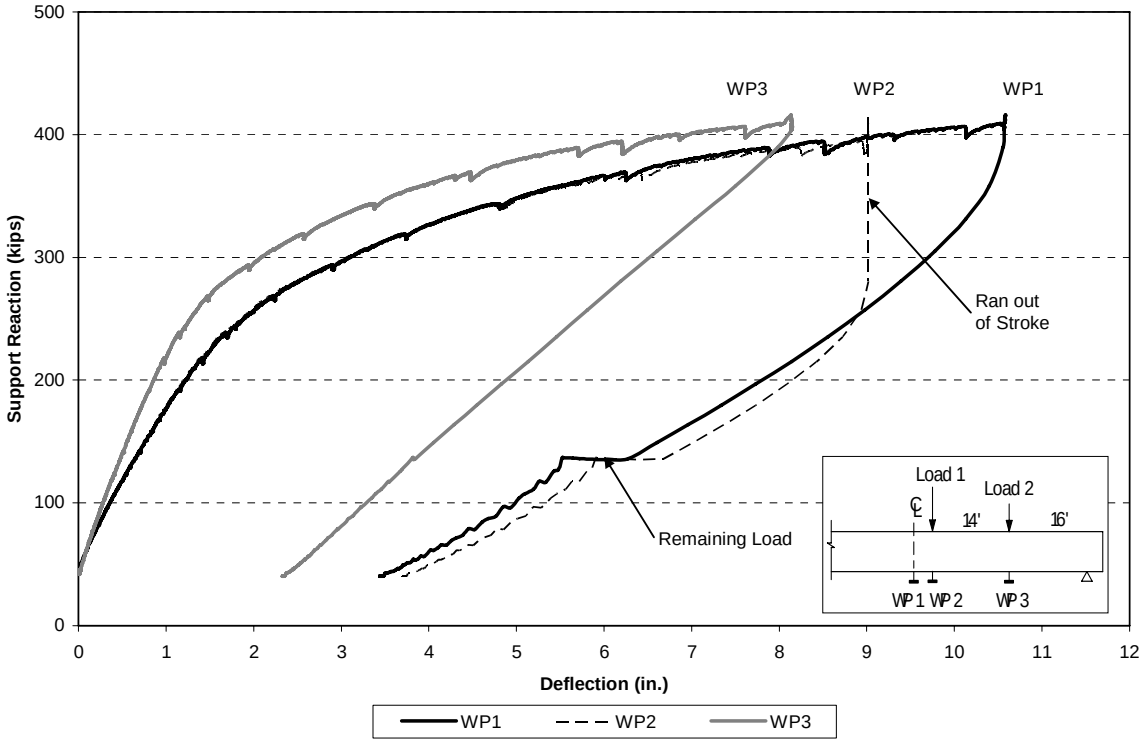

Figure 52. Flexure-shear test #1 displacements

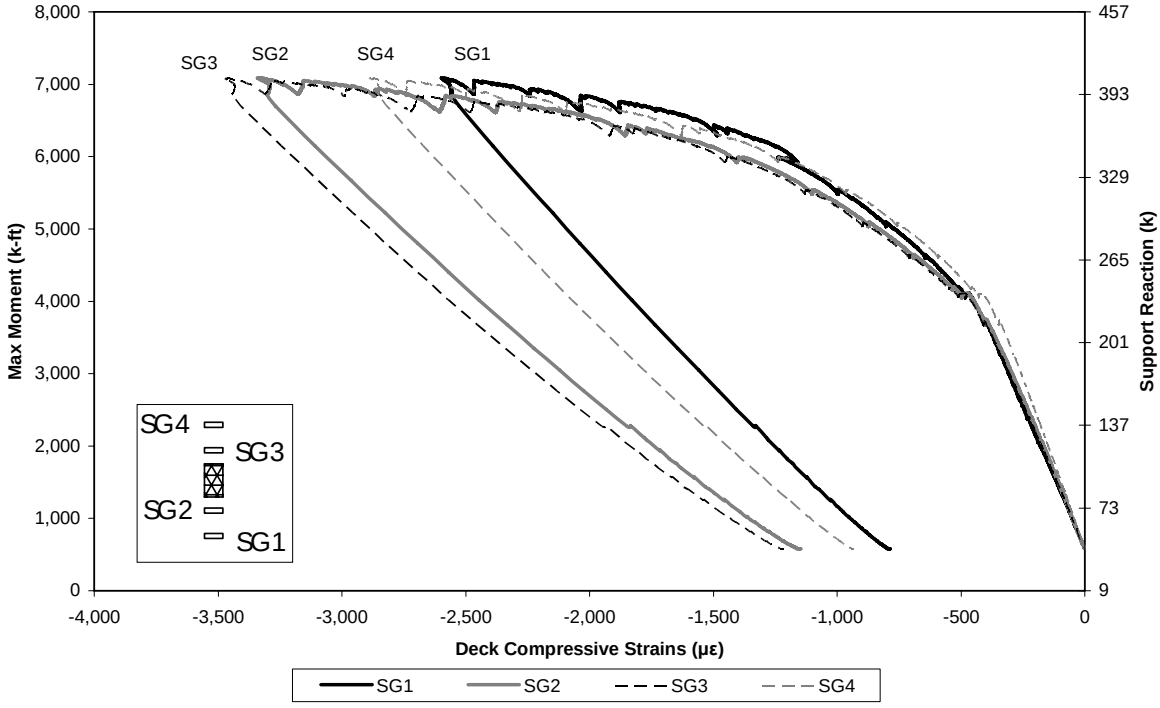

Figure 53. Flexure-shear test #1 deck strains under the load 30 ft from girder end

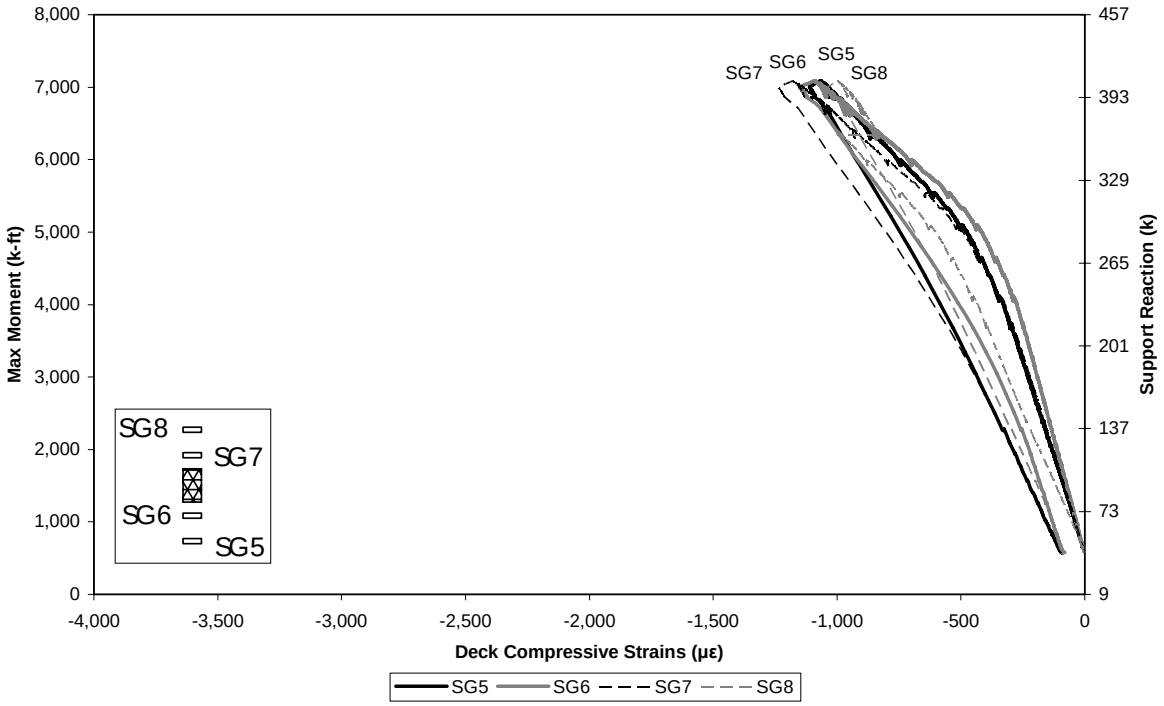

Figure 54. Flexure-shear test #1 deck strains under load 16 ft from girder end

Flexure-Shear Test with Added Stroke

The PCBT-53 was unloaded after the actuator ran out of stroke and then re-loaded in stage two of the flexure-shear testing with more steel plates between the simulated tire patch and the actuator. This allowed for roughly 3-4 in of additional stroke. The girder was again loaded directly to 220 kips per actuator. This is the second stage of the flexure-shear test from which the data are not reported because at this point, and continuing through the maximum load reached during this test of approximately 260 kips per actuator, the researchers noticed the roller support (support 1) in the pin-and-roller support system moving too far. The roller was deemed unsafe because it was close to rolling off the edge of the steel plate. This test was stopped at 260 kips per actuator so that the researchers could lift the girder with small hydraulic pumps and re-adjust the roller support system. After the roller was fixed, flexure-shear test #2 commenced.

Flexure-Shear Test #2

The final flexure-shear test (third overall stage) took place with a constant loading until 150 kips per actuator was reached. At this applied load, the adjusted roller and pin support conditions looked good upon inspection. The girder was then loaded continuously until 260 kips per actuator was reached. From this point, the girder was loaded at 10 kip increments until the final load of 303 kips per actuator was reached. The ultimate failure of the PCBT-53 was initiated with top flange crushing, and an extremely fast and sudden failure commenced. The web of the girder blew out, the bottom flange dropped off of the girder, and a compression strut formed in the web of the girder. During the abrupt failure, a single leg of one double leg vertical shear stirrup was also ruptured. The failure occurred very close to midspan of the girder, between midspan of the girder and the loading point 30 ft from the end of the beam. Figure 55

shows the girder after failure; the compression strut is visible to the left of the load frame. Figure 56 illustrates the crushing that occurred in the top of the composite system.

Figure 55. Ultimate failure of the PCBT-53

Figure 56. Crushing in the top of the deck

The maximum deflection achieved during this test, as shown in Figure 57, was approximately 9.5 in. This value was measured at the center line of the 65 ft girder. This deflection was achieved when a maximum support reaction of 415 kips was applied. This load also pushed the wire pots to the extent of their stroke. Again, no significant amount of strand slip was noticed from visual inspection or from the data recorded.

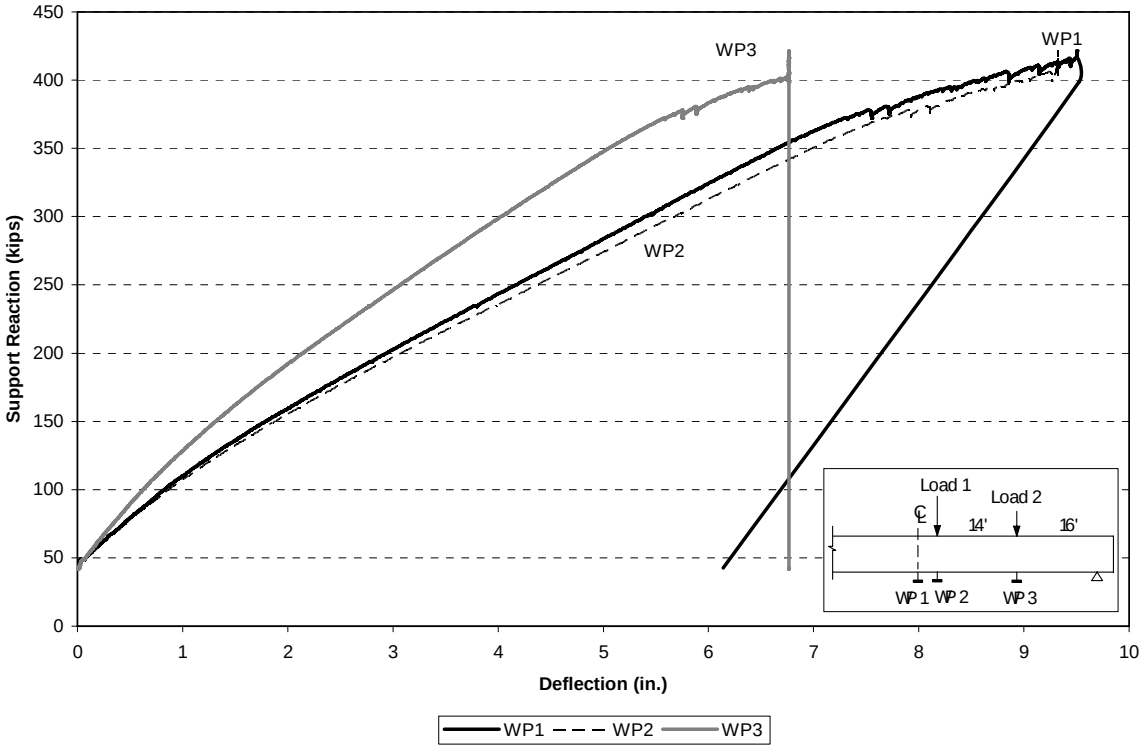

Figure 57. Flexure-shear test #2 displacements

The maximum compressive strain achieved during this test was approximately 3,500 με. This strain was recorded under the point load located at 30 ft from the end of the beam. A plot of maximum moment vs. strain, as seen in Figure 58, shows that this strain was present under an applied moment of approximately 7,100 k-ft. It can be noted that this value exceeds the assumed design failure strain of concrete in compression of 0.003 in/in, but at this recorded value the top of the concrete deck did crush. Figure 59 shows a plot of the maximum moment vs. strain in the composite deck from the gages located at 16 ft from the end of the girder.

DISCUSSION

Girder Concrete Material Properties

Measured girder concrete material properties over time are summarized in Table 13. This table shows the average compressive strength, tensile strength, and modulus of elasticity test results for the specified concrete age. The average compressive strength for the girder was greater than the target strength of 8,000 psi; in fact, the design strength was reached after the steam curing ended. AASHTO LRFD (2006) equations for the tensile strength and the modulus of elasticity are also included in the table. These values are based on the concrete compressive strength (and the concrete unit weight for modulus of elasticity). The measured tensile strengths from split cylinder tests were slightly greater than calculated, and in general, the measured modulus of elasticity was significantly less than the calculated modulus of elasticity. Also note, as discussed in the "Results" section and illustrated in Figure 27, the modulus dropped over time.

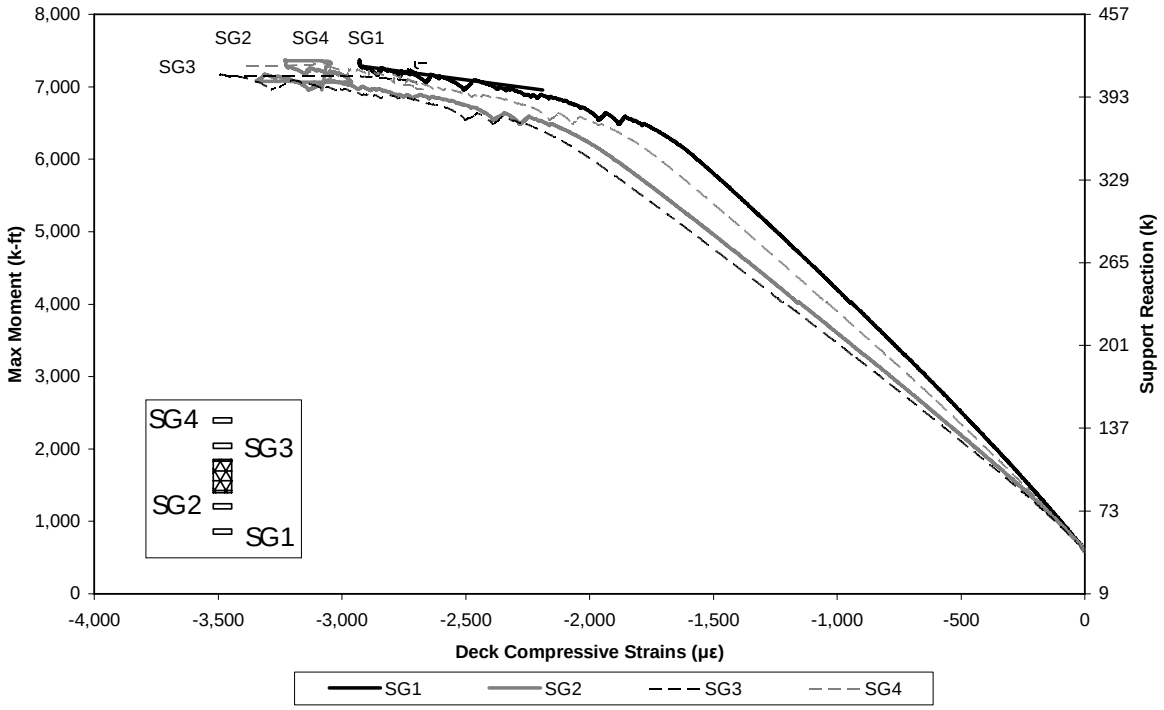

Figure 58. Flexure-shear test #2 deck strains under the load 30 ft from girder end

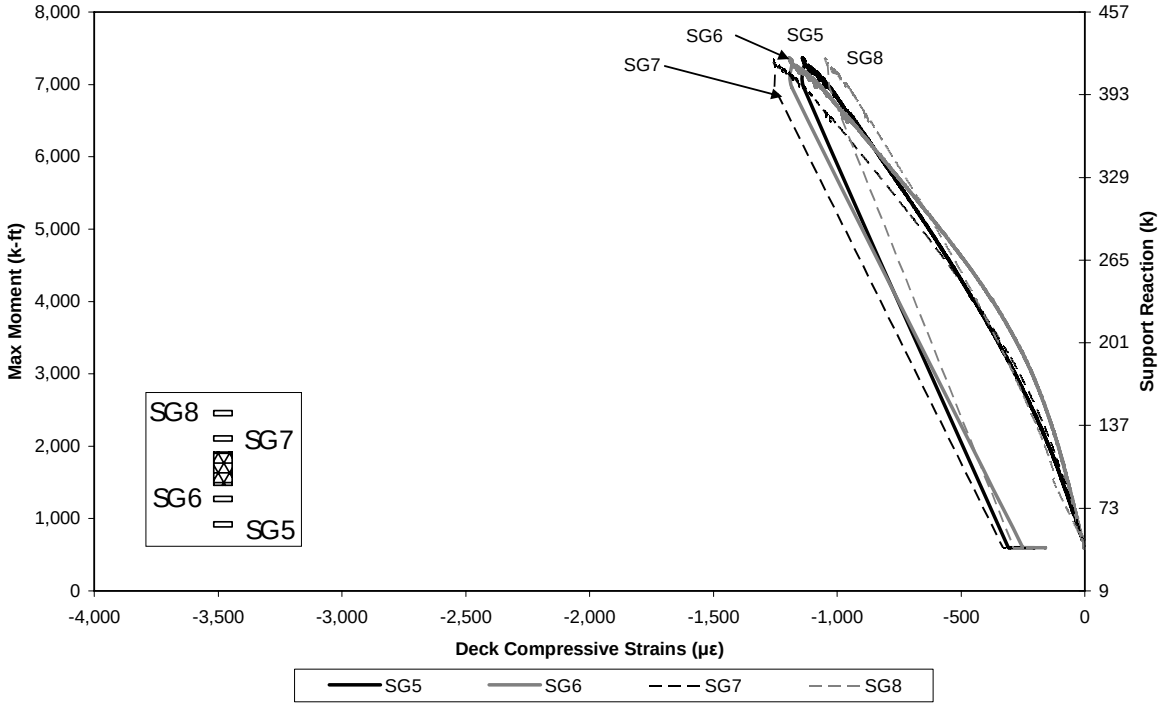

Figure 59. Flexure-shear test #2 deck strains under the load 16 ft from girder end

Table 13. PCBT-53 material properties

Concrete Age (days)	f'_c (ksi)	f_{ct} (ksi)		E_c (ksi)	
		Meas.	$0.20f'^{0.5}_c$	Meas.	$33{,}000w_c^{1.5}f'^{0.5}_c$
Transfer	8.34	0.592	0.578	3,600	3,860
7	8.14	0.620	0.571	3,550	3,820
14	9.04	0.668	0.601	3,310	4,020
28	8.96	0.653	0.599	3,450	4,000
Shear Test	10.55	0.796	0.650	3,277	4,350
Flexure-Shear Test	10.70	0.865	0.654	3,197	4,380

* Unit Weight = 0.118 k/ft^3

It is evident from Table 13 that the equation used to calculate the modulus of elasticity in the AASHTO LRFD Specifications (2006) over estimated the measured modulus. Table 14 presents a comparison of three other available equations for modulus of elasticity. These equations are based on the concrete unit weight (w_c) and the concrete compressive strength (f'_c). The first equation shown comes from the AASHTO LRFD Specifications (2006) and was previously discussed. The second equation was adopted by ACI Committee 363 (1992) in their State-of-the-Art Report on High Strength Concrete. Finally, the third equation was presented by Cook (1989) as a power curve fit equation from experimental data. Table 15 and Figure 60. Provide a comparison over time of the measured girder modulus of elasticity to the predicted modulus of elasticity using these three equations.

Table 14. Comparison of E_c equations

Equation		w_c units	f'_c units	E_c units
AASHTO LRFD	$33{,}000w_c^{1.5}f'^{0.5}_c$	k/ft^3	ksi	ksi
ACI 363	$(40{,}000\sqrt{f'_c} + 1{,}000{,}000)(w_c / 145)^{1.5}$	lb/ft^3	psi	psi
Cook	$w_c^{2.55}f'^{0.315}_c$	lb/ft^3	psi	psi

Table 15. Comparison of girder measured and calculated Ec

Concrete Age (days)	f'_c (psi)	E_c (ksi)			
		Meas.	AASHTO	ACI 363	Cook
0	0	0	0	0	0
1	8,340	3,600	3,860	3,420	3,300
7	8,140	3,550	3,820	3,380	3,280
14	9,040	3,310	4,020	3,530	3,380
28	8,960	3,450	4,000	3,510	3,380
56	9,460	3,320	4,110	3,590	3,430
77	10,000	3,220	4,230	3,670	3,500
119	10,550	3,280	4,350	3,750	3,550
154	10,700	3,200	4,380	3,770	3,570

* Unit Weight = 118 lb/ft^3

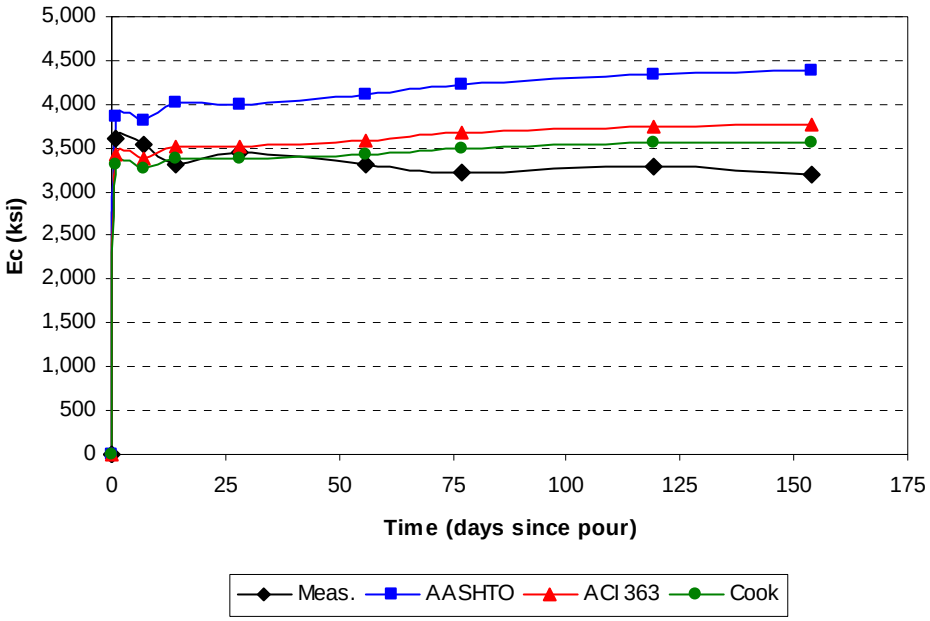

Figure 60. Comparison of girder measured and calculated E_c

From Table 15 and Figure 60, it can be seen that the predicted modulus of elasticity using the ACI 363 equation and the Cook equation fits the data from the PCBT-53 girder better than the predicted modulus of elasticity from the AASHTO LRFD equation. It should be noted that during the bridge design process an engineer will be using the design value of the concrete compressive strength instead of the final measured compressive strength. Typically, the design compressive strength is lower than the final measured compressive strength, and thus, the final modulus of elasticity is higher than that used during the design process. While there is some inherent caution in using alternate equations to predict the final modulus of elasticity, it is realistic to use the ACI 363 equation or the Cook equation during the design process because higher than expected modulus of elasticity values are typically beneficial.

Deck Concrete Material Properties

Measured deck concrete material properties over time are summarized in Table 16. This table shows the average compressive strength, tensile strength, and modulus of elasticity test results for the specified concrete age. The average compressive strength for the deck was greater than the target strength of 5,000 psi. AASHTO LRFD equations for the tensile strength and the modulus of elasticity are also included in the table. These values are based on the concrete compressive strength. The measured tensile strengths from split cylinder tests were greater than calculated, and in general, the measured modulus of elasticity was significantly less than the calculated modulus of elasticity.

Table 16. Deck material properties

Concrete Age (days)	f'_c (ksi)	f_{ct} (ksi)		E_c (ksi)	
		Meas.	$0.20f'^{0.5}_c$	Meas.	$33{,}000w_c^{1.5}f'^{0.5}_c$
7	4.76	0.534	0.436	2,790	3,140
14	6.02	0.587	0.491	3,040	3,540
28	7.08	0.673	0.532	2,850	3,830
Shear Test	7.63	0.683	0.552	2,860	3,980
Flexure-Shear Test	8.30	0.701	0.576	3,130	4,150

* Unit Weight = 0.124 k/ft^3

Table 17 and Figure 61 provide a comparison over time of the measured deck modulus of elasticity to the predicted modulus of elasticity using the AASHTO equation, the ACI 363 equation, and the Cook equation as previously discussed.

Table 17. Comparison of deck measured and calculated E_c

Concrete Age (days)	f'_c (psi)	E_c (ksi)			
		Meas.	AASHTO	ACI 363	Cook
0	0	0	0	0	0
7	4760	2,790	3,140	2,970	3,140
14	6020	3,040	3,540	3,250	3,380
28	7080	2,850	3,830	3,450	3,560
42	7630	2,860	3,980	3,550	3,640
77	8300	3,130	4,150	3,670	3,740

* Unit Weight = 124 lb/ft^3

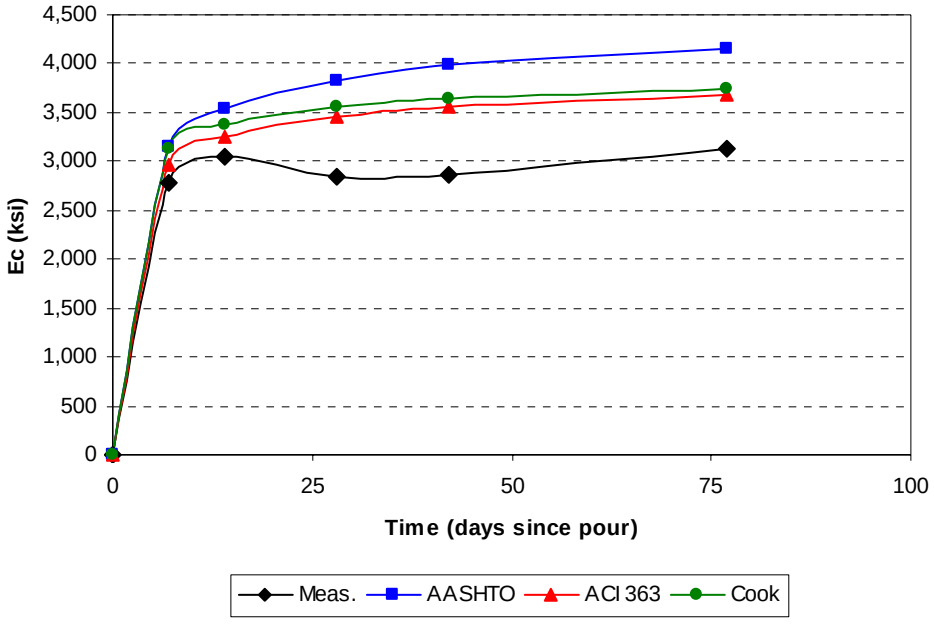

Figure 61. Comparison of deck measured and calculated E_c

From Table 17 and Figure 61, it can be seen that the predicted modulus of elasticity using the ACI 363 equation and the Cook equation fits the data from the lightweight cast-in-place deck better than the predicted modulus of elasticity from the AASHTO LRFD equation. The measured modulus of elasticity was still lower than the predicted modulus of elasticity using all three equations.

Shear Strength Testing

Both the web-shear strength and the flexure-shear strength of the PCBT-53 were theoretically predicted and experimentally determined in two separate tests. Theoretical predictions were made using four different models where applicable: the AASHTO Standard Specifications (2002), the Sectional Model from the AASHTO LRFD Specifications (2006), a Strut-and-Tie model created using the AASHTO LRFD Specifications, and the Simplified Procedure proposed in NCHRP Report 549 (Hawkins and Kuchma, 2007). In addition, comparisons between critical web-shear cracks angles are made using the LRFD approach, a Mohr's circle analysis, and the strut-and-tie model. Experimental measurements of web-shear strength were obtained by testing the girder on its south end, and experimental measurements of flexure-shear strength were obtained by testing the girder on its north end.

The focus of the first tests on the beam was to collect data pertaining to the predicted web-shear strength of the girder. These tests will be referred to from here on as shear test #1 or shear test #2 depending on the loading configuration. During shear test #1, the girder was loaded with two point loads located 7.5 ft and 21.5 ft from the south end of the beam. During shear test #2, the girder was loaded with two point loads located 7.5 ft and 10.5 ft from the south end of the beam. The focus of the third and final test on the beam was to collect data pertaining to the predicted flexure-shear failure. This test will be referred to from here on as the flexure-shear test. During the flexure-shear test, the girder was loaded at a distance of 16 ft and 30 ft from the north end of the beam.

Theoretical predictions of shear strength were done using both the measured material properties and the design material properties. The differences between the two sets of properties are shown in Table 18.

Table 18. Measured and design material properties

Property	Design	Measured
Beam f'_c (psi)	8,000	10,550
Deck f'_c (psi)	5,000	7,600
Beam Unit Weight (pcf)	120	118
Deck Unit Weight (pcf)	120	124
Beam E_c (ksi)	3,880	3,280
Deck E_c (ksi)	3,067	2,860
Strand E_p (ksi)	28,500	29,000
Strand f_{pu} (ksi)	270	284
Strand f_{py} (ksi)	243	259
Strand f_{pe} (ksi)	159	177

The measured concrete properties are those measured by Virginia Tech during cylinder tests, and the measured strand properties are those reported by the prestressing strand provider, American Spring Wire Corporation. The measured effective prestress value corresponds to the data recorded by the vibrating wire gages from concrete placement to the time of the initial shear test (Dymond, 2007); the design effective prestress value is from the LRFD prediction of prestress losses using the design material properties. The vertical stirrup spacing was 7 in at the middle of the shear span for both the web-shear test and the flexure-shear test. All theoretical calculations take into account the use of sand-lightweight concrete by using the correction factor $\lambda = 0.85$ where specified, and in all calculations the resistance factor, ϕ, was 1.0.

Theoretical Shear Strength Predictions

Theoretical predictions were made using four different models where applicable: the AASHTO Standard Specifications, the Sectional Model from the AASHTO LRFD Specifications, a Strut-and-Tie model created using the AASHTO LRFD Specifications, and the Simplified Procedure based on NCHRP Report 549. The Strut-and-Tie model was not used to predict the flexure-shear strength because the model is developed specifically for a web crushing failure (which was expected in only the web-shear test). Sample calculations for the web-shear strength predictions are shown in Dymond (2007).

AASHTO Standard Method

The AASHTO Standard Specifications 17th Edition (2002) specifies that the nominal shear strength, V_n, multiplied by a resistance factor, ϕ, must be greater than or equal to the factored shear force at the section in consideration, V_u. The nominal shear strength is made up of both the shear strength provided by the concrete, V_c, and the shear strength provided by the shear reinforcement, V_s. Within this, the concrete shear strength, V_c, is the lower of the flexure-shear strength, V_{ci}, and the web-shear strength, V_{cw}.

The shear strengths determined using this method were calculated at the center of the shear span (a/2), because that was the region of failure and initial web-shear cracks. This region was outside of the transfer length for both the web-shear tests and the flexure-shear tests so the prestress force was not reduced in the calculation of V_{cw}. The results for both the theoretical web-shear strength and the flexural-shear strength can be seen in Table 19.

Table 19. AASHTO Standard theoretical shear strength

Test	V_{ci}	V_{cw}	V_s	V_n
Measured Properties (k)				
Web-Shear	560	184	280	465
Flexure-Shear	264	191	286	478
Design Properties (k)				
Web-Shear	501	164	264	428
Flexure-Shear	236	170	270	440

It can be seen in this table that the overall concrete shear strength was controlled by V_{cw} in all of the tests. When design material properties were used to calculate the steel contribution to the shear strength, the AASHTO upper limit, $8\sqrt{f'_c}b_w d$, controlled in both of the tests.

Figure 62 shows the AASHTO Standard shear strength (V_n) for the web-shear test along one half the length of the girder. The theoretical predictions were based on measured material properties. This plot also includes the applied shear over the length of the beam. The applied shear value is based upon the load reached at failure during the web-shear test. The researchers deemed the girder was close to a web-shear failure when a load of 353 kips per actuator was applied to the beam, as discussed previously.

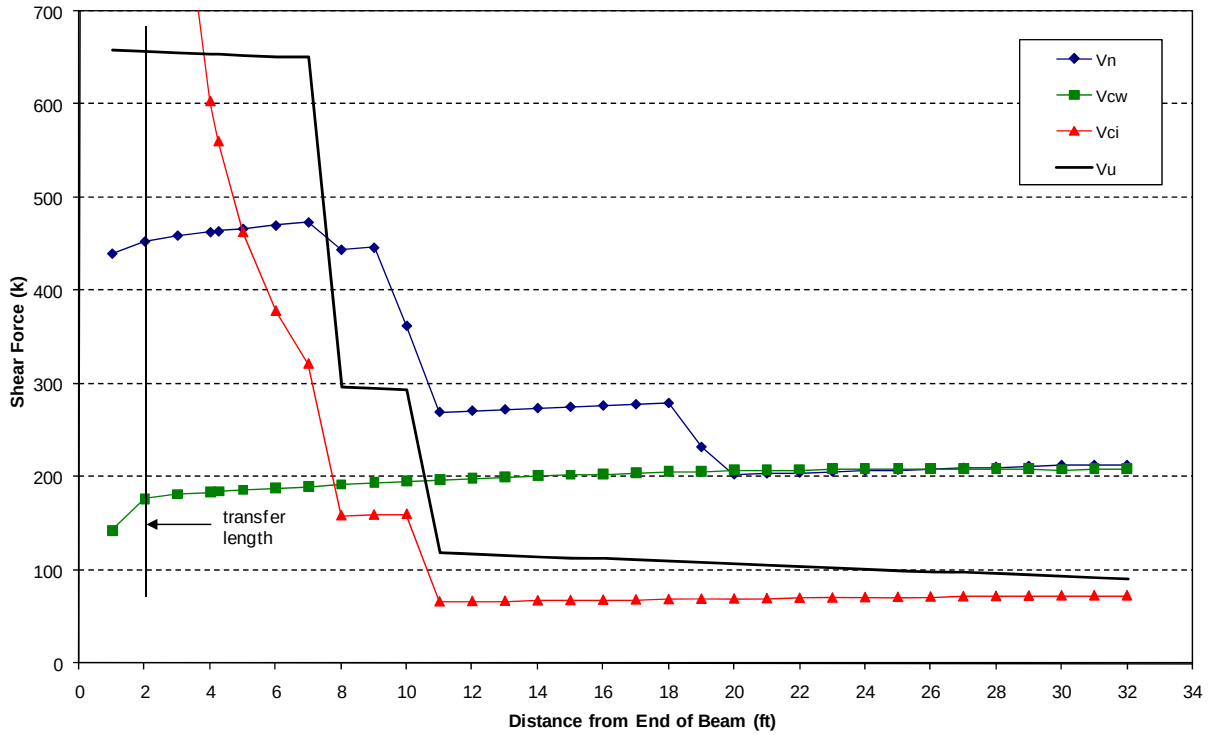

Figure 62. AASHTO Standard shear force diagram

NCHRP Simplified Method

The NCHRP Simplified Method was recommended by Hawkins and Kuchma (2007) and it presents an alternative shear design method similar to the AASHTO Standard Method using V_{ci} and V_{cw}. The simplified method very much resembles the AASHTO Standard Specifications in that the equations for the shear design of members includes modified V_{ci}, V_{cw}, and V_s terms. Table 20 provides a summary of the differences between the Simplified Method equations and the AASHTO Standard equations.

Table 20. Comparison between V_{ci}, V_{cw}, and V_s terms

	AASHTO Standard	NCHRP Simplified
V_{ci}	$= 0.6\sqrt{f'_c}\,b'd + V_d + \frac{V_i M_{cr}}{M_{\max}} \geq 1.7\sqrt{f'_c}\,b'd$	$= 0.632\sqrt{f'_c}\,b_v d_v + V_d + \frac{V_i M_{cr}}{M_{\max}} \geq 1.9\sqrt{f'_c}\,b_v d_v$
V_{cw}	$= \left(3.5\sqrt{f'_c} + 0.3 f_{pc}\right) b'd + V_p$	$= \left(1.9\sqrt{f'_c} + 0.30 f_{pc}\right) b_v d_v + V_p$
V_s	$= \frac{A_v f_{sy} d}{s} \leq 8\sqrt{f'_c}\,b'd$	$= \frac{A_v f_y d_v}{s}\cot\theta$

Where:

V_{ci} = nominal flexure-shear strength provided by concrete (lb)
f'_c = compressive strength of the concrete at 28 days (psi)
b', b_v = web width of a flanged member (in)
d = distance from extreme compressive fiber to centroid of the prestressing force (in)
d_v = effective shear depth (in) taken as the maximum of:

(1) $d_p - \frac{a}{2}$ (2) $0.9d_e$ (3) $0.72h$

V_d = shear force at section due to unfactored dead load (lb)
V_i = factored shear at section due to applied loads occurring simultaneously with M_{max} (lb)
M_{cr} = moment causing flexural cracking at section due to externally applied loads (lb-in)
M_{max} = maximum factored moment at section due to externally applied loads (lb-in)
V_{cw} = nominal web-shear strength provided by concrete (lb)
f_{pc} = compressive stress in the concrete at centroid of cross section (psi)
V_p = vertical component of effective prestress force at section (lb)
V_s = nominal shear strength provided by shear reinforcement (lb)
f_y, f_{sy} = yield stress of non-prestressed reinforcement in tension (≤ 60,000 psi) (psi)
s = longitudinal spacing of the web reinforcement (in)
A_v = area of web reinforcement (in^2)
θ = angle of inclination of diagonal compressive stresses as shown below (°)

$$\cot\theta = \sqrt{1 + \frac{f_{pc}}{f_t}}$$

The shear strengths using this method were calculated at the center of the shear span (a/2), because that was the region of failure and initial web-shear cracks. The results for both the theoretical web-shear strength and the flexural-shear strength can be seen in Table 21.

Table 21. NCHRP Simplified theoretical shear strength

Test	V_{ci}	V_{cw}	V_s	V_n
Measured Properties (k)				
Web-Shear	561	133	346	479
Flexure-Shear	265	139	286	425
Design Properties (k)				
Web-Shear	502	119	407	526
Flexure-Shear	237	125	426	440

Much like the AASHTO Standard Method, it can be seen in Table 21 that the overall concrete shear strength was again controlled by V_{cw} in all tests. The steel contribution to shear was calculated much differently in this method than in the AASHTO Standard method. The NCHRP Simplified method takes into account the crack angle. For the shear strength calculations, when measured material properties were used, this crack angle was assumed to be 39 degrees for the web-shear tests and 45 degrees for the flexure-shear tests based on observation. When design material properties were used to calculate the steel contribution to the shear strength, the crack angle was calculated using the equation presented by Hawkins and Kuchma (2007). For both the web-shear and the flexure-shear strength calculations the equation used to calculate cot(θ) yielded a value of 1.5, which was below the upper limit of 1.8. This value was higher than those used in the measured material property calculations and thus resulted in a higher steel contribution to the shear strength for the design cases.

Figure 63 shows the NCHRP Simplified Method shear strength (V_n) for the web-shear test along one half the length of the girder. The theoretical predictions were based on measured material properties. This plot also includes the applied shear over the length of the beam. The applied shear value is again based upon the load reached at failure during the web-shear test.

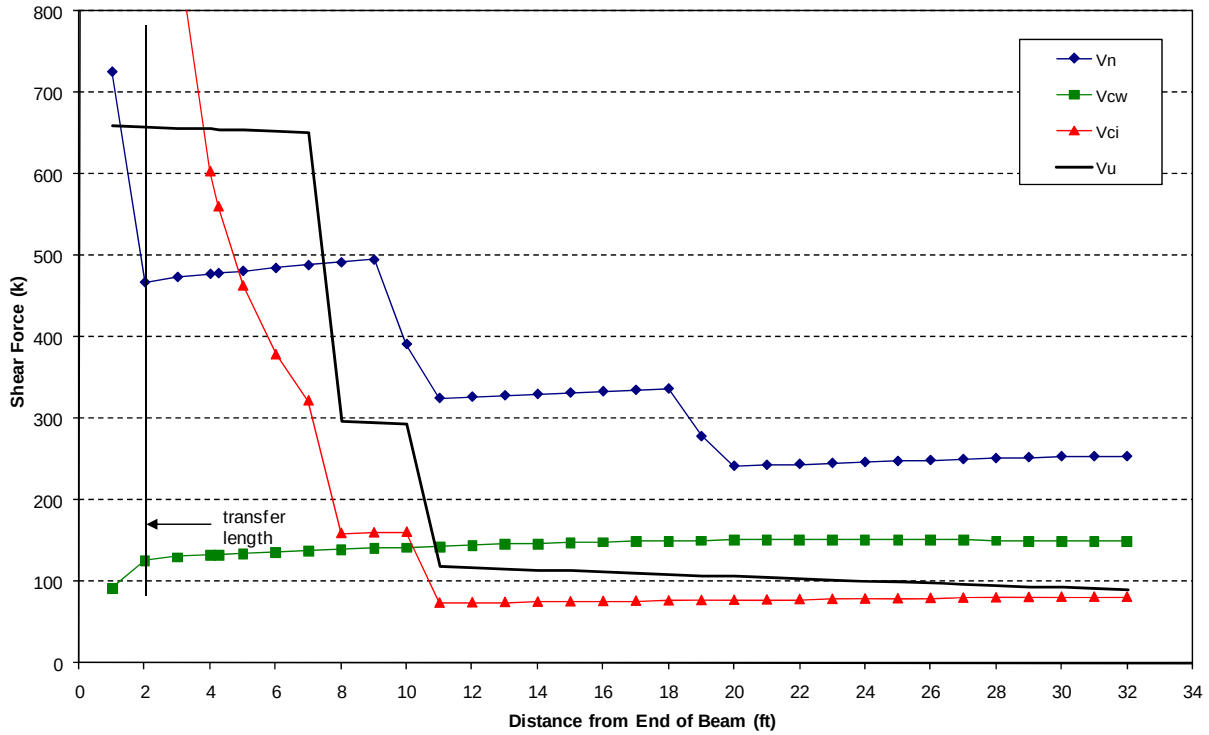

Figure 63. NCHRP Simplified method shear force diagram

AASHTO LRFD Sectional Model

The Sectional Model from the AASHTO LRFD Specifications 3rd Edition (2006) specifies that the nominal shear resistance, V_n, multiplied by a resistance factor, ϕ, must be greater than or equal to the factored shear force at the section in consideration, V_u. The AASHTO LRFD Sectional Model for calculating the nominal shear resistance is based on the

modified compression field theory and is discussed in depth in Dymond (2007). This calculation process is very different than the procedure discussed for the AASHTO Standard Specifications due to the iterative nature of the method. The results for both the theoretical web-shear strength and the flexural-shear strength (using both the code based angle and the test based angle) can be seen in Table 22. Additionally, this table shows the calculated maximum shear strength values for the region in consideration. The maximum shear strength is calculated as follows:

$$V_{n\max} = 0.25 f'_c b_v d_v + V_p \quad (1)$$

Table 22. LRFD theoretical shear strength

Test	θ (°)		V_c	V_s	V_p	V_n	V_{nmax}
Measured Properties (k)							
Web-Shear	LRFD	32.5	74	430	20	523	970
	Test	39	95	338	20	453	
Flexure-Shear	LRFD	36.6	70	378	20	468	992
	Test	45	99	280	20	399	
Design Properties (k)							
Web-Shear	LRFD	33.3	61	411	18	490	731
	Test	39	75	334	18	427	
Flexure-Shear	LRFD	36.9	58	369	18	445	747
	Test	45	79	277	18	374	

The Sectional Model from the AASHTO LRFD Specifications (2006) requires calculation of the longitudinal strain on the tension side of the member, ε_x, when calculating the nominal shear strength. Within the equation for longitudinal strain, the area of prestressing strand was reduced to an effective area based on the location of the critical section and the percent of strand fully developed at that location. In both test setups, half of the shear span was located between the transfer length and the development length. It was assumed that the strand stress varied linearly from the transfer length to the development length. Further within the nominal shear strength calculations, the compression angle was estimated and iteration was required until both the predicted compression angle matched the tabulated angle and the nominal shear strength, V_n, was equal to the applied shear, V_u. When these values were equal, the shear strength at the section of interest was obtained. Example calculations using the AASHTO LRFD Specifications can be seen in Dymond (2007).

The LRFD Sectional Model was applied in two different ways taking into account the angle of the crack that formed during testing and using the crack angle predicted by the LRFD equation; the difference in the two angles is shown in Table 22. In the first method, the compression angle was estimated and then iterated upon (in conjunction with the applied shear) until the shear strength of the section was reached. This involved determining both θ and β from AASHTO Table 5.8.3.4.2-1. The second method took into account the critical crack angle that formed during testing of the girder. This angle was held constant and the applied shear was iterated upon until the overall shear strength of the section was found. This involved only determining β from AASHTO Table 5.8.3.4.2-1. Sample calculations of both methods are

shown in Dymond (2007). Calculations for a longitudinal reinforcement check were also done using the AASHTO LRFD Specifications to predict if strand slip would control during web-shear testing. Results from this check revealed that strand slip would not control during testing, and experimental results confirmed this prediction.

Strut-and-Tie Model

A basic strut-and-tie model (STM) was developed to determine the ultimate strength of the girder when tested in the final web-shear configuration only. This STM was used to analyze and also predict at what load the applied stress exceeded the available concrete stress in a compression strut that formed in the shear span. During shear test #2, the researchers believe that the girder came close to reaching the ultimate shear failure desired because there was clear evidence of concrete spalling in the web of the PCBT-53. This phenomenon occurred at the top of the bottom bulb (13.5 in from the bottom of the beam) and approximately 2.5 ft from the end of the girder as previously shown in Figure 46.

Using this STM, the nominal compressive stress in the web at that location was calculated using AASHTO Article 5.6.3.3.3 and compared to the applied stress at failure. For these calculations, the failure load, and hence the failure stress, do not include the self-weight of the composite system. Furthermore, the forces from the draped strands, which deviate at an angle from the harping point to the end of the beam, are not included in the analysis.

The strut-and-tie model, created using AASHTO Article 5.6.3, was developed by proportioning two different node regions. The first node was a compression-compression-tension (CCT) node at the end of a strut anchored by the support bearing area and the reinforcement as shown in Figure 64.

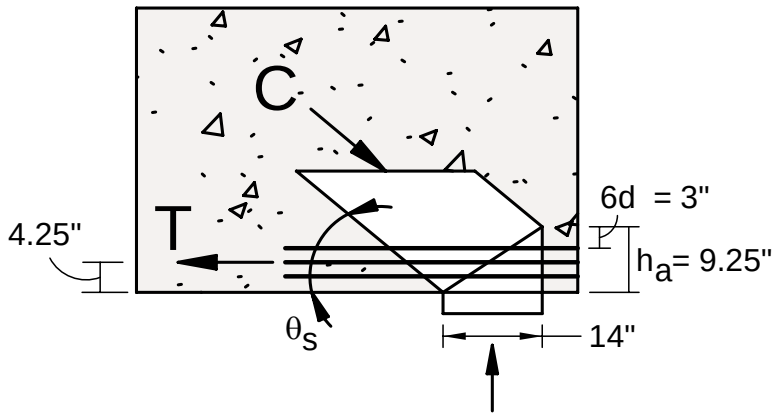

Figure 64. Strut anchored by bearing and reinforcement (CCT node)

The dimensions of this node were based solely upon existing geometry. The bearing width, prestressing strand spacing, and strand diameter were already known. The angle θ_s can be found from geometry by connecting this node to node at the point of load application.

The second node in this STM was a compression-compression-compression (CCC) node at the end of a strut anchored by a bearing area and another strut. This node can be seen in

Figure 65 and is determined both by physical geometry of the beam and by the forces acting on the beam.

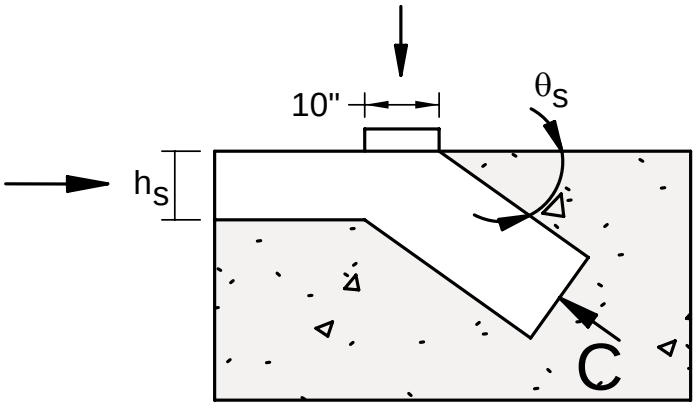

Figure 65. Strut anchored by bearing and strut (CCC node)

The final strut-and-tie model dimensions can be determined by summing moments about the CCT node as shown in Figure 66. Summing moments in this manner eliminates the need to find the prestressing strand force, which is a function of the effective prestress. Additionally, the reaction has a moment arm of zero so the only forces included are the applied load and the compressive force from the CCC node. Thus, the height of the top compression strut, h_s, can be found by limiting the compressive stress in the CCC node region to $0.85(f'_c)$, which is specified in AASHTO Article 5.6.3.5. Once the compression strut height is known, the angle at which the strut is orientated, θ_s, can be derived from geometry.

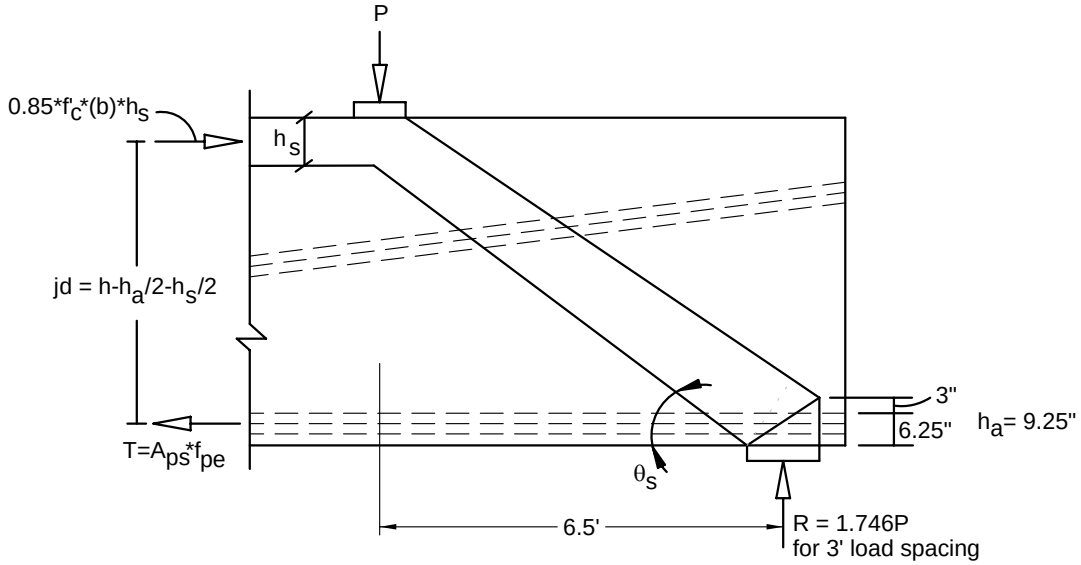

Figure 66. Strut-and-Tie model dimensions

Finally, using the angle, θ_s, the shear at the section of interest is transformed to be in line with the strut and the applied stress can be calculated using the equation shown below.

$$f_{app} = \frac{V_{app} / \sin(\theta_s)}{w_w w_s} \quad (2)$$

Where:

f_{app} = applied stress in the compression strut at section of interest (ksi)
V_{app} = shear from applied loads at section of interest (kip)
θ_s = orientation angle of the compressive strut with respect to the bottom of the girder (°)
w_w = width of the web (in)
w_s = width of the compression strut taken perpendicular to the angle θ_s (in)

This calculation was done at the location where web spalling was evident during shear test #2. This location, at the top of the bottom bulb (13.5 in from the bottom of the beam) and approximately 2.5 ft from the end of the girder, is most likely where the web would have crushed if more load could have been applied.

The point at which the concrete in the web would have crushed is taken as the limiting compressive stress in the strut. This value is determined using AASHTO Equation 5.6.3.3.3-1 as shown below.

$$f_{cu} = \frac{f'_c}{0.8 + 170\varepsilon_1} \leq 0.85 f'_c \quad (3)$$

in which:

$$\varepsilon_1 = \varepsilon_s + (\varepsilon_s + 0.002)\cot^2 \alpha_s \quad (4)$$

Where:

f_{cu} = limiting compressive stress of concrete (ksi)
f'_c = specified compressive strength (ksi)
ε_1 = principle tensile strain in cracked concrete due to loads (in/in)
ε_s = tensile strain in the concrete in the direction of the tension tie (in/in)
α_s = the smallest angle between the compressive strut and the adjoining tension tie (°)

The angle between the compressive strut and the tension tie was taken to be equal to θ_s because they are the same value in this case. Additionally, according AASHTO Article C5.6.3.3.3 for a tension tie consisting of prestressing strands, ε_s may be taken as 0.0 until the precompression of the strut is overcome ,which simplifies Equation 4.12 to $0.002\cot^2\alpha_s$. This article also states that the limiting stress for regions not crossed by or joined by tension ties is taken as $0.85(f'_c)$, which is the upper limit shown in Equation 3.

The results of the strut-and-tie model for the specified location and load at which the testing stopped can be seen in Table 23. These results present both the load at which the compression strut was predicted to crush and also the load at which the applied stress is equal to the ultimate stress. Sample calculations for the strut-and-tie method are presented in Dymond (2007).

Table 23. Applied stress and ultimate stress of compression strut

Load per Actuator (k)	Applied Shear at Angle θ_s (k)	h_s (in)	θ_s (°)	Strut Width Normal to θ_s (in)	f_{app} (ksi)	f_{cu} (ksi)	f_{app} / f_{cu}
353	967	0.62	39.6	14.2	9.7	8.1	1.20
295	808	0.62	39.6	14.2	8.1	8.1	1.00

Crack Angle Comparison and Discussion

The initial web-shear cracks were physically measured during shear test #1 and the predicted crack angles were calculated using the Sectional Model from the AASHTO LRFD Specifications, the strut-and-tie model used to predict the web-crushing failure, and Mohr's circle. The LRFD angle was taken as that used in calculating the shear strength of the section with AASHTO Table 5.8.3.4.2-1. The shear strength at the section of interest was calculated in two different ways using both the design material properties and the measured material properties. Thus, a crack angle is predicted from each set of calculations.

The strut-and-tie model was based on the geometry of the test setup and the girder. The initial web-shear crack is assumed to form along the compression strut that was used to predict the web crushing failure. This strut angle, θ_s, was calculated using geometry after the height of the top compression strut, h_s, was found by limiting the compressive stress in the CCC node region as previously discussed.

Finally, Mohr's circle was also used to predict the initial web-shear cracking angle. In this approach, the principle stresses and the orientation of the principle planes were found from the loading configuration used for shear test #1. The initial web-shear crack angle was predicted by setting the maximum principle stress equal to the maximum allowable stress according to the model proposed by Kupfer and Gerstle (1973). The maximum allowable stress in their model is a function of the minimum principle stress, the measured tensile strength of the concrete, and the compressive strength of the concrete. Sample calculations for this method can be seen in Dymond (2007). Table 24 provides a comparison of the experimental and predicted cracking angles.

Table 24. Web-shear crack angle comparisons

Type of Angle	Crack θ (deg)	Exp. / Pred.
Experimental	39	1.00
LRFD (measured props.)	32.5	1.20
LRFD (design props.)	33.3	1.17
STM	39.6	0.98
Mohr's circle	37.2	1.05

From Table 24 it can be seen that the strut-and-tie model most accurately predicted the web-shear crack angle. This was to be expected because it was largely dependent on the test setup geometry. The strut-and-tie model predicted a crack angle of 39.6 degrees, which had an experimental-to-predicted ratio of 0.98. Additionally, an analysis done using Mohr's circle predicted the cracking angle with an experimental-to-predicted ratio of 1.05. The LRFD shear

strength method under predicted the angle using both the measured concrete properties and the design material properties. The average experimental-to-predicted ratio for the LRFD method was 1.19. The results also agree with statements made by McGowan (2007) stating that the LRFD provisions predicted crack angles too shallow for PCBT girders.

Shear Model Comparisons and Discussion

Comparison of Tests to Calculated Strengths using Measured Material Properties

There were four different methods used to calculate the shear strength of the girder for each test: the AASHTO Standard Specifications (2002), the Sectional Model from the AASHTO LRFD Specifications (2006), a Strut-and-Tie model created using the AASHTO LRFD Specifications, and the Simplified Procedure based on NCHRP Report 549. All load and resistance factors were taken as one for the calculations. The shear capacities for each test (web-shear and flexure-shear), using all of the applicable methods, were calculated at half of the shear span for the corresponding test. In the web-shear test, this location is very close to that where the girder was expected to fail. In the flexure-shear test, it is important to note that the girder did not fail at this location because it failed prematurely close to the centerline of the girder. Additionally, the shear strength calculations for the flexure-shear test were done with a crack angle of 45 degrees as previously mentioned. The crack with this critical angle was located between the middle of the shear span and the load point 16 ft from the end of the girder. Calculations were still done at half of the shear span for consistency.

Table 25 summarizes the shear strength for each test and corresponding section using the measured material properties by presenting a ratio of experimental to theoretical.

Table 25 . Shear strength results using measured material properties

Test	Exp. / Standard	Exp. / NCHRP	Exp. / LRFD[1]	Exp. / LRFD[2]	Exp. / STM
Web-Shear	1.42	1.38	1.26	1.46	1.18
Flexure-Shear*	0.88	0.99	0.90	1.06	----

* Flexural strength was exceeded during this test.

[1] Using LRFD θ

[2] Using measured θ

Further investigating the web-shear strength values in Table 25, it can be seen that both the AASHTO Standard Method and the NCHRP Simplified Method provided conservative results (42 and 38 percent, respectively). The LRFD Sectional Model provided results that were 26 percent conservative when using the LRFD tabulated crack angle, and 46 percent conservative when using the crack angle measured during testing. Finally, the strut-and-tie model provided an overall web-shear strength prediction that was 18 percent conservative.

The strength values for the flexure-shear test, also shown above in Table 25 are almost all unconservative when compared to the applied load at failure. This is because the girder did not fail in shear at the critical location for this load case. The failure occurred near the center line of

the girder because the flexural strength of the PCBT-53 was exceeded at the location of maximum applied moment. The calculated flexural strength of the beam, ignoring the courtesy strands and deck reinforcing, is 6680 k-ft. Considering the self weight and the applied load of 303 kips per actuator, the total moment at the failure location was 7440 k-ft. The calculations and the explosive crushing of the top flange indicate a flexural failure, not a shear failure. Therefore, a comparison of the measured shear at failure to theoretical predictions is not valid. However, comparisons are presented for completeness.

The strengths presented in Tables 19, 21 and 22 were calculated using the recommended reduction factor of 0.85 for sand lightweight concrete. This modifier is applied to the $\sqrt{f'_c}$ term in the V_c equations. This modifier was applied even though the lightweight concrete used in the beam had a relatively high tensile strength. The Standard and LRFD Specifications state that the modifier is not to be applied if the specified tensile strength of the lightweight concrete is greater than $6.7\sqrt{f'_c}$. At the time of the web shear test the tensile strength was $7.7\sqrt{f'_c}$, and at the time of the flexure shear test the tensile strength was $8.4\sqrt{f'_c}$.

The reduction factor, λ, makes a surprisingly small difference in the calculated shear strength. Table 26 illustrates the calculation of web shear strength, broken down into its various components, for the Standard Specification method and the simplified NCHRP method. For the NCHRP method, the measured crack angle of 39 degrees is used.

Table 26. V_{cw} Calculations with and without λ

Method		Term 1	Term 2	Term 3	Term 4	Total	Test
AASHTO Standard with λ	Equation	$3.5\lambda\sqrt{f'_c}b'd$	$0.3f_{pc}b'd$	V_p	$\frac{A_v f_{sy} d}{s}$	465 kips	661 kips
	Value	113 kips	52 kips	20 kips	280 kips		
AASHTO Standard without λ	Equation	$3.5\sqrt{f'_c}b'd$	$0.3f_{pc}b'd$	V_p	$\frac{A_v f_{sy} d}{s}$	485 kips	
	Value	133 kips	52 kips	20 kips	280 kips		
NCHRP Simplified with λ	Equation	$1.9\lambda\sqrt{f'_c}b_v d_v$	$0.3f_{pc}b_v d_v$	V_p	$\frac{A_v f_y d_v}{s}\cot\theta$	479 kips	
	Value	61 kips	52 kips	20 kips	346 kips		
NCHRP Simplified without λ	Equation	$1.9\sqrt{f'_c}b_v d_v$	$0.3f_{pc}b_v d_v$	V_p	$\frac{A_v f_y d_v}{s}\cot\theta$	490 kips	
	Value	72 kips	52 kips	20 kips	346 kips		

The calculations presented in Table 26 illustrate that the lightweight reduction factor, λ, makes a very small difference in the overall calculation of shear strength. With the AASHTO Standard method, the difference is 20 kips and with the NCHRP method the difference is approximately 10 kips. These constitute very small percentages of the overall calculated strengths of over 450 kips. Therefore, it is impossible to evaluate the effectiveness of the λ factor to properly account for the lightweight concrete.

Comparison of Tests to Calculated Strengths using Design Material Properties

The shear strength of each section was also calculated using the design material properties. Table 27 presents a ratio of experimental to theoretical shear strength for each test and corresponding section using the design material properties.

Table 27. Shear strength results using design material properties

Test	Exp. / Standard	Exp. / NCHRP	Exp. / LRFD[1]	Exp. / LRFD[2]
Web-Shear	1.54	1.26	1.35	1.55
Flexure-Shear*	0.96	0.96	0.95	1.13

* Flexural strength was exceeded during this test.

[1] Using LRFD θ

[2] Using measured θ

The ratios of experimental to calculated strength in Table 27 indicate that the AASHTO Standard Method and the NCHRP Simplified method provided results that were 54 and 26 percent conservative, respectively. The LRFD Sectional Model provided results that were 35 percent conservative when using the LRFD tabulated crack angle, and 55 percent conservative when using the crack angle measured during testing. Additionally, the flexure-shear strength values exhibited the same tendency as previously discussed because the girder failed in flexure before the shear strength of the section was reached.

Comparison of Tests to Calculated V_{nmax}

The Sectional Model from the AASHTO LRFD Specifications (2006) recommend that the shear strength is taken as the lesser of two equations. Equation 1 presents the second equation, which is often taken as the maximum shear strength (V_{nmax}). It is interesting to examine the ultimate web-shear strength predictions (V_n) in comparison with the code recommended maximum value (V_{nmax}) as shown in Table 28.

Table 28. Comparison of V_n to V_{nmax}

Test	θ (°)		V_n	V_{nmax}	V_n / V_{nmax}
Measured Properties (k)					
Web-Shear	Code	32.5	523	970	0.54
	Test	39	453		0.47
Design Properties (k)					
Web-Shear	Code	33.3	490	731	0.67
	Test	39	427		0.58

From Table 28, it can be seen that the value of V_{nmax} does not ever control the shear strength; it is often considerably larger than the calculated shear strength V_n. Ratios of the nominal shear strength to the maximum shear strength (V_n/V_{nmax}) show that for the web shear

test the calculated strength, even with very dense reinforcing, was far less than the maximum allowed.

The V_n values obtained at the section of interest for web-shear testing can also be presented in the same fashion as the V_{nmax} equation. The value of V_{nmax} (as calculated with Equation 1) is a function of many different variables, including a numerical constant. In the equation for V_{nmax}, the numerical constant is a multiplier of 0.25. Table 29 provides a comparison between the V_n numerical constants and the V_{nmax} numerical constants.

Table 29. Comparison of V_n constants to V_{nmax} constants

Test	θ (°)		V_n Constant	V_{nmax} Constant	V_n / V_{nmax}
Measured Properties (k)					
Web-Shear	Code	32.5	0.13	0.25	0.52
	Test	39	0.11		0.44
Design Properties (k)					
Web-Shear	Code	33.3	0.17	0.25	0.68
	Test	39	0.14		0.56

Further consideration of Table 29 reveals that the V_{nmax} equation results in far higher shear strengths than calculated for V_n. The nominal shear strength, V_n, is based on both the concrete contribution to shear strength, V_c, and the steel contribution to shear strength, V_s. Evidence from testing suggested that during the web-shear test, the concrete contribution to shear strength had been reached because concrete spalling was beginning to occur in an area with high shear forces. As previously shown, the stirrup spacing at the location of web crushing was No. 5 bars at 7 in; even with this tight spacing, the concrete was able to consolidate properly and achieve the expected strength. Thus, from tests done within this research project, it seems that the constant multiplier of 0.25 used in the equation for V_{nmax} may be too high. However, experimental evidence, from research done by Tadros et al. (2000), suggests that the upper limit on the nominal shear strength equation ($0.25f'_c b_v d_v$) is sufficient. The research focused on shear testing of two prestressed I-girders. These girders had vertical shear reinforcement consisting of two planes of welded wire fabric; this type of shear reinforcement allowed for crack control in the compression strut during testing, eventually leading to crushing of the web concrete.

Cracking Load and Angle

The AASHTO Standard Specifications 17th Edition (2002) and the NCHRP Simplified procedure specify that the nominal shear strength, V_n, is made up of both the shear strength provided by the concrete, V_c, and the shear strength provided by the shear reinforcement, V_s. Within this, the concrete shear strength, V_c, is the lower of the flexure-shear strength, V_{ci}, and the web-shear strength, V_{cw}. The web-shear strength (V_{cw}) by itself can be used as a predictor for the initial web-shear crack. Table 30 and Table 31 compare the web-shear strength values from the AASHTO Standard Specifications, the NCHRP Simplified procedure, and finally the cracking load from a Mohr's circle analysis. The initial web-shear crack formed at a load of approximately 180 kips per actuator, or an applied shear in the section of 327 kips.

Table 30. AASHTO and NCHRP cracking load comparison

Test	V_{cw}	V_{app}	V_{app} / V_{cw}
Measured Properties (k)			
AASHTO Std.	184	327	1.78
NCHRP	133	327	2.46
Design Properties (k)			
AASHTO Std.	164	327	1.99
NCHRP	119	327	2.75

Table 31. Mohr's circle cracking load comparison

$V_{theoretical}$ (k)	V_{app} (k)	$V_{app} / V_{theoretical}$
342	327	0.96

The web-shear strength calculated using the AASHTO Standard Specifications provided conservative results when compared to the cracking load measured experimentally. The code based approach was 78 percent conservative when using the measured material properties and 99 percent conservative when using the design material properties. The web-shear strength values calculated using the NCHRP Simplified method results were 146 percent conservative when using the measured material properties and 175 percent conservative when using the design material properties. Additionally, an analysis done using Mohr's circle to predict the crack angle was the most accurate and yielded a theoretical cracking load that was 4 percent unconservative. This cracking load was calculated using the Kupfer and Gerstle (1973) method for maximum principle stresses previously discussed.

CONCLUSIONS

Conclusions from Material Testing

- The AASHTO LRFD equation for tensile strength, $f_{ct} = 0.20\sqrt{f'_c}$ (in ksi), predicted tensile strengths less than those measured for both the deck and the girder concrete.
- The AASHTO LRFD equation for modulus of elasticity, $E_c = 33{,}000 w_c^{1.5} \sqrt{f'_c}$ (in ksi), predicted moduli considerably higher than those measured for the girder and deck concrete.
- The equations presented by ACI 363 (1992) and by Cook (1989) provided better predictions of modulus of elasticity.
- The modulus of elasticity dropped slightly over time after attaining a maximum value at approximately 14 to 28 days.

Conclusions from Shear Testing

- The theoretical predictions calculated with a 39 degree crack angle for the web-shear strength were all conservative when compared to the experimentally measured failure strength. For

the web shear test, the AASHTO Standard Specifications (2002) and the Simplified Procedure recommend in NCHRP Report 549 were approximately 40 percent conservative while the Sectional Model from the AASHTO LRFD Specifications (2006) were between 26 and 46 percent conservative depending on the method of calculation. An additional strut-and-tie model was conservative when predicting the web-shear strength by approximately 18 percent.

- The theoretical predictions of the flexure-shear strength cannot be compared to the results from the flexure-shear test, because the girder reached the nominal flexural strength and a flexural failure occurred prior to a shear failure.

- Shear strength was also predicted using the design material properties. For the web shear test, the AASHTO Standard Specifications (2002) and the Simplified Procedure recommended in NCHRP Report 549 provided conservative results (54 and 26 percent, respectively). Additionally, the AASHTO LRFD Specifications (2006) were between 35 and 55 percent conservative depending on the method of calculation.

- The calculated maximum nominal shear strength never controlled and appears to be unconservative.

- Predictions of the initial web-shear cracking load using both the AASHTO Standard Specifications and the Simplified Method suggested in NCHRP Report 549 were 78 percent and 146 percent conservative, respectively, when using the measured material properties. A Mohr's circle analysis was 4 percent unconservative when predicting the initial web-shear crack.

- The initial web-shear crack angle was predicted using the Sectional Model from the AASHTO LRFD Specifications, the strut-and-tie model used to predict the web-crushing failure, and a Mohr's circle analysis. All of the models under-predicted the critical crack angle except for the strut-and-tie model (2 percent different from the actual angle), which was largely based upon existing geometry and the loading configuration. The LRFD Sectional Model predicted a crack angle of approximately 33 degrees, while the actual crack angle was 39 degrees; additionally, Mohr's circle predicted the crack angle to be approximately 37 degrees.

- It was difficult to assess the validity of the reduction factor for shear strength, λ, because it has a small influence on the overall shear strength.

RECOMMENDATIONS

1. *VDOT's Structure and Bridge Division should use the ACI 363 Equation for determining the modulus of elasticity for LWSCC.*

2. *VDOT's Structure and Bridge Division should use either the LRFD Sectional Model or the Simplified Procedure (for prestressed sections) for shear design.* The newly introduced Simplified Shear Design method and the current LRFD Sectional Model provided conservative results.

3. *VDOT's Structure and Bridge Division should exercise caution in designs in which V_n is approaching the maximum allowable V_n.* Tests indicate that the maximum allowable shear strength may be unconservative.

BENEFITS AND IMPLEMENTATION POTENTIAL

The cost of lightweight aggregate concrete (LWC) is somewhat higher than conventional, normal weight aggregate concrete. However, overall economy of a bridge can be achieved with LWC due to the lower self-weight, which can result in smaller sub-structure and longer span lengths. Likewise, self-consolidating concrete has a higher cost per cubic yard of materials, but savings can be achieved by more rapid concrete placement, with no labor costs associated with vibrator operators. The costs and benefits should be assessed on a job-by-job basis, but it is anticipated that on most prestressed bulb-tee bridge projects, LWSCC will result in an overall cost savings.

This study indicates that LWSCC can be successfully used in prestressed beams and bridge decks. Current AASHTO or ACI standards are adequate for use in the design of bridge beams and decks.

ACKNOWLEDGMENTS

The authors acknowledge and thank VDOT for providing funding for this project as part of the 2005 Innovative Bridge Research and Construction Program. This project was a collaborative effort between Virginia Tech and the Virginia Transportation Research Council (VTRC). Material design for the PCBT-53 was done at VTRC with the help of the Carolina Stalite Company. Material testing for the girder was done by staff at Virginia Tech and VTRC, and load testing was done at Virginia Tech. The authors also thank Chad Saunders of Bayshore Concrete Products for helping in scheduling and delivery of the girder. Finally, the authors thank Scott Stanley, the director of quality assurance, and ConRock Concrete for technical assistance with the deck mix design.

REFERENCES

American Concrete Institute Committee 363. (1992). State-of-the-Art Report on High Strength Concrete. ACI 363R-92 Reapproved 1997, American Concrete Institute, Farmington Hills, MI.

American Association of State and Highway Transportation Officials. (2002). *Standard Specifications for Highway Bridges,* 17th Ed. Washington, DC.

American Association of State and Highway Transportation Officials. (2004). *AASHTO LRFD Bridge Construction Specifications,* 2nd Ed. Washington, DC.

American Association of State and Highway Transportation Officials. (2006). *AASHTO LRFD Bridge Design Specifications,* 3rd Ed. Washington, DC.

ASTM A416/A 416M-05. (2005). *Standard Specification for Steel Strand, Uncoated Seven-Wire for Prestressed Concrete.* American Society for Testing and Materials, West Conshohocken, PA.

ASTM A615/A 615M-04b. (2005). *Standard Specification for Deformed and Plain Carbon Steel Bars for Concrete Reinforcement.* American Society for Testing and Materials, West Conshohocken, PA.

ASTM C39/C 39M-05e1. (2005). *Standard Test Method for Compressive Strength of Cylindrical Concrete Specimens.* American Society for Testing and Materials, West Conshohocken, PA.

ASTM C469-02e1. (2005). *Standard Test Method for Static Modulus of Elasticity and Poisson's Ratio of Concrete in Compression.* American Society for Testing and Materials, West Conshohocken, PA.

ASTM C496/C496M-04e1. (2005). *Standard Test Method for Splitting Tensile Strength of Cylindrical Concrete Specimens.* American Society for Testing and Materials, West Conshohocken, PA.

Cook, J. E. (1989). 10,000 psi Concrete. *Concrete International,* 11(10), 67-75.

Crispino, E. D. (2007). *Anchorage Zone Design for Pretensioned Bulb-Tee Bridge Girders in Virginia*. Master's Thesis, Virginia Tech, Blacksburg.

Dymond, B. (2007). *Shear Strength Of A Pcbt-53 Girder Fabricated With Lightweight, Self-Consolidating Concrete.* Master's Thesis, Virginia Tech, Blacksburg, VA.

Hawkins, N. M., and Kuchma, D. A. (2005). Simplified Shear Design of Structural Concrete Members. NCHRP Report 549. Transportation Research Board, Washington, DC.

Kupfer, H. B., and Gerstle, K. H. (1973). Behavior of Concrete under Biaxial Stress. *American Society of Civil Engineers Journal of Engineering Mechanics*, 99(4), 853-866.

McGowan, P. D. (2007). *Proposal for a Rational Shear Design Model for Prestressed Concrete Bulb-T Bridge Beams*. Master's Thesis, University of Virginia, Charlottesville.

APPENDIX

PLOT OF LOAD VS. STRAIN

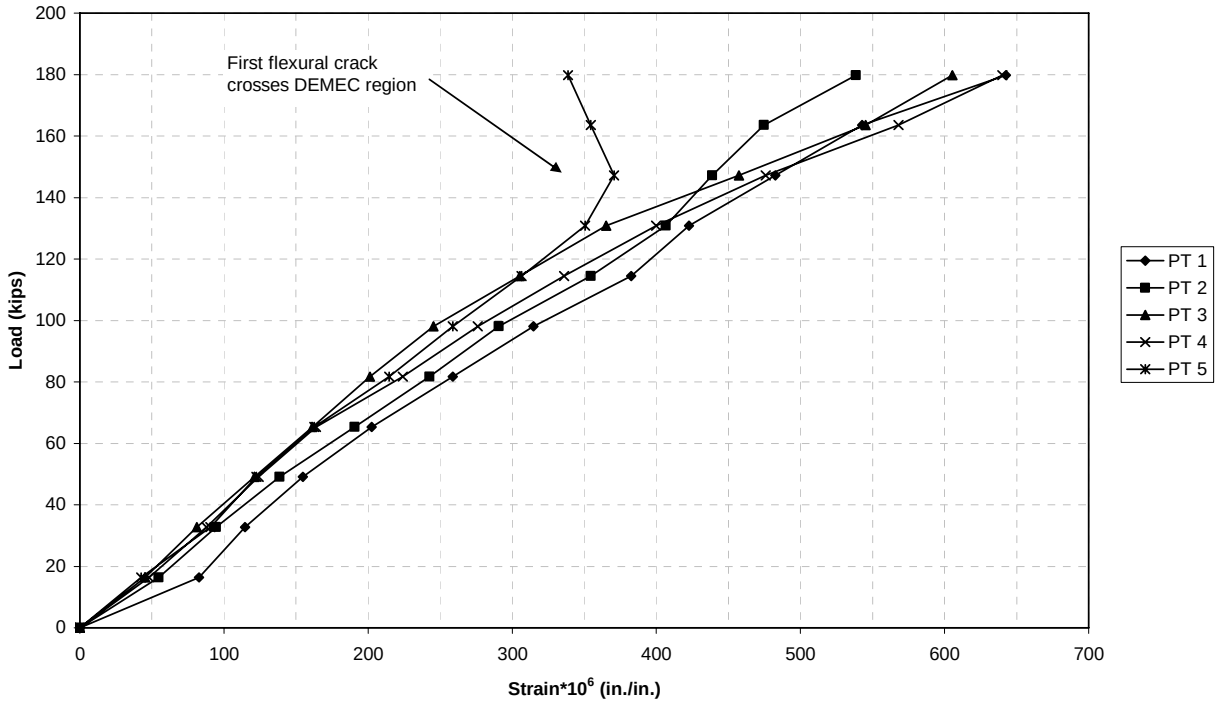

Figure A-1. DEMEC load vs. strain plot on shop side of girder

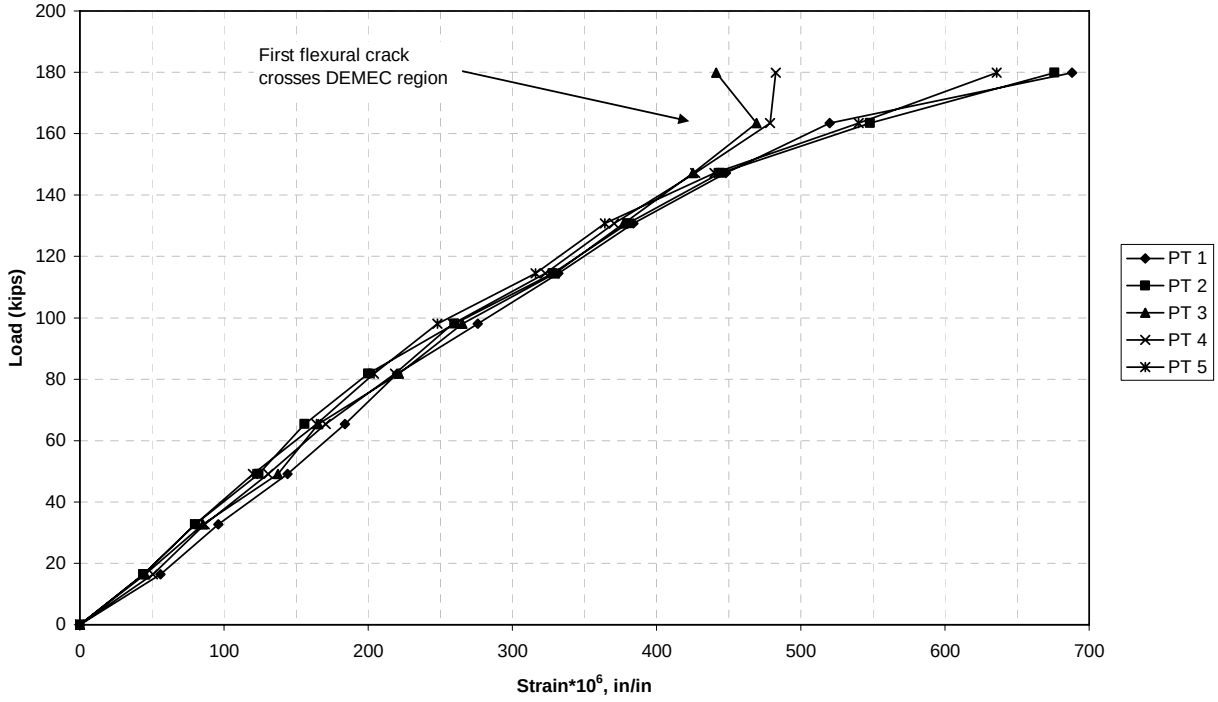

Figure A-2. Load vs. strain plot on Plantation Rd. side of girder